University of Central Florida
STARS

Electronic Theses and Dissertations, 2020-

2022

# Decoding Task-Based fMRI Data Using Graph Neural Networks, Considering Individual Differences

Maham Saeidi
*University of Central Florida*

 Part of the Industrial Engineering Commons
Find similar works at: https://stars.library.ucf.edu/etd2020
University of Central Florida Libraries http://library.ucf.edu

This Doctoral Dissertation (Open Access) is brought to you for free and open access by STARS. It has been accepted for inclusion in Electronic Theses and Dissertations, 2020- by an authorized administrator of STARS. For more information, please contact STARS@ucf.edu.

STARS Citation
Saeidi, Maham, "Decoding Task-Based fMRI Data Using Graph Neural Networks, Considering Individual Differences" (2022). *Electronic Theses and Dissertations, 2020-*. 1433.
https://stars.library.ucf.edu/etd2020/1433

# DECODING TASK-BASED FMRI DATA WITH GRAPH NEURAL NETWORKS, CONSIDERING INDIVIDUAL DIFFERENCES

by

MAHAM SAEIDI
B.S. Mashhad University, 2007
MS. Semnan University, 2010
M.S. University of Central Florida, 2019

A dissertation submitted in partial fulfilment of the requirements
for the degree of Doctor of Philosophy
in the Department of Industrial Engineering and Management Systems
in the College of Engineering and Computer Science
at the University of Central Florida
Orlando, Florida

Fall Term

2022

Major Professor: Waldemar Karwowski

© 2022 Maham Saeidi

# ABSTRACT

Functional magnetic resonance imaging (fMRI) is a non-invasive technology that provides high spatial resolution in determining the human brain's responses and measures regional brain activity through metabolic changes in blood oxygen consumption associated with neural activity. Task fMRI provides an opportunity to analyze the working mechanisms of the human brain during specific task performance. Over the past several years, a variety of computational methods have been proposed to decode task fMRI data that can identify brain regions associated with different task stimulations. Despite the advances made by these methods, several limitations exist due to graph representations and graph embeddings transferred from task fMRI signals. In the present study, we proposed an end-to-end graph convolutional network by combining the convolutional neural network with graph representation, with three convolutional layers to classify task fMRI data from the Human Connectome Project (302 participants, 22–35 years of age). One goal of this dissertation was to improve classification performance. We applied four of the most widely used node embedding algorithms—NetMF, RandNE, Node2Vec, and Walklets—to automatically extract the structural properties of the nodes in the brain functional graph, then evaluated the performance of the classification model. The empirical results indicated that the proposed GCN framework accurately identified the brain's state in task fMRI data and achieved comparable macro F1 scores of 0.978 and 0.976 with the NetMF and RandNE embedding methods, respectively. Another goal of the dissertation was to assess the effects of individual differences (i.e., gender and fluid intelligence) on classification performance. We tested the proposed GCN framework on sub-datasets divided according to gender and fluid intelligence. Experimental results indicated significant differences in the classification

predictions of gender, but not high/low fluid intelligence fMRI data. Our experiments yielded promising results and demonstrated the superior ability of our GCN in modeling task fMRI data.

To my love, Bahar, who constantly stands behind me while I am pursuing my dream.

# ACKNOWLEDGEMENTS

I would like to thank my advisor, Dr. Waldemar Karwowski, for his guidance, superhuman patience, and thoughtful insights throughout this research. I feel incredibly fortunate to have learned from and worked with him. Many thanks to the members of my committee, Dr. Peter A. Hancock, Dr. Ben D. Sawyer, and Dr. Pamela K. Douglas for their time and constructive feedback.

I would also like to express my thanks to my mentors and friends, Dr. Farzad Farahani and Dr. Krzysztof Fiok, who have been with me from the beginning and provided me with their generous support and valuable comments. It was a pleasure to collaborate and work with them.

My last thanks go to my love, Bahar, and my son, Arvin, for their unconditional love and support, which underlies everything I do.

# TABLE OF CONTENTS

# LIST OF FIGURES

# LIST OF TABLES

# LIST OF ABBREVIATIONS

| | |
|---|---|
| AD | Alzheimer's Disease |
| ADHD | Attention-Deficit Hyperactivity Disorder |
| ANNs | Artificial Neural Networks |
| ASD | Autism Spectrum Disorder |
| BOLD | Blood Oxygenation Level-Dependent |
| CNN | Convolutional Neural Network |
| DCNN | Diffusion Convolutional Neural Network |
| DL | Deep Learning |
| DTI | Diffusion Tensor Imaging |
| EEG | Electroencephalography |
| EV-GCN | Edge-Variational Graph Convolutional Network |
| FBIRN | Function Biomedical Informatics Research Network |
| fMRI | Functional Magnetic Resonance Imaging |
| GAT | Graph Attention Network |
| GCN | Graph Convolutional Network |
| GCRNN | Graph Convolutional Recurrent Neural Network |
| gF | Fluid Intelligence |
| GIN | Graph Isomorphism Network |
| GNN | Graph Neural Network |
| GRN | Graph Recurrent Network |
| GRU | Gated Recurrent Units |

| | |
|---|---|
| HCP | Human Connectome Project |
| Hi-GCN | Hierarchical Graph Convolutional Network |
| HM-gF | High Median Fluid Intelligence Score |
| KNN | K-Nearest Neighbor |
| LDA | Linear Discriminant Analysis |
| LM-gF | Low Median Fluid Intelligence Score |
| LR | Logistic Regression |
| LSTM | Long Short-Term Memory |
| MCC | Mathews correlation coefficient |
| MEG | Magnetoencephalography |
| ML | Machine Learning |
| MNI | Montreal Neurological Institute |
| NB | Naïve Bayes |
| PET | Positron Emission Tomography |
| RandNE | Iterative Random Projection Network Embedding |
| RF | Random Forest |
| RNN | Recurrent Neural Network |
| ROI | Region of Interest |
| rs-fMRI | Resting-State fMRI |
| SGC | Simple Graph Convolution |
| STAGIN | Spatio-Temporal Attention Graph Isomorphism Network |
| STGNN | Spatial-Temporal Graph Neural Network |
| SVM | Support Vector Machine |

# CHAPTER ONE: INTRODUCTION

## Human Brain Connectivity

The human brain is a complex system containing approximately 100 billion neurons and trillions of synaptic connections (Pakkenberg et al., 2003; Herculano-Houzel, 2009). The brain's electrical activity became a research focus in the 19th century when Richard Caton recorded brain signals from rabbits (Al-Kadi, Reaz and Mohd Ali, 2013; Molfese, Molfese and Kelly, 2016). Human brain research has since increased significantly, and brain networks research is now the most commonly used method to understand information underlying cognition, behavior, and perception (Reijneveld et al., 2007; Bullmore and Sporns, 2009; He and Evans, 2010; Craddock et al., 2013; Park and Friston, 2013; Farahani, Karwowski and Lighthall, 2019; Saeidi et al., 2021). Human brain networks can be acquired from anatomical connections in neural fiber (Huang and Chung, 2020) or statistical relationships between successive time points (Anirudh and Thiagarajan, 2019; Felouat and Oukid-Khouas, 2020; Huang et al., 2020), resulting in structural and functional networks, respectively. Structural connectivity generally refers to white matter volume changes between pairs of brain regions (Rubinov and Sporns, 2010), whereas functional brain connectivity refers on the basis of the temporal correlations among regional interactions of brain activities. Human connectome—the map of neural connections—provides a sense of fMRI-based studies and can be studied through computational techniques that offer new insights into brain functional connectivity to extract topological features from fMRI (Sporns, 2022). Extracted information from functional connectivity networks can be fed to machine learning (ML) algorithms as input data to identify biomarkers of the brain networks (Kazeminejad and Sotero, 2019).

## Machine Learning on Neural Connections

ML methods have become rapidly growing areas with applications in brain imaging and computational neuroscience, owing to higher levels of neural data analysis efficiency and decoding of brain function (Huang, Xiao and Wu, 2021). In ML, various algorithms are used to simplify processing pipelines and improve the learning process. For instance, supervised ML algorithms first learn on training data. The model and learned parameters are then applied to unseen or new data to predict the class label of the new data (Sen, Hajra and Ghosh, 2020).

There are two broad categories of ML algorithms including conventional/traditional ML methods and Deep Learning (DL) models. Conventional ML algorithms heavily rely on handcrafted graph topological features that use traditional graph analytics such as centrality measures, connectivity, and path analysis (Xu, 2021). For example, local and global connectivity from brain regions as graph features can be extracted from fMRI data to classify metabolic states with a linear support vector machine (Al-Zubaidi et al., 2019). On the other hand, DL introduced the concept of end-to-end learning and is trained automatically at multiple levels of abstraction. Instead of using handcrafted features in Conventional ML methods, which are usually based on expert domain knowledge and heuristics, high-level complex features can be automatically extracted from the original fMRI data and helped to improve the performance of classification models using deep learning algorithms (Huang, Hu, Dong, et al., 2018; Huang, Hu, Zhao, et al., 2018; Hu et al., 2019; Gui, Chen and Nie, 2020; Wang et al., 2020; Huang, Xiao and Wu, 2021). Convolutional neural networks (CNNs), for instance, can efficiently extract spatial features that are shared with the entire grid-like data (e.g., 2D and 3D images) (Azevedo, Campbell, et al., 2020). These features are then combined and fed into the higher-level layers within the network architecture (Spasov et al., 2019). Recurrent neural networks (RNNs), however, are able to learn

the temporal feature from input sequence data (Azevedo, Campbell, et al., 2020). With the availability of big data in neuroscience that represents complex functions with computational analysis, the application of DL algorithms shows remarkable progress in neuroimaging research using fMRI data (Razavian et al., no date; Wang et al., no date; L. Liu et al., 2020). However, they cannot directly work on graph-structured input data due to considering the brain network features as a vector of one dimension (D. Wu et al., 2021). The human connectome represents the brain as a graph with interacting nodes in non-Euclidean space (Zhu et al., no date; X. Bi et al., 2020), and existing DL methods generally disregard the interaction and association of brain connectivity networks (Liégeois et al., no date; Yao et al., 2021).

## Graph Neural Networks

One of the most effective ways to tackle the aforementioned limitations of ML and DL algorithms on a graph is with Graph Neural Networks (GNNs). GNN is a combination of neural networks with graph representation and has been successfully applied in many domains including social networks (Z. Wang et al., 2018), traffic networks (Guo et al., 2019), and protein networks (Fout et al., 2017) for solving various tasks including node classification, edge prediction, and graph classification (see illustration in Figure 1.1). GNNs have shown improvement in learning the representation of graph-structured data by creating an embedding of the nodes in a low-dimensional space (Xu et al., 2018). The end-to-end training allows this representation to be learned from the structural properties of the graph that are associated with the problem at hand. The representation of nodes uses an iterative procedure and passes information via a message-passing algorithm from the neighbors of each node (Casas et al., 2020). Unlike neural networks, GNNs update the representations of nodes while maintaining the

graph topology (Z. Wu et al., 2021). However, the computational cost will be growing with the number of graph nodes, which is why modern implementations are focused on reducing the number of iterations or using sampling methods to improve the speed of the model.

More recently, GNNs have seen a rapid increase in research activity in the field of fMRI data analysis (Ahmedt-Aristizabal et al., 2021) since the human connectome represents the brain as a graph with interacting nodes in non-Euclidean space (Zhu et al., no date; X. Bi et al., 2020). The study of GNNs for fMRI data analysis can be generally classified into two classes based on the definition of nodes: (1) the individual scale that uses graphs in which nodes represent brain parcels and edges represent functional connectivity (Ji, Maurits and Roerdink, 2019; Ventresca, 2019); (2) the population scale that involves a graph in which each subject is modeled as a node with corresponding brain connectivity data, and the similarities based on the modalities are defined by the edges (Stankevičiūtė et al., 2020). In this thesis, we focus on the first category. We study the robustness of the model for node classification where each node represents the ROIs, and two nodes are connected based on their functional connectivity.

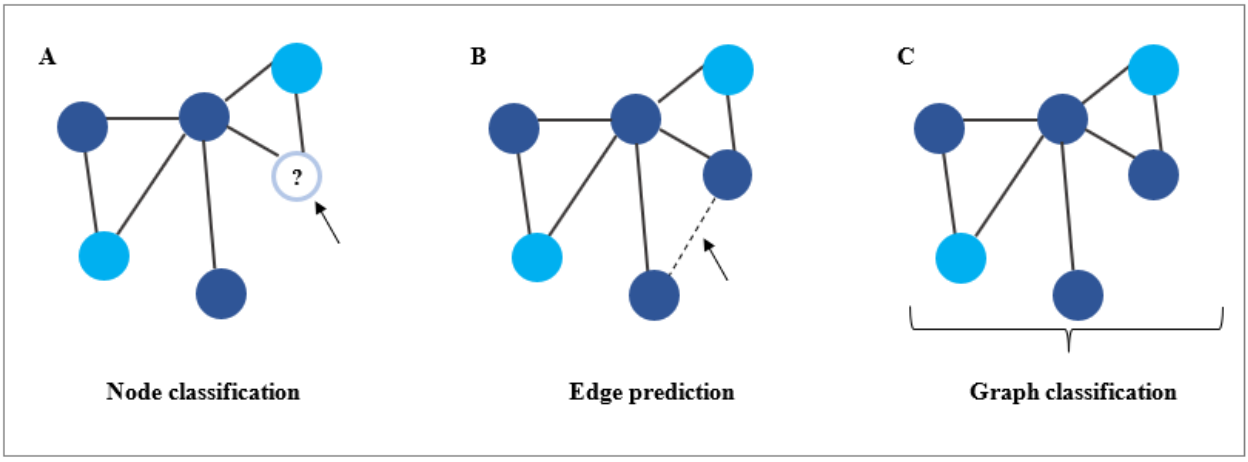


Figure 1.1. Problems that can be solved by graph neural networks. Node classification (A) to predict the node embedding for the unlabeled nodes in a graph. Edge prediction (B) to predict the relationship between nodes in a graph. Graph classification (C) to classify the whole graph into various classes.

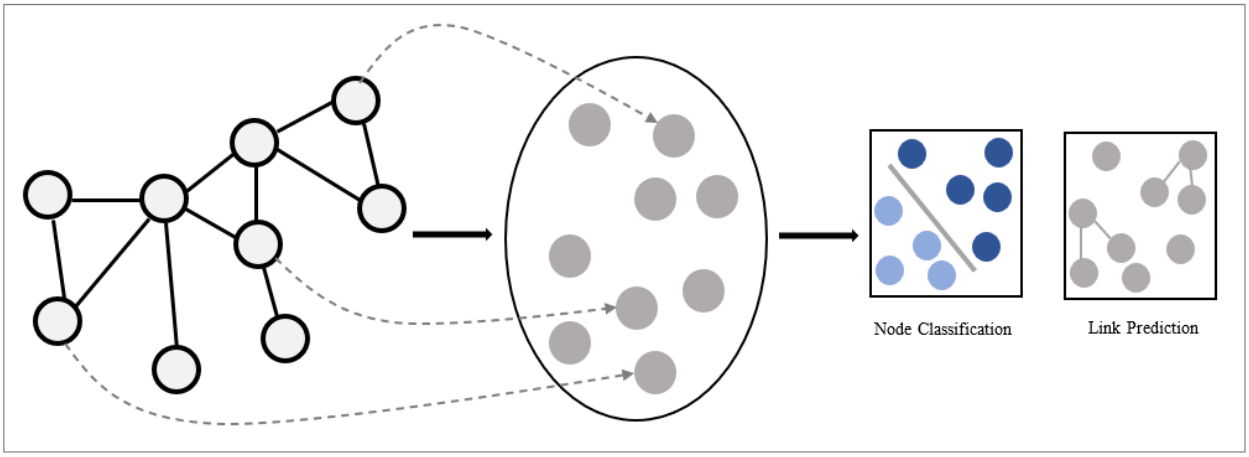


Figure 1.2. Illustration of graph embedding. First, each node is mapped to a low-dimensional vector embedding, based on the node's position in the graph. Then, the embedding methods have been successfully applied to solve many different tasks.

## Unsupervised Representation Learning

The traditional approach for extracting features from graph data relies on handcrafted topological features that use traditional graph analytics such as degree statistics, centrality measures, connectivity, and path analysis (Xu, 2021). In contrast, network representation learning aims to directly extract the features (i.e., representation learning or embeddings) from data by creating an embedding of the nodes in a low dimensional space such that similar nodes are close to each other in the Euclidian space (Xu et al., 2018). The embeddings should keep relevant structural information of the graph and the node features. As a result, the embedding methods have been successfully applied to solve many different tasks (see illustration in Figure 1.2). Depending on the particular data structure of a graph, the performance of embedding methods varies in extracting the structural properties of graph nodes, thus the classification algorithms may perform differently by using various node embeddings (Goyal and Ferrara, 2018). In this thesis, we show the power of the learning node embeddings for extracting features. We also compare the performance of several embedding algorithms on our proposed classification model.

## Research Objectives

The primary objective of this thesis is to improve the classification performance of task fMRI data by proposing a classification model that can accurately identify brain regions associated with different task stimulation using Human Connectome Project (HCP) dataset (Van Essen et al., 2013). Herein, we propose an end-to-end graph convolutional network (GCN) framework to classify task-evoked fMRI data. We conducted a series of experiments to evaluate the model's classification performance by using four well-known node embedding algorithms: NetMF, RandNE, Node2Vec, and Walklets. Furthermore, on the basis of prior studies indicating a close link between individual variability and the organization of brain function, we aimed to examine the effects of individual differences (i.e., gender and fluid intelligence (gF)) on the classification performance of the proposed GCN model. For this purpose, we performed extensive experiments on four sub-datasets: gender-associated sub-datasets (female and male) and gF score-associated sub-datasets (sub-datasets associated with individuals with gF scores lower than the median value, denoted LM-gF, or higher than the median value, denoted HM-gF). The main objectives are divided into the following segments.

Objective 1: To develop a classification model based on GCN to accurately classify task-evoked fMRI data. The proposed model should achieve comparability of results with previous findings.

Objective 2: To investigate whether the pre-processing step has an effect on the classification performance. If so, which node embedding methods have the most improvement on the GCN model.

Objective 3: To study whether individual differences (i.e., gender and the fluid intelligence) have an effect on the classification performance of the proposed GCN model.

## Thesis Organization

The rest of this thesis is organized as follows.

Chapter Two

Some parts of this chapter are adapted from the systematic review paper by (Saeidi et al., 2021), which has been published in the Brain Science journal. This chapter introduces the concepts of brain connectivity and provides an overview of machine learning/deep learning approaches. We illustrate how limitations in these approaches to analyze fMRI data have led researchers to develop GNN models. In this chapter, we mainly review graph neural network models for fMRI data analysis through a systematic literature review. We further discuss the application of the graph neural network approach in three main categories: neurological and psychiatric disease, gender classification, and brain response cognitive stimuli. Accordingly, we provide study limitations in task fMRI data analysis, research gaps, and future directions.

Chapter Three

In this chapter, we introduce the Human Connectome Project that is a popular large-scale fMRI dataset including resting-state and task fMRI data. Then, we discuss node embedding method application to extract topological features of graph nodes on fMRI data. We further propose a task-evoked fMRI data analysis pipeline for classification purpose and introduce our GCN architecture for fMRI analysis.

Chapter Four

In this chapter, we summarize the results of task fMRI classification based on the various node embedding methods. We have tested the classification performance of our GCN framework by

employing different node embedding methods. Our results indicate that our GCN is effective and promising in task fMRI classification.

Chapter Five

This chapter provides discussion of results, the limitations of the work, and future directions.

Chapter Six

This chapter summarizes the concluding remarks as well as research contribution.

# CHAPTER TWO: LITERATURE REVIEW

Some parts of this chapter are taken from the published systematic review paper by (Saeidi *et al.*, 2021) which has been published in the Brain Sciences[1] journal.

## Brain imaging technologies

Brain imaging technologies are divided into two main categories: structural imaging and functional imaging that are used for studying structural brain connectivity and functional brain connectivity, respectively. Structural connectivity describes anatomical connections in neural fiber between brain regions (Huang et al., 2020), and its changes in the brain network can be demonstrated with different properties including gray matter and white matter volume, cortical thickness, and texture-based approach (Karas et al., 2004; Li et al., 2017; Liu et al., 2018). An example of structural brain imaging is Magnetic Resonance Imaging (MRI). Functional connectivity, on the other hand, is a statistical measurement that is derived from time-series observations, and describes patterns of regional interactions of brain activities (Anirudh and Thiagarajan, 2019; Felouat and Oukid-Khouas, 2020; Huang et al., 2020), and can be obtained using model-based (e.g., cross-correlation, spectral coherence, and statistical parametric mapping) and model-free (e.g., mutual information, clustering, and decomposition-based analysis) approaches (Rocca et al., 2014; García-Prieto, Bajo and Pereda, 2017; Farahani, Karwowski and Lighthall, 2019; Felouat and Oukid-Khouas, 2020; Mahmood et al., 2021). Electroencephalography (EEG), magnetoencephalography (MEG), Positron Emission Tomography (PET), and functional Magnetic Resonance Imaging (fMRI) are examples of brain functional imaging.

[1] https://www.mdpi.com/2076-3425/11/11/1525.

Time series data may be inferred from measuring changes in electrical activity and changes in magnetic fields generated by electrical activity in the brain through EEG and MEG, respectively, or evaluating metabolic changes through PET and changes in blood oxygenation level-dependent (BOLD) over time through fMRI (Crosson et al., 2010; Farahani, Karwowski and Lighthall, 2019). Among various advanced neuroimaging techniques to directly observe brain activities, MRI and fMRI are non-invasive technologies that provide higher spatial resolution to determine the brain's responses (Goense, Bohraus and Logothetis, 2016) and significantly reduce radiation exposure (Crosson et al., 2010) (see illustration in Figure 2.1).

## Functional Magnetic Resonance Imaging technology

fMRI is a non-invasive technique for studying brain activity. In fMRI technology, we demonstrate the activated regions of the brain based on BOLD contrast. This method measures the oxygen consumption of active neurons to make the active areas observable. During an fMRI experiment, time series of the three-dimensional volume of the brain are acquired within a task block while the participant's brain actively performs an explicit task. Therefore, changes in the measured signal between individual images are used to make inferences regarding task-related activations in the brain. In each single experiment, several hundred images are acquired, and each image consists of a large number (~ 100000) of voxels (i.e., the smallest distinguishable element of fMRI data). Each voxel corresponds to a spatial location and has a number associated with it that represents its intensity. Therefore, the related information can be extracted from a single voxel by measuring intensity changes across that voxel in its spatial location. This process can generate the time series of these intensities which shows how its activity changes over the course of scanning. This concept is presented in Figure 2.2.

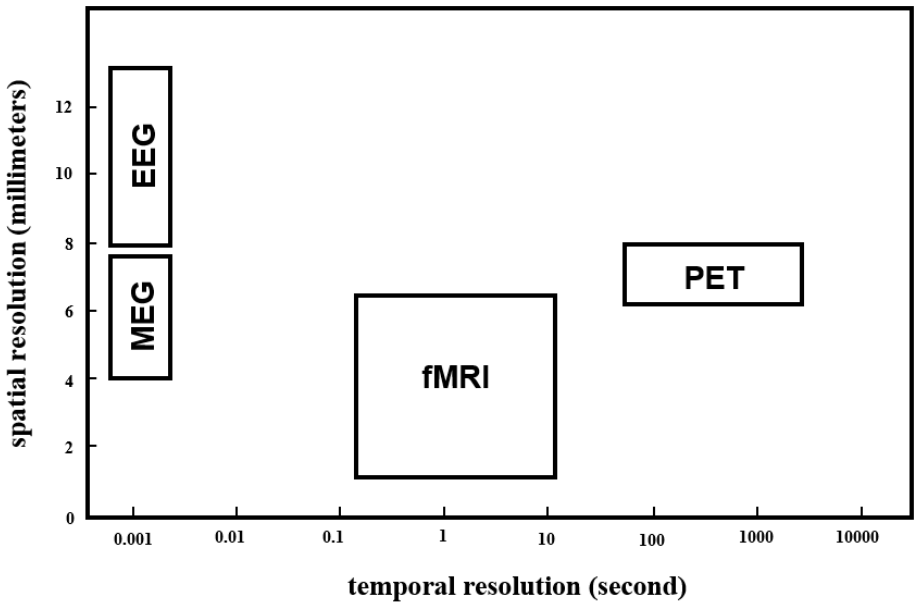


Figure 2.1. Spatial and temporal resolution. Spatial resolution refers to our ability to distinguish changes in image across different spatial locations. Temporal resolution refers to our ability to separate brain events in time.

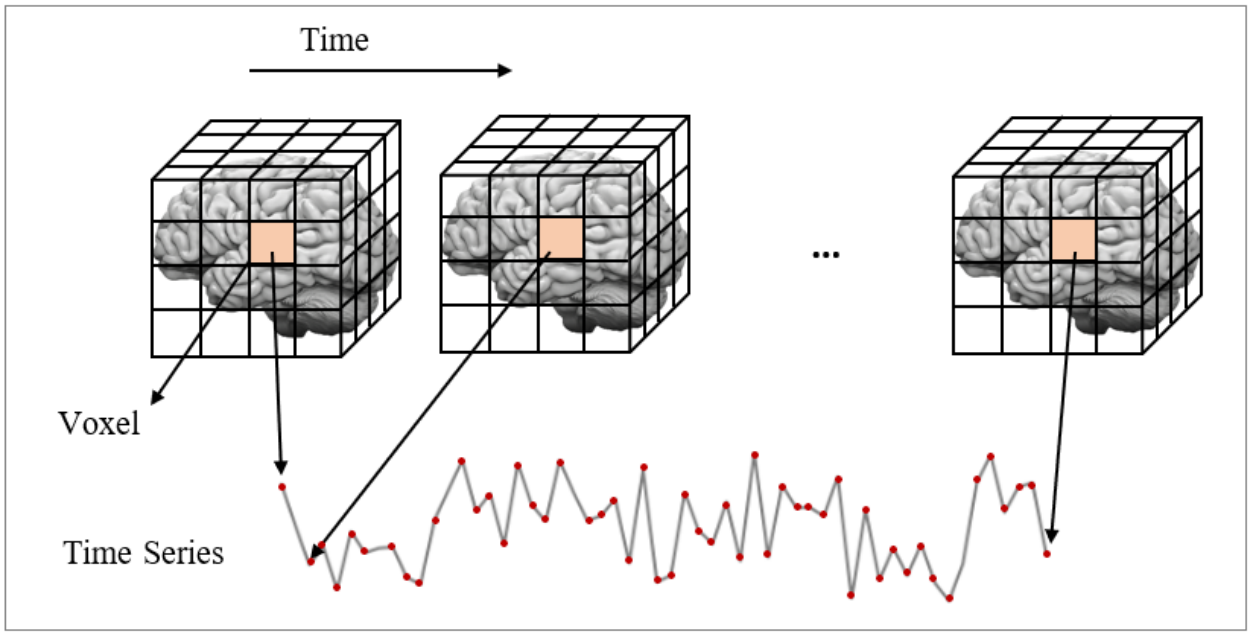


Figure 2.2. Illustration of a single voxel time series.

## Task and Resting State fMRI

There are two primary paradigms of fMRI studies: resting-state fMRI (rs-fMRI) and task-based fMRI. The former records brain activity to detect synchronous BOLD changes associated with brain regions while participants lie in the scanner and do not perform a task or think about any specific thing. In contrast, in the latter paradigm, fMRI data is acquired while the participant's brain is active with or without performing an explicit task. Rs-fMRI and task-based fMRI have gained widespread applications in neurological disorders such as Epilepsy (Bernhardt, Bonilha and Gross, 2015), Schizophrenia (Mastrovito, Hanson and Hanson, 2018), Autism Spectrum Disorder (ASD) (Ecker, Spooren and Murphy, 2012), and Attention-Deficit Hyperactivity Disorder (ADHD) (Cocchi et al., 2012), age and gender prediction (Gadgil et al., 2020; Kim and Ye, 2020), and brain responses to the cognitive stimulus by tasks (Gong et al., 2016; Markett et al., 2018; Kim, Ye and Kim, 2021; Zhang et al., 2021).

## Functional Brain Network

The brain is a complex network that includes structural and functional connections. Human connectomes, complex maps that explain the set of functional connections in the brain, provide insights into fMRI-based studies and represent the brain as a graph where the regions of interest (ROIs) are nodes and the connections among interacting ROIs are known as edges. The whole brain could be divided into different regions using atlases and parcellation schemes. Functional connectivity that determines temporal correlation among brain ROIs, could be obtained using fMRI. Most conventionally, cross-correlation is computed using the Pearson correlation coefficient (Bishara and Hittner, 2012) which denotes the weight of the edge between two brain

parcels. In most cases, a pre-defined threshold value has been applied, so that if the correlation is higher than the threshold value, it can be considered as an edge connecting two nodes.

Graph theoretical metrics such as clustering coefficient, geodesic path, small-worldness, and assortativity (Farahani, Karwowski and Lighthall, 2019) provide an effective tool to analyze the brain's connectivity network and have numerous applications in understanding the neural correlates of neurological and psychiatric disorders, and predicting human behavioral and cognitive traits (Park and Friston, 2013; Bernhardt, Bonilha and Gross, 2015; Petersen and Sporns, 2015; Mastrovito, Hanson and Hanson, 2018).

## Introduction to Machine Learning

Machine learning as a field of artificial intelligence, is a rapidly growing area with applications in computational neuroscience, owing to higher levels of neural data analysis efficiency and decoding of brain function (Huang, Xiao and Wu, 2021). Three main categories of ML include supervised learning, unsupervised learning, and semi-supervised learning. Supervised learning teaches the model based on the labeled data and draws pre-classified patterns that use to classify new patterns. However, in unsupervised learning, we let the model work on its own to discover information since there are no exact target outputs associated with each input. Semi-supervised learning is halfway between supervised and unsupervised learning including a number of labeled instances and a number of unlabeled instances.

In ML, various algorithms are used to simplify processing pipelines and improve the learning process. For instance, supervised machine learning algorithms first learn on training data. The model and learned parameters are then applied to unseen or new data to predict the class label of the new data (Sen, Hajra and Ghosh, 2020). Among different types of classification tasks, binary

and multi-label classifications are widely used in clinical studies, and in studies of cognitive function and brain disorders. The objective of classification is to predict the class label of the new data points in various tasks (Sen, Hajra and Ghosh, 2020). Classification algorithms can be divided into two categories: conventional classification algorithms and DL algorithms (Wang, Cang and Yu, 2019). Conventional classification algorithms represent a precise effort to build classification models by using input data and applying statistical analysis to classify output values. Most conventional classification algorithms use hand-crafted input features to train the model. This process, called feature creation, has limitations in handling input in high-dimensional datasets (Wang, Cang and Yu, 2019). DL algorithms rely on representation learning (Bengio et al., 2012) and can accommodate the limitations of conventional classification algorithms through learning features automatically at multiple levels of abstraction (Wang, Cang and Yu, 2019). Table 2.1 presents a brief comparison of conventional classification and DL algorithms (Wang, Cang and Yu, 2019).

Table 2.1. Brief comparison of conventional classification algorithms and deep learning algorithms.

| | Conventional classification algorithms | Deep learning algorithms |
|---|---|---|
| Input features | Hand-crafted | Automatically based on representation learning |
| Feature selection process | Required | Not Required |
| Model architecture | Based on statistical concepts | Consists of a diverse set of architecture based on sample data |
| Computational cost | Computational cost is based on the conventional classification models but is lower than that of deep learning algorithms | Computational cost is very high, because hyper parameters must be tuned |

## Conventional Classification Algorithms

Among different conventional classification algorithms including supervised learning and unsupervised learning, supervised algorithms are the most well-known methods used in fMRI data analysis. One of the most commonly used supervised algorithms is artificial neural networks (ANNs). ANNs are computational models (Haykin and network, 2004) that use multilayered networks of neurons with weighted connections between units, typically followed by a static non-linearity function (e.g., Rectified Linear Unit (ReLu)). During the learning phase, the network can learn by modifying its weights to enhance the performance outcomes in test data classification (Behri, Subasi and Qaisar, 2018). Similar examples of well-performed and well-known supervised algorithms include naive Bayes (NB), support vector machine (SVM), k-nearest neighbor (KNN), logistic regression (LR), random forest (RF), and linear discriminant analysis (LDA). Each supervised model applies a learning algorithm to generate a more accurate model.

NB is a probabilistic classifier that applies Bayes' theorem to classify data on the basis of certain features (Hosseini et al., 2020). It is a simple and effective classifier that needs only small training datasets to estimate the parameters for classification. This advantage makes NB a robust classifier for brain signals analysis in several types of tasks. However, NB is based on the assumption that all attributes are independent of one another, and feature vectors have equal effects on the outcome (Hosseini et al., 2020).

SVM has been demonstrated to be a useful supervised model based on a statistical learning tool with high generalization. The principle underlying SVM is the separation of two datasets. This separation can be linear or non-linear. In the case of linear separation, SVM uses a discriminant hyperplane to distinguish classes. However, in the case of nonlinear separation, SVM uses the

kernel function to identify decision boundaries. Compared with that of other supervised algorithms, such as ANNs and KNN, the computational complexity of SVM is low (Osowski, Siwek and Markiewicz, 2004; Palaniappan, Sundaraj and Sundaraj, 2014). Although the computational complexity of KNN decreases by increasing the k-value, its classification performance also decreases (Beyer et al., 1999; Palaniappan, Sundaraj and Sundaraj, 2014). Furthermore, with the advent of deep learning algorithms, SVM has remained widely used in fMRI data classification, because its computation has a solid mathematical basis. However, the performance of SVM is affected by the kernel function and penalty coefficient parameters; thus, optimizing the parameters introduced into SVM classifiers is essential (Du, Huang and Wang, 2015). (Huang and Wang, 2006) have applied a genetic algorithm, and (Wang, Qiu and Li, 2010) have proposed particle swarm optimization to optimize SVM parameters. According to our investigation (Saeidi *et al.*, 2021), SVM has been widely used in brain data classification because of its simplicity and adaptability in solving classification problems such as diagnosis of brain disorders.

RF is a tree-based supervised algorithm that constructs an ensemble of decision trees. Each decision tree is generated during the training phase. RF makes predictions from each tree and selects the final decision via a voting method or averaging the results (Ramzan and Dawn, 2019) to identify the most commonly used class. The main idea underlying this, and related ensemble methods is that a group of weak classifiers can collectively generate a strong classifier to create a successful learning algorithm. However, the overfitting and instability of trees can affect RF model performance, particularly with varying sizes of trees (Hosseini et al., 2020). In contrast to the LR model, which is a probabilistic classification model for both binary and multi-class classification tasks (Conklin, 2002), RF works on both discrete and continuous data, thus

providing models for classification and regression problems. Furthermore, the parallelization structure of RF results in better performance than that of the other supervised algorithms on large fMRI datasets in addressing classification problems (Sarica, Cerasa and Quattrone, 2017).

LDA is a linear transformation technique used to identify linear combinations of the variables that most effectively separate the classes (Bandos, Bruzzone and Camps-Valls, 2009; Tharwat et al., 2017). LDA is based on the assumption that the density for the data is normally distributed, with equal covariance for both classes. The separating hyperplane is achieved by maximizing the distance between the two classes, while minimizes the distance points within each class (Lotte et al., 2007). This technique is simple to use and has very low computational requirements. However, the main limitation of this model is its linear nature which prevents competitive results on nonlinear brain data (Balakrishnama, Ganapathiraju and Picone, 1999; Garcia, Ebrahimi and Vesin, 2003).

## Deep Learning Algorithms

Deep learning is a new branch of machine learning that has received widespread attention in fMRI classification tasks. Although conventional classification algorithms have been very effective in analyzing massive datasets and understanding the relationship between variables, such algorithms often lead to poor generalization behavior and low classification performance when highly dynamic features are encountered (Sakhavi, Guan and Yan, 2018). Deep learning algorithms inspired by neuroscience (McCulloch and Pitts, 1943) exploit learning features from raw data without depending completely on preprocessing (Lecun, Bengio and Hinton, 2015). Humans can transfer knowledge and memory throughout their lifespan, whereas deep learning algorithms immediately forget the previous learning after being trained on a new dataset (van de

Ven, Siegelmann and Tolias, 2020). For instance, (Borgomaneri et al., 2020) have confirmed that fear memory remains in humans after memory reactivation and affects the future learning process. Such a life-long learning task is a large challenge in developing neural network algorithms (Parisi et al., 2019). Deep learning algorithms apply multiple layers of perceptrons that obtain representation learning (Lecun, Bengio and Hinton, 2015). Recent developments in graphics processing unit technology have enabled the development of deep learning architectures on large datasets. This advantage has significantly improved the performance on large datasets with high-dimensional data (Craik, He and Contreras-Vidal, 2019).

Convolutional neural network (CNN) is a type of deep neural network that has gained attention, particularly in computer vision and neuroimaging (Lecun, Bengio and Hinton, 2015). CNN can identify the image of an object by using convolutions within its architecture; including convolutional layers that have parameters to create a feature map; pooling layers that reduce the number of features for computational efficiency; dropout layers that help avoid overfitting by randomly turning off perceptron; and an output layer that map the learned features into the final decision, such as classification (Abiodun et al., 2018; Valliani, Ranti and Oermann, 2019). The recent emergence of the CNN algorithm has enabled outstanding performance in several applications such as image processing (Bhattacharya et al., 2021), natural language processing (Fiok et al., 2021), and fMRI data analysis (Wen et al., 2018). However, CNN performance is highly dependent on hyperparameters such as the number of convolution layers, and the size and number of kernels and pooling windows (Al-Saegh, Dawwd and Abdul-Jabbar, 2021). Fortunately, CNN architectures have led to automatic optimization of parameters through several iterations (Craik, He and Contreras-Vidal, 2019); therefore, CNN is very commonly used for addressing classification problems involving large datasets (see illustration in Figure 2.3.A).

Recurrent neural network (RNN) is a time series-based deep learning algorithm that uses sequential data and learns from training data, similar to feed-forward and CNN methods (see illustration in Figure 2.3.B). Unlike traditional deep neural networks, which assume independence of the input and output, RNN takes information from inputs continually. Consequently, the output of RNN depends on the prior outputs and the current inputs within the sequence (Al-Saegh, Dawwd and Abdul-Jabbar, 2021). Thus, the architecture of this network includes inbuilt memory cells for storing information from previous output states (Faust et al., 2018). The form of RNN architecture has enabled these types of networks to effectively analyze time-series data for applications such as speech recognition (Miao, Gowayyed and Metze, 2016), natural language processing (Wiggins et al., 2021), and disease signal identification (Tan et al., 2018).

The most commonly used RNN variants are long short-term memory (LSTM) (Hochreiter and Schmidhuber, 1997), LSTM peephole connections (P. Wang et al., 2018), gated recurrent units (GRU) (Roy, Kiral-Kornek and Harrer, 2019), and multiplicative LSTM (Krause et al., 2016). The ability of these variants to preserve and retrieve memories is part of the generic structure of these networks. However, CNNs have a different architecture and use filters and pooling layers. According to differences in the internal network structure of CNNs and RNNs, CNNs are effective for the analysis of spatial data, because CNN models consider the complete trial as an object and can extract features. In contrast, RNN models are suited for the analysis of temporal and sequential data by slicing the trail into several sub-trails (Al-Saegh, Dawwd and Abdul-Jabbar, 2021).

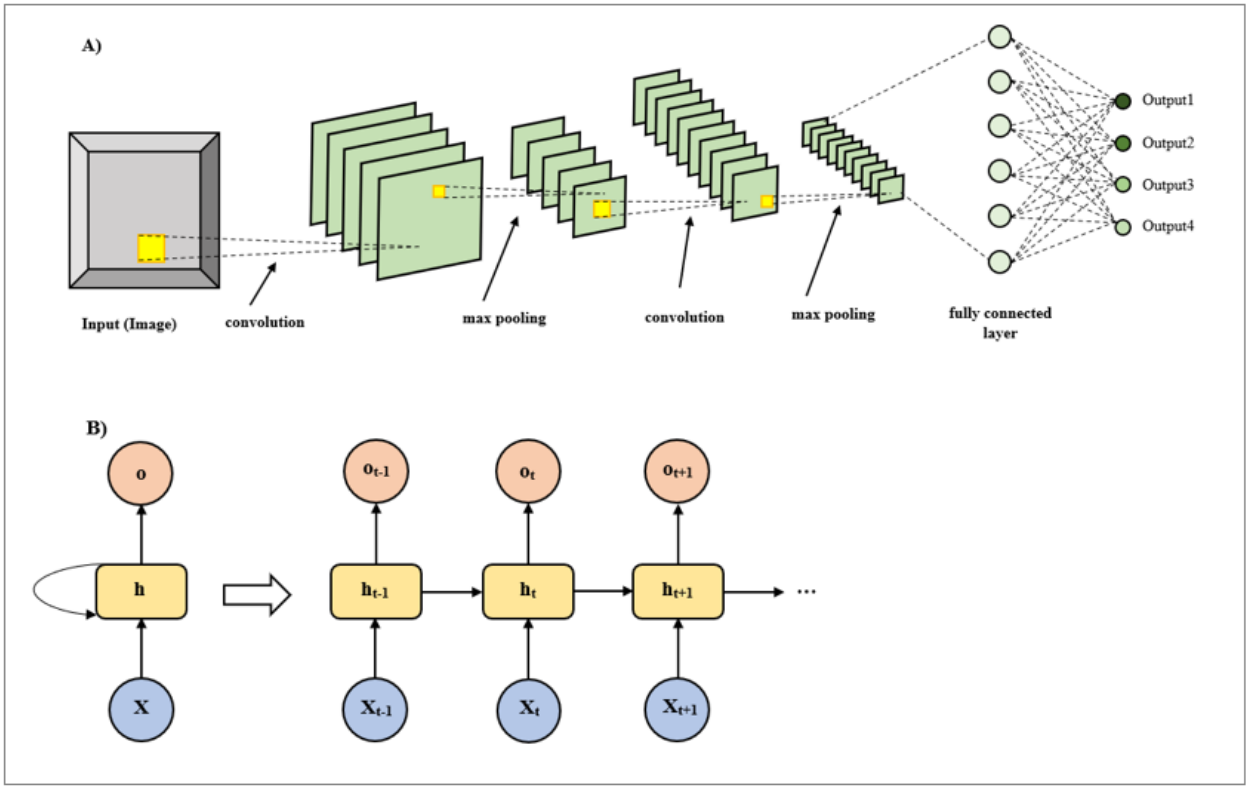


Figure 2.3. Illustration of the A) Convolutional Neural Network architecture and B) Recurrent Neural Network architecture.

## Graph Neural Networks

The first introduction of GNNs goes back to the study by (Gori, Monfardini and Scarselli, 2005) and (Scarselli et al., 2009) who generalized existing recursive neural networks to learn graph-structured data. Since that time, GNNs have attracted great attention in a large number of technological domains, including social networks (Zhang and Chen, 2018), chemical molecules networks (Duvenaud et al., 2015), drug interaction networks (Zitnik, Agrawal and Leskovec, 2018), and many other research areas (Bojchevski and Günnemann, 2017; Dai et al., 2017). Generally, GNNs utilize graph structure and node features to learn a representation vector of each node. Modern GNN architectures proceed with a neighborhood aggregation step in which the representation of each node has been constantly updated with the aggregating representations

of its neighbors. After h iterations of aggregation, the structural information for each graph node has been captured from h-hop network neighborhood.

The idea behind GNNs is to learn a mapping that represents graph nodes into low-dimensional vectors, so that provide geometric relationships in the embedding space to reflect the structure of the original graph (Hamilton, Ying and Leskovec, 2017b). The main contribution of GNN methods is to address the limitations of traditional approaches to learning on graphs in which fixed, and hand engineering parameters have been used, by employing methods to learn the embeddings that represent the desired graph structure. In this section, we will briefly review some basic concepts and the set of required definitions of graph theory that are used in this dissertation. Then, we will present the main variants of GNNs.

Theoretical Aspects of Graph Theory

We used the basic notions described in reference (Gross, Yellen and Anderson, 2018). A graph is defined as $G = (V, E)$ that consists of the set of nodes $\{v_1, v_2, \dots, v_n\}$ and set of edges that $e_{ij} = (v_i, v_j) \in E$ and $E \subseteq V \times V$. An edge e has two endpoints $v_i$ and $v_j$, that are said to be joined by e. In this case, these two nodes are adjacent. A graph can either be directed or undirected. With an undirected graph, edges have no orientation. In contrast to undirected graphs, directed graphs are the set of nodes connected by edges that have a direction associated with them. Furthermore, a graph is a weighted graph if weight is assigned to each edge. These weights quantify the degree of interaction between the nodes or the volume of exchange. Table 2.2 illustrates a list of notations used in this dissertation.

Table 2.2. Notations used in this dissertation

| Notations | Description |
|---|---|
| $\boldsymbol{N = 1, 2, \dots, n}$ | number of ROIs |
| $\boldsymbol{v_i}$ | node $i$ (ROI $i$) in the graph |
| $\boldsymbol{e_{ij}}$ | edge connecting node $v_i$ and $v_j$ |
| $\boldsymbol{V}$ | nodes set |
| $\boldsymbol{E}$ | edge set |
| $\boldsymbol{G}$ | graph, $G = (V, E)$ |
| $\boldsymbol{A}$ | adjacency matrix, $A = [e_{ij}] \in R^{N \times N}$ |
| $\boldsymbol{x_i}$ | node feature vector associated with $v_i$ |
| $\boldsymbol{d}$ | node feature dimension |
| $\boldsymbol{X}$ | node feature matrix, $X \in R^{V \times d}$ |
| $\boldsymbol{p}$ | edge feature dimension |
| $\boldsymbol{X^e}$ | edge feature matrix, $X^e \in R^{M \times p}$ |

**Definition 1 (Adjacency Matrix):** The adjacency matrix $A$ for a graph $G$ with $n$-nodes is an $n \times n$ matrix representation with $A_{ij} = 1$ if the direct connections exist between $v_i$ and $v_j$, and $A_{ij} = 0$ if no direct connection exist. If the graph is weighted, the entry of the adjacency matrix $A_{ij} > 0$ if $(v_i, v_j) \in E$ and $A_{ij} = 0$, otherwise.

**Definition 2 (Feature Matrix):** The node feature matrix $X \in R^{V \times d}$, where $V$ is the number of nodes in the graph and $d$ is the number of node features, is a matrix with $x_i \in R^d$ representing the $d$- dimensional feature vector of the node $v$. Similarly, the edge feature matrix $X^e \in R^{M \times p}$ is a matrix with $X^e_{v_i, v_j} \in R^P$ representing the $p$- dimensional feature vector of the edge $e_{ij}$.

**Definition 3 (Laplacian Matrix):** The Laplacian matrix (or graph Laplacian) $L \in R^{N \times N}$ is defined as $L = D - A$, where $D$ is the degree matrix, $D_{ij} = \sum_{j=1}^{n} A_{ij}$, and $A$ is the adjacency matrix of the unweighted graph. Similarly, for a weighted graph, $L = D - W$, where $W$ is a

weighted adjacent matrix. The Symmetric normalized Laplacian matrix can be defined as $L_{sym} = I - D^{-\frac{1}{2}}AD^{-\frac{1}{2}}$, where $I$ is the Identity matrix.

Graph Convolutional Networks

The structure of GCNs is inspired by the Convolutional Neural Networks (CNNs) to learn hierarchical representations of irregular data (i.e., graph and manifold). Despite increasing efforts to generalize the CNN models on graph-structured data, several challenges still exist to extract spectral-spatial features (Zhou et al., 2020; Zhang, Cui and Zhu, 2022). GCNs, however, can be categorized into two major algorithms as spectral GCNs (Kipf and Welling, 2016) and spatial GCNs (Simonovsky and Komodakis, 2017). Spectral GCNs implement convolutional operation on graph spectral domains based on the Fourier transform and graph Laplacian. Spatial GCNs, on the other hand, implement convolutional operations based on spatial relationships between nodes to aggregate neighborhood information for each node. In the following, we will represent an introduction to spectral- and spatial-based GCNs.

Spectral-Based GCN

Spectral GCNs use the Laplacian matrix to compute the eigen-decomposition of the graph Laplacian in the Fourier domain (see illustration in Figure 2.4.A). Let $\mathrm{L_{sym}}$ be the symmetric normalized Laplacian matrix of graph $\mathrm{G}$. $\mathrm{L_{sym}}$ can be decomposed into $\mathrm{L_{sym}} = \mathrm{U}\Lambda\mathrm{U^T}$, where $\mathrm{U} = (\mathrm{u_0}, \mathrm{u_1}, \dots, \mathrm{u_{n-1}}) \epsilon \mathrm{R^{n\times n}}$ is the eigenvector matrix, and $\Lambda$ is the diagonal matrix of eigenvalues, $\Lambda = \mathrm{diag}(\lambda_1, \lambda_2, \dots, \lambda_\mathrm{n})$. In graph signal processing, node features are mapped to feature vectors (i.e., $\mathrm{x_0}, \mathrm{x_1}, \dots \mathrm{x_{n-1}}$) which may be formed as a feature vector of all nodes of a graph, $\mathrm{X} \in \mathrm{R^n}$. The graph Fourier transform to a signal $\mathrm{X}$ is defined as $\widehat{\mathrm{X}} = \mathrm{U^T X}$, and the inverse

graph Fourier transform is defined as $X = U\widehat{X}$. The graph convolution operation of X in the Fourier domain is defined as follows:

$$X * g = U\Big((U^T g) \odot (U^T X)\Big) \tag{2.1}$$

where $*$ represents convolution operation, $\odot$ represents the pointwise product and $g \in R^N$ represents the learnable parameters of the graph convolutional kernel. By defining $g_\theta = \mathrm{diag}(U^T g)$ as a spectral filter in the spectral domain, the graph convolution operation can be simply defined as follows:

$$X * g_\theta = U g_\theta(\Lambda) U^T X \tag{2.2}$$

Equation (2) has been used for the first spectral network proposed (Bruna et al., 2013). However, this operation was computationally expensive because of multiplication eigenvector matrix U which is a full matrix with n Fourier functions. To avoid the quadratic complexity, (Defferrard, Bresson and Vandergheynst, 2016) proposed ChebNet model which avoids the eigen-decomposition by directly a learning function of the Laplacian. ChebNet model uses Chebyshev polynomials of the diagonal matrix of eigenvalues to estimate filter $g_\theta$ as shown below:

$$g_\theta = \sum_{i=0}^{K} \theta_i T_k(\widetilde{\Lambda}) \tag{2.3}$$

where $\widetilde{\Lambda} = 2\Lambda/\lambda_{max} - I_N$, and $\Lambda \in [-1,1]$. The model uses a Chebyshev polynomial for recursive calculation as $T_k(x) = 2xT_{k-1}(x) - T_{k-2}(x)$ with $T_0(x) = 1$ and $T_1(x) = x$. Therefore, the definition of the convolution of the graph signal x with a filter $g_\theta$ is as shown below:

$$X * g_\theta = U(\sum_{i=0}^{K} \theta_i T_i(\tilde{L}))U^T X \tag{2.4}$$

where $\tilde{L} = 2L_{sym}/\lambda_{max} - I_N$, and maps the eigenvalues from $[0, \lambda_{max}]$ to $[-1,1]$ (Yi Ma et al., 2019).

The filters defined by ChebNet are unstable for localizing frequency bands of interest, which are essentially the graph communities. To improve the above-mentioned ChebNet model and reduce the overfitting problem (Zhou et al., 2020), (Kipf and Welling, 2016) have proposed the CayleyNet model to capture narrow frequency band by using Cayley polynomials. ChebNet assumes a linear function with respect to $K = 1$ and $\lambda_{max} = 2$, which results in a simplification of Equation (4) as shown below:

$$X * g_\theta = f(\tilde{D}^{-\frac{1}{2}}\tilde{A}\tilde{D}^{-\frac{1}{2}}X\Theta) \tag{2.5}$$

where $\tilde{A} = I + A$, is an adjusted adjacency matrix A, $\tilde{D}_{ij} = \sum j\tilde{A}_{ij}$, f is the activation function, and $\Theta$ is a matrix of filter parameters. Spectral GCNs are powerful tools for graph-structured data. However, this method is difficult to calculate for a dense graph.

Spatial-Based GCN

Spatial GCNs define graph convolutions by aggregating the neighborhood's information based on the node's spatial relations. This process generally consists of aggregation and combine functions (Kim and Ye, 2020). Unlike the spectral GCNs, spatial-based methods update the representation for the central node with its neighbors' representations (see illustration in Figure 2.4.B). Diffusion convolutional neural network (DCNN) (Atwood and Towsley, 2015) regards a process of diffusion between nodes for graph convolutions, i.e., the information is transferred between nodes with a certain diffusion transition probability after random walking. Specially, the structure of the diffusion graph convolution is as follows:

$$H^{l+1} = f(\theta P^k H^l) \tag{2.6}$$

where $P^k$ is the transition probability of a length-k between two nodes (i.e., random walk) and $\theta$ is a learnable model parameter. DCNN describes the high-order information between nodes through a series of operations. As such, the computational complexity of the model for a large graph is $O(n^2K)$.

GraphSAGE (Hamilton, Ying and Leskovec, 2017a) solved this problem by proposing a batch-training algorithm for GCNs. Instead of applying all nodes during the training process of the embedding, GraphSAGE randomly samples the local neighboring nodes and aggregates their features to generate the embedding function for unseen data. The graph convolutions are as follows:

$$h_v^{(k)} = \sigma(W^k . f_K\left(h_v^{(k-1)}, \left\{h_u^{(k-1)}, \forall u \in S_{N_{(v)}}\right\}\right)) \tag{2.7}$$

where $f_k(.)$ is an aggregation function, and $S_{N_{(v)}}$ is a random sample of neighbors node v. GraphSAGE proposes three different aggregator functions: mean aggregator, LSTM-based aggregator, and max pooling aggregator. GraphSAGE with a mean aggregator takes the element-wise average values of the input nodes without the concatenation with the previous layers representation of the current node while the LSTM-based aggregator requires order invariant of the nodes. A max pooling aggregator is implemented as a trainable fully connected neural network which stands as the most general argument for the overall structure of the GraphSAGE algorithm (X. Bi et al., 2020).

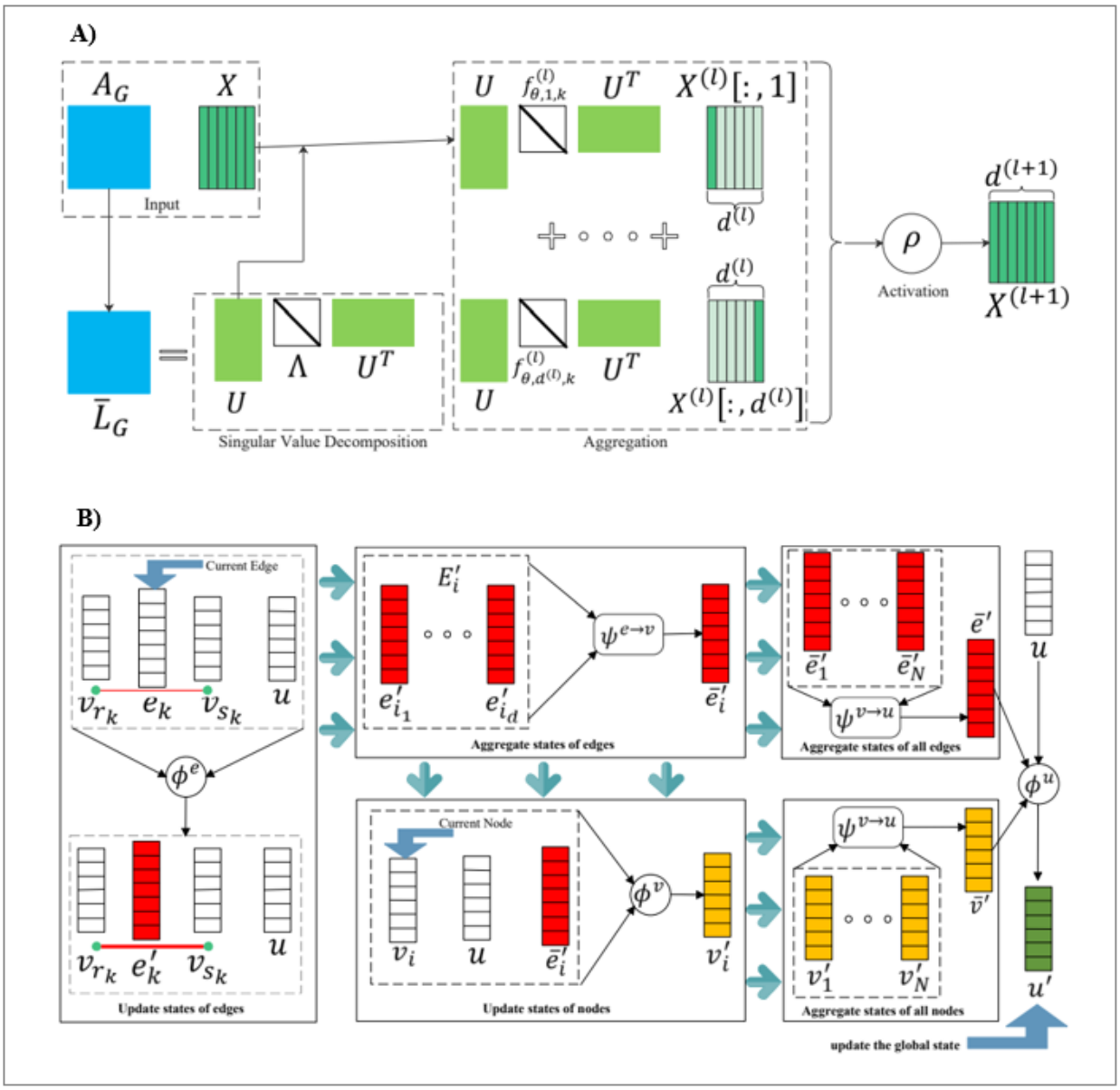


Figure 2.4. Graph Convolutional Network architecture. A) spectral-based GCN; convolutional operation is implemented based on the Fourier transform and graph Laplacian, B) spatial-based GCN; convolutional operation is implemented based on spatial relationships between nodes to aggregate neighborhood information for each node. Images adapted from (Zhou et al., 2022)

Graph Isomorphism Network (GIN) (Xu et al., 2018) proposes a generalization of GraphSAGE and GCNs frameworks by adapting the aggregation and update functions that make discriminative and representational power of GIN equivalent to the Weisfeiler-Lehman test

(Weisfeiler et al., no date). GIN considers the node features and implements the aggregate and combine functions as the sum of them:

$$h_v^{(k)} = \mathrm{MLP}^{(k)}\left(\left(1+\epsilon^{(k)}\right).h_v^{(k-1)} + \sum_{u\in\mathcal{N}(v)} h_u^{(k-1)}\right) \tag{2.8}$$

where $h_v^{(k)}$ is the k-th layer feature vector at the v-th node, $\epsilon^{(k)}$ is a learnable parameter, and MLP is a multi-layer perceptron with non-linearity. Hence, the proposed architecture achieves maximum discriminative power for classification tasks (Schweitzer PASCAL et al., 2011; Xu et al., 2018).

Graph Attention Networks

The graph attention network (GAT) (Veličković et al., 2017) adopts attention mechanisms to learn the attention coefficient between two connected nodes. The attention coefficient denotes how important node j are for node i and is defined as $e_{ij} = a(Wh_i, Wh_j)$, where $h_i, h_j$ are node feature vectors that are multiplied with the weight matrix, W, and a is an attention mechanism that is adapted to learn the relative weights between two connected nodes and return the attention coefficient. The normalized attention coefficient is represented by $\propto_{ij}$ and can be defined by using softmax function as

$$\propto_{ij} = \mathrm{softmax}_j\left(e_{ij}\right) = \frac{\exp\left(a\left(Wh_i, Wh_j\right)\right)}{\sum_{k\in\mathcal{N}_i}\exp\left(a(Wh_i, Wh_k)\right)} \tag{2.9}$$

Similarly, the full attention coefficient between the node i and its neighbor j is defined as:

$$\propto_{ij} = \frac{\exp\left(\mathrm{LeakyReLU}(a^T\left[Wh_i||Wh_j\right])\right)}{\sum_{k\in\mathcal{N}_i}\exp\left(\mathrm{LeakyReLU}\left(Wh_i||Wh_k\right)\right)} \tag{2.10}$$

where || denotes the concatenation operation. The output representations of each node according to GAT are calculated by the following equation:

$$h_i' = \sigma(\sum_{j \in \mathcal{N}_i} \alpha_{ij} W h_j) \tag{2.11}$$

Additionally, GAT performs the multiple attention heads that applies K independent attention mechanisms to increase the stability of the learning process as below:

$$h_i' = \sigma(\frac{1}{K}\sum_{k=1}^{K} \sum_{j \in \mathcal{N}_i} \alpha_{ij}^k W^k h_j) \tag{2.12}$$

GAT performs computing operations of the node-neighbor pairs in parallel, resulting in computational efficiency, and is helpful for inductive learning to generalize the training process to unseen nodes and graphs (Zhou et al., 2020).

Graph Recurrent Networks

Graph Recurrent Networks (GRNs) as the particular cases of Recurrent Neural Networks (RNNs), capture a sequential representation of a given graph and can be designed for classification tasks in both graph-level and node-level. The assumption of these models is to information/messages exchange between nodes until a stable equilibrium is reached. The termed recurrent in RNNs refers to the dependency between the output of the prior element and the current inputs within the sequence (Saeidi et al., 2021). Similarly, GRNs reduce the limitation of solving long-term dependencies between graph-structured data in GNNs by extending gate mechanisms from RNNs (Li et al., 2015) such as LSTM (Hochreiter and Schmidhuber, 1997) and GRU (Cho et al., 2014).

LSTM-Based Approach

(Hochreiter and Schmidhuber, 1997) proposed the LSTM model to reduce the impact of the vanishing gradients problem by employing an internal memory. The basic architecture of LSTM includes an input gate, memory unit, output gate, and hidden state (Tai, Socher and Manning, 2015), and can be described as below:

$$\begin{gathered} f_t = \sigma_F(W_f x_t + U_f h_{t-1} + b_f), \\ i_t = \sigma_I(W_i x_t + U_i h_{t-1} + b_i), \\ o_t = \sigma_O(W_o x_t + U_o h_{t-1} + b_o), \\ \tilde{c}_t = \tanh(W_c x_t + U_c h_{t-1} + b_c), \\ c_t = f_c \odot c_{t-1} + i_t \odot \tilde{c}_{t-1}, \\ h_t = o_t \odot \tanh(c_t) \end{gathered} \tag{2.13}$$

where $x_t$ is the input data at time step $t$; $\sigma_F(\cdot)$ is the activation function of the forget gate; $\sigma_I(\cdot)$ is the activation function of the input gate; $\sigma_O(\cdot)$ is the activation function of the output gate; $W_f$ and $U_f$ are the weights of the forget gate; $W_i$ and $U_i$ are the weights of the input gate; $W_o$ and $U_o$ are the weights of the output gate; $W_c$ and $U_c$ are the weights of the LSTM; $b_f$ is the bias vector of the forget gate; $b_i$ is the bias vector of the input gate; $b_o$ is the bias vector of the output gate; $b_c$ is the bias vector of the LSTM; $h_t$ is the hidden state at time step $t$; and $\odot$ denotes the element-wise product.

GRU-Based Approach

GRU is another common gated architecture for graph-structure data that calculate the gradients by back-propagating timestep and has fewer parameters than LSTM (Li et al., 2015). In this approach, the given node aggregates messages from its neighbors. Then the hidden state of each node is updated by its previous hidden states and its neighboring hidden states (Zhou et al., 2020). The GRU-based approach propagation formula is as follows:

$$
\begin{aligned}
r_t &= \sigma_R(W_r x_t + U_r h_{t-1} + b_r), \\
z_t &= \sigma_Z(W_z x_t + U_z h_{t-1} + b_z), \\
\tilde{h}_t &= \tanh(W_h x_t + U_h(r_t \odot h_{t-1}) + b_h), \\
h_t &= (1 - z_t) \odot h_{t-1} + z_t \odot \tilde{h}_t
\end{aligned}
\tag{2.14}
$$

where $x_t$ is the input data at time step t; $\sigma_R(\cdot)$ is the activation function of the reset gate; $\sigma_Z(\cdot)$ is the activation function of the update gate; $W_r$ and $U_r$ are the weights of the reset gate; $W_z$ and $U_z$ are the weights of the update gate; $W_h$ and $U_h$ are the weights of the gated GNNs at time step t; and $r_t, z_t, \tilde{h}_t, h_t$ denotes the reset gate, update gate, candidate activation, and hidden state respectively. The advantage of GRU over the LSTM is the speed of convergence and less complexity than LSTM.

Spatial-Temporal Graph Neural Networks

Conceptually, spatial-temporal graph neural networks (STGNNs) are the type of graphs in that graph structure is dynamic and feature information keeps changing over time. Specifically, STGNNs simultaneously model spatial and temporal dependencies to predict values and perform graph node classification. For example, a human brain connectome can be represented as a spatio-temporal graph, where the temporal graph represents the dynamics of brain activity in each region of interest and the spatial graph represents the dynamic properties of the functional interaction between different brain regions (Azevedo, Passamonti, Liò, et al., 2020; Kim, Ye and Kim, 2021).

Existing STGNNs can be divided into RNN-based approaches and CNN-based approaches. RNN-based approaches take into consideration spatial-temporal dependencies by filtering both input data and hidden states passed to recurrent units using convolutional operations on graphs

(Seo et al., 2018). According to this, suppose that hidden states of RNNs at time step $t$ is defined as:

$$H_{RNN}^{t} = \sigma(W_{RNN}^{t} X_{RNN}^{t} + U_{RNN}^{t} H_{RNN}^{t-1} + b_{RNN}^{t}) \quad (2.15)$$

where $W_{RNN}^{t}$ and $U_{RNN}^{t}$ are the weights of RNNs; $b_{RNN}^{t}$ is the bias vector; $X_{RNN}^{t}$ is the node feature matrix at time step $t$; and $\sigma(\cdot)$ is the activation function. Adding graph convolutional operations to $(15)$, the hidden states of RNN-based models become:

$$H_{RG}^{t} = \sigma(\mathrm{Gconv}(X_{RNN}^{t}, A; W_{RNN}^{t}) + \mathrm{Gconv}(H^{t-1}, A; U_{RNN}^{t}) + b_{RNN}^{t}) \quad (2.16)$$

Where $\mathrm{Gconv}(\cdot)$ is a graph convolutional layer; and $A$ is the adjacency matrix (Z. Wu et al., 2021).

Furthermore, edge-level RNNs and node-level RNNs have been used in (Y. Bi et al., 2020) to deal with various aspects of the temporal information of nodes. For example, (Jain et al., 2015) proposed the edge-level RNN and the node-level RNN to capture temporal features and classify labels of nodes at each time step. To do that, the temporal information of edges and nodes is passed through the edge-level RNN and node-level RNN respectively. Then, to merge spatial information, the inputs of the node-level RNN use the outputs of edge-level RNN (Z. Wu et al., 2021).

The RNN-based approaches have a deficiency in iterative propagation and have gradient vanishing problems. To overcome the mentioned deficiencies of existing RNN-based models, CNN-based approaches have been introduced to handle the temporal-spatial graphs issues in a non-recursive manner. This solver uses parallel computing, stable gradient, and low memory requirement (Y. Zhang et al., 2020). For example, a 1-D convolutional layer is used to create a

temporal-spatial block and generate the final prediction in (Azevedo, Passamonti, Lio, et al., 2020).

## Computational methods for fMRI data analysis

Over the past several decades, a variety of computational methods have been proposed to analyze fMRI time-series data, such as the generalized linear model (GLM) (Friston *et al.*, 1994; Barch *et al.*, 2013), sparse dictionary learning (Hu *et al.*, 2015; Lv *et al.*, 2017; W. Zhang *et al.*, 2019), and blind source separation techniques including independent component analysis (Calhoun *et al.*, 2001; Beckmann *et al.*, 2005; Calhoun, Liu and Adali, 2009; Calhoun and Adali, 2012) and tensor decomposition (Sen and Parhi, 2017, 2019b). For example, an analysis by Tavor et al. (Tavor *et al.*, 2016) has confirmed that GLM analysis can provide trustworthy results for fMRI data analysis to predict tasks by showing interparticipant variability in task activation. However, these methods are fundamentally limited because they cannot address the needs of modeling the hierarchical structures of task fMRI functional connectivity (Ferrarini *et al.*, 2009; Meunier *et al.*, 2009): they only build shallow models that overlook all information in the task fMRI data (Huang, Hu, Zhao, *et al.*, 2018).

Deep learning (DL) based methods can achieve satisfactory classification performance, in contrast to traditional machine learning algorithms. In DL methods, rather than using manual features, which are usually based on expert domain knowledge and heuristics (Xu, 2021), high-level complex features can be automatically extracted from the original fMRI data, thus providing meaningful information to improve the performance of classification models. For example, Huang et al. (Huang, Xiao and Wu, 2021) have proposed a deep neural network framework, consisting of both convolutional and recurrent layers, that automatically extracts

spatial and temporal features of fMRI data. In the past several years, a growing body of literature has applied DL algorithms to decoding fMRI data. Among those DL models, convolution autoencoder (Huang, Hu, Dong, *et al.*, 2018; Huang, Hu, Zhao, *et al.*, 2018; Wang *et al.*, 2020; Zhao *et al.*, 2020), recurrent autoencoder (Wang *et al.*, 2019; Q. Li *et al.*, 2021), and deep belief networks (Jang *et al.*, no date; Hjelm *et al.*, 2014; Dong *et al.*, 2020) have shown a superior ability to decode fMRI data. Huang et al. have developed a deep convolutional autoencoder to model fMRI data (Huang, Hu, Dong, *et al.*, 2018; Huang, Hu, Zhao, *et al.*, 2018); Zhao et al. have used a spatio-temporal convolutional neural network to obtain both spatial and temporal features of functional networks (Zhao *et al.*, 2020); Wang et al. have applied a deep sparse recurrent neural network on task fMRI data that has shown promising performance in extracting the temporal dependencies of input fMRI volumes (Wang *et al.*, 2019); and a deep belief network with a restricted Boltzmann machine (Hjelm *et al.*, 2014) has been used to identify networks in fMRI data. Similarly, Jang et al. have applied the same deep belief network algorithm as that in reference (Hjelm *et al.*, 2014) to initialize the weights of fully connected deep neural networks (Jang *et al.*, no date). Despite the advances made by these methods, the proposed DL algorithms have been limited in neuroimaging data applications, because the complex interactions within brain regions cannot be naturally encoded in deep features by deep neural network algorithms, particularly when the data have high dimensionality and are generated from non-Euclidean domains (Z. Wu *et al.*, 2021).

## Review of Literature in fMRI data analysis with Graph Neural Networks

### Search Strategy

The comprehensive literature searches were performed within databases based on a search strategy using the following databases and search engines such as Science Direct, arXiv, IEEE Xplore, and PubMed. To meet the eligibility criteria for defining search space, the combinations of keywords in the title, keywords or abstract were applied, with no restrictions on publication date, as follows: ("graph neural networks" OR "GNNs" OR "graph convolutional networks" OR "GCNs" OR "graph recurrent networks" OR "GRNs" OR "graph attention networks" OR "GATs" OR "geometric deep learning") AND ("graph topology" OR "brain connectome") AND ("fMRI" OR "functional MRI" OR "functional magnetic resonance imaging"). These keywords resulted in identifying relevant studies and keeping focused on publications addressing the research questions. All titles and abstracts of the selected articles were reviewed, and the full text review of the remaining articles were independently performed by two authors (MS and WK) for inclusion and exclusion criteria.

### Criteria for Identification of Studies

The following criteria were applied to exclude unqualified published original articles and limit the final selection of studies: (a) be included fMRI data only, studies with fMRI analysis combined with physiological recordings (e.g., EEG, MEG, etc.) were excluded; (b) be written in English; (c) be applied to the human brain network, this review focused solely on a graph representation of the human brain connectome. Other exclusion criteria set applied during the screening process were: (a) studies not in a peer-reviewed journal; (b) published abstracts, book chapters, and dissertations; (c) studies that were irrelevant to the research questions. According

to the aforementioned inclusion and exclusion criteria, the relevant studies were selected to further investigation through the four stages featured in the PRISMA guidelines process (Moher *et al.*, 2009).

## Synthesis of Results

Figure 2.5 indicates PRISMA guidelines of the study selection process (Moher *et al.*, 2009). According to this flow diagram, at the first step, we obtained 123 articles after the removal of duplicates. Next, we applied a formal abstract screening process to determine relevant scientific articles based on our inclusion criteria. A total of 71 articles remained after this stage. The full text of these 71 articles was reviewed, resulting in 39 relevant articles that met all the aforementioned criteria.

Our extensive literature investigation indicates that the application of GNNs to process fMRI data has been rapidly developed in the last three years, and the number of publications in this field has shown significant growth. Based on various tasks, the existing application of GNNs in fMRI data analysis can be organized into three main topics: neurological and psychiatric disease prediction, gender classification, and brain response cognitive stimuli. Note that the application of GNNs in fMRI data analysis is relatively limited. A summary of existing applications of GNNs in fMRI data analysis is presented in Table 2.3.

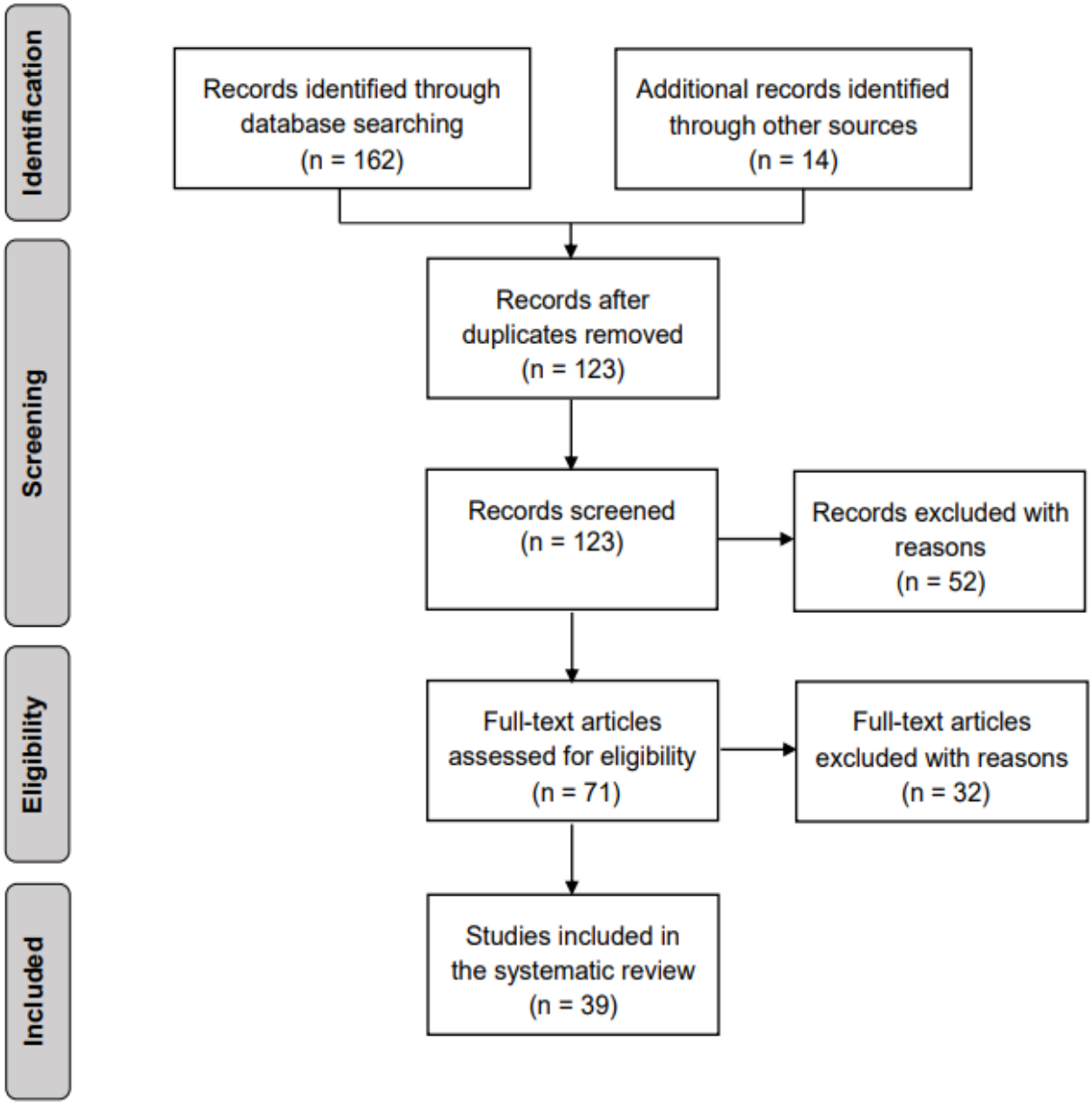


Figure 2.5. Flow diagram based on the PRISMA guideline (Moher et al., 2009), including identification, screening, eligibility, and inclusion stages.

Table 2.3. Existing applications of GNNs in fMRI data analysis. Abbreviation: GNN, graph neural network; GCN, graph convolutional network; GIN, graph isomorphism network; SGC, simple graph convolution; EV-GCN, edge-variational GCN; Hi-GCN, hierarchical GCN; GAT, graph attention network; GCRNN, graph convolutional recurrent neural network; GNEA, GNN with extreme learning machine aggregator; ST-GCN, spatio-temporal GCN; STAGIN, spatio-temporal attention GIN.

| Article | Year | Algorithm | Database | Highlights |
|---|---|---|---|---|
| (Parisot *et al.*, 2017) | 2017 | Spectral-based GCN | ABIDE (Di Martino *et al.*, 2013) | One of the pioneers of GCN for group-level disease prediction applications. |
| (Ktena *et al.*, 2017) | 2017 | Spectral-based GCN | ABIDE | Siamese GCN has been applied to learn the similarity between a pair of graphs. |
| (Ktena *et al.*, 2018) | 2018 | Spectral-based GCN | ABIDE | Siamese GCN has been applied to learn the similarity between a pair of graphs. |
| (Parisot *et al.*, 2018) | 2018 | Spectral-based GCN | ABIDE | An extension of their previous study on GCN model that considered characteristics and features of nodes as well as interactions between them. |
| (X. Li *et al.*, 2019) | 2019 | GIN | Yale Child Study Center (X. Li *et al.*, 2019) | Feature importance scores are identified for the GNN model by applying an extensive comparison between the proposed GNN and random forest. |
| (Rakhimberdina and Murata, 2020) | 2019 | SGC | ABIDE | The complexity of the GCN model is reduced by removing nonlinearities between consecutive layers. |
| (Kazi, Shekarforoush, *et al.*, 2019) | 2019 | Inception GCN | ABIDE | Inception modules with different kernel sizes are considered in each layer, then the output of each layer is used in the aggregator function. |

| Article | Year | Algorithm | Database | Highlights |
|---|---|---|---|---|
| (Yao *et al.*, 2019) | 2019 | Multi-scale triplet GCN | ABIDE | Multiple templates are applied for coarse-to-fine brain parcellation to create functional connectivity graphs. Then, a triplet GCN model is used to learn each graph obtained from functional connectivity networks. |
| (Anirudh and Thiagarajan, 2019) | 2019 | Spectral-based GCN | ABIDE | A bootstrapped version of GCN is used to reduce the sensitivity of the initial graph construction phase. The proposed model is trained by multiple random graphs from the initial graph. |
| (Felouat and Oukid-Khouas, 2020) | 2020 | Spectral-based GCN | ABIDE | Complex network measures and GCN structure are used with a large multi-site dataset. |
| (Li, Dvornek, et al., 2020) | 2020 | Graph Embedding Learning | Yale Child Study Center | Improving the graph classification task by adding an extra loss including mutual information loss to regularize the embedding of noisy fMRI. |
| (Huang and Chung, 2020) | 2020 | EV-GCN | ABIDE | Monte-Carlo edge dropout improves the learning process of multi-modal data to approximate the uncertainty of the graph topology. |
| (H. Jiang *et al.*, 2020) | 2020 | Hi-GCN | ABIDE | Hierarchical GCN framework is used for graph embedding resulting in better training and convergence performances in the brain network. |

| Article | Year | Algorithm | Database | Highlights |
|---|---|---|---|---|
| (Li, Zhou, et al., 2020) | 2020 | GAT | ACD Biopoint task (Kaiser *et al.*, 2010) | Pooling Regularized-GNN framework with a new loss term for the biomarker analysis in both the individual and population levels. |
| (X. Li *et al.*, 2021) | 2021 | GAT | Biopoint (Venkataraman *et al.*, 2016) | The proposed BrainGNN framework contains a pooling layer and a regularization loss term to modify the distribution of the node pooling scores. |
| (Rakhimberdina and Murata, 2020) | 2019 | SGC | COBRE | The complexity of the GCN model is reduced by removing nonlinearities between consecutive layers. |
| (Mahmood et al., 2021) | 2021 | Gated GNN | FBIRN (Keator *et al.*, 2016) | Novel attention based GNN to capture the functional connectivity matrices resulted in improving the model interpretability. |
| (Rakhimberdina and Murata, 2020) | 2019 | SGC | ADHD-200 (Bellec *et al.*, 2017) | The complexity of the GCN model is reduced by removing nonlinearities between consecutive layers. |
| (Yao et al., 2019) | 2019 | Multi-scale triplet GCN | ADHD-200 | Multiple templates are applied for coarse-to-fine brain parcellation to create functional connectivity graphs. Then, a triplet GCN model is used to learn each graph obtained from functional connectivity networks. |
| (Saboksayr, Foxe and Wismüller, 2020) | 2020 | Spectral-based GCN | ADHD-200 | Successfully applied GCN model in the identifications of ADHD from subjects. |

| Article | Year | Algorithm | Database | Highlights |
|---|---|---|---|---|
| (Yao et al., 2021) | 2021 | Mutual multi-scale triplet GCN | ADHD-200 | A triplet GCN framework is employed to learn the representation of each functional connectivity network. |
| (Parisot et al., 2017) | 2017 | Spectral-based GCN | ADNI2 (Beckett *et al.*, 2015) | One of the pioneers of GCN for group-level disease prediction applications. |
| (Parisot et al., 2018) | 2018 | Spectral-based GCN | ADNI (Petersen *et al.*, 2010) | An extension of their previous study on the GCN model that considered characteristics and features of nodes as well as interactions between them. |
| (Banka and Rekik, 2019) | 2019 | GCN | ADNI | Adversarial Connectome Embedding architecture is proposed with graph convolutional layers. The proposed framework uses GCN for the encoding network operations. |
| (Kazi, Krishna, et al., 2019) | 2019 | Multi-GCN | TADPOLE (Marinescu *et al.*, 2018) | An automatic learning layer for weights elements of the demographic data increases the performance of the model. |
| (L. Zhang *et al.*, 2019) | 2019 | GCRNN | ADNI | An RNN framework captured the temporal features of functional brain activity along with a GCN to model spatial and temporal characteristics of MRI data. |
| (Yu et al., 2019) | 2019 | Multi-Scale GCN | ADNI | A GCN model with a combination of neuroimaging and demographic information. |

| Article | Year | Algorithm | Database | Highlights |
|---|---|---|---|---|
| (Kazi, Shekarforoush, et al., 2019) | 2019 | Inception GCN | TADPOLE | Inception modules with different kernel sizes are considered in each layer, then the output of each layer is used in the aggregator function. |
| (Park and Friston, 2013) | 2019 | Spectral-based GCN | ADNI2 | A combination of GCN architecture with a long-short term memory network is shown to reinforce the performance of classification tasks. |
| (J. Liu et al., 2020) | 2020 | Spectral-based GCN | ADNI | A new recognition framework based on multimodal data is proposed to improve the efficiency of the feature selection process. |
| (Huang and Chung, 2020) | 2020 | EV-GCN | ADNI/TADPOLE | Monte-Carlo edge dropout improves the learning process of multi-modal data to approximate the uncertainty of the graph topology. |
| (An et al., 2020) | 2020 | Spectral-based GCN | Private dataset from Xuanwu Hospital, China | Compering the combination of three types of features with a GCN framework. The proposed framework uses dynamic functional connectivity to consider changes in the brain over time. |
| (Cosmo et al., 2020) | 2020 | Spatial-based GCNs | TADPOLE | The complexity of the model is reduced by proposing a single graph learning method. |

| Article | Year | Algorithm | Database | Highlights |
|---|---|---|---|---|
| (S. Yu et al., 2020) | 2020 | Multi-Scale Enhanced GCN | ADNI | Automatically extracting the topological information of brain networks through the local weighted clustering coefficients resulted in significantly improving the performance of the model. |
| (X. Bi et al., 2020) | 2020 | GNEA | ADNI | The aggregator based on an extreme learning machine can boost learning performance in brain network classification tasks. |
| (H. Jiang *et al.*, 2020) | 2020 | Hi-GCN | ADNI | Hierarchical GCN framework is used for graph embedding resulting in better training and convergence performances in the brain network. |
| (Xing et al., 2021) | 2021 | Spectral-based GCN | ADNI2 | Dynamic functional connectivity with sliding windows is computed as input for the GCN model along with two subnetworks for assistance to improve disease prediction tasks. |
| (Yao et al., 2021) | 2021 | Mutual multi-scale triplet GCN | ADNI | A triplet GCN framework is employed to learn the representation of each functional connectivity network. |
| (Zhang and Huang, 2019) | 2019 | Spectral-based GCN | HCP S1200 (Van Essen *et al.*, 2013) | Leveraging the brain graph embedding using GCN. |

| Article | Year | Algorithm | Database | Highlights |
|---|---|---|---|---|
| (Yao et al., 2020) | 2020 | Temporal-adaptive GCN | MDD (Yan *et al.*, 2019) | An adaptive GCN has been used to extract topological features from brain regions. In addition, to consider brain status changes, temporal changes for each ROI are modeled. |
| (Arslan et al., 2018) | 2018 | Spectral-based GCN | UK Biobank (Sudlow *et al.*, 2015) | Spectral convolutional network classifier is used for ROI identification task based on network functional connectivity in males and females. |
| (Ktena et al., 2017) | 2018 | Spectral-based GCN | UK Biobank | Siamese GCN has been applied to learn the similarity between a pair of graphs. |
| (Kim and Ye, 2020) | 2020 | GIN | HCP S1200 | GIN-based analysis method can be used for improving the performance of GNN architecture for graph classification. |
| (Gadgil et al., 2020) | 2020 | ST-GCN | HCP S1200 | ST-GCN has been used to extract temporal dynamic information and functional connectivity between brain regions resulting in improving the performance and interpretability of the model. |
| (Azevedo, Passamonti, Lio, et al., 2020) | 2020 | ST-GCN | HCP S1200 | Spatial and temporal information has been used in a GNN model, followed by linear transformations to generate the final gender classification. |

| Article | Year | Algorithm | Database | Highlights |
|---|---|---|---|---|
| (W. Zhang et al., 2020) | 2020 | GAT | HCP S1200 | A graph autoencoder framework has been applied to fuse multimodal brain networks. The proposed framework is based on a multi-stage graph convolution kernel. |
| (Filip et al., 2020) | 2020 | GAT | HCP S1200 | The aggregation strategies for the GAT architecture is developed to classify the entire graph. |
| (Kim, Ye and Kim, 2021) | 2021 | STAGIN | HCP S1200 | A spatio-temporal attention graph is used to obtain dynamic graph representation. |
| (X. Li *et al.*, 2021) | 2021 | GAT | HCP S1200 | The proposed BrainGNN framework contains a pooling layer and a regularization loss term to modify the distribution of the node pooling scores. |
| (Zhang et al., 2021) | 2021 | Spectral-based GCN | HCP S1200 | The performance of brain decoding has been improved by using an automated learning tool to interpret human brain activity within a short time window. |
| (Kim, Ye and Kim, 2021) | 2021 | STAGIN | HCP S1200 | A spatio-temporal attention graph is used to obtain dynamic graph representation. |

## Application of Graph Neural Network in fMRI data analysis

Deeper discussions about the existing applications of GNNs in neurological and psychiatric disease, gender classification, and brain response cognitive stimuli are provided in three separate subsections. Note that, due to the novelty of the domain, the applications of GNNs in fMRI data analysis are relatively limited. In this section, further explanations of the contents of the articles reviewed and the proposed GNN frameworks are provided in more detail.

### Application of GNNs in Neurological and Psychiatric Disease

Diagnosing neurological disorders is challenging due to the uncertainty of medical assessment to identify the symptoms (Ecker, Spooren and Murphy, 2012; Mastrovito, Hanson and Hanson, 2018). Significant progress has been made using rs-fMRI and task fMRI to characterize the functional architecture of the brain to analyse network properties and metrics extracted from brain topology (Bassett and Bullmore, 2009; Wang, Zuo and He, 2010; Stam, 2014; Zhou et al., 2017). Recently, the advances in GNNs to arbitrarily fMRI and non-imaging data, make these architectures a promising solution to the disease classification (X. Li et al., 2019). The node classification problems that GNNs solve can be broadly classified into two categories: graph-based and population-based models. Graph-based models use a brain graph where nodes denote brain Regions of Interest (ROIs), and edges represent the functional correlations of the sets of brain nodes. In contrast, population-based models consider a graph of subjects where nodes correspond to specific subjects with their own brain connectivity data, and edges denote similarity between subjects' non-imaging information such as age, gender, and handedness. In the following, studies that have applied GNNs models to classify common neurological disorders, including autism spectrum disorder (ASD), Schizophrenia (SZ), Alzheimer's disease

(AD), and attention-deficit/hyperactivity disorder (ADHD) are discussed. However, other psychiatric research was found in the study selection process, predicting clinical depression scores and comprising major depression (Zhang and Huang, 2019; Yao et al., 2020) that make a negligible contribution to this systematic review.

### Autism Spectrum Disorder

ASD is a neurodevelopmental disability that can cause difficulties in social, communication, and behavior (Roux et al., 2012). ASD disrupts the functional network organization of the brain so many studies attempt to investigate how this network changes by using functional connectivity analysis and graph analysis (Zeng et al., 2017; Farahani, Karwowski and Lighthall, 2019). As pioneering works for brain analysis, Parisot et al. (Parisot et al., 2017, 2018) applied GCNs in a population graph with both imaging and non-imaging information. The population was represented as a sparse graph where the imaging feature vector was used as the feature representation of the node, and their edges were associated with phenotypic information. Further, in two rs-fMRI studies using spectral-based GCN, Ktena et al. proposed a Siamese GCN model to learn a graph similarity metric in the spectral domain in a supervised setting (Ktena et al., 2017, 2018). They evaluated their model with individual graphs constructed to identify ASD patients from HC and the results showed an improvement in the classification accuracy compared to the previous works. The other type of spectral-based GCN model was proposed by Felouat and Oukid-khouas (Felouat and Oukid-Khouas, 2020) in which the voting classifier integrated multi-classifiers into a single model based on the majority voting (Al-Shboul et al., 2016). However, the proposed GCN models used a special template to construct the functional connectivity network. Such restriction of using the single spatial scale for brain regions of interest (ROIs) has been addressed by (Yao et al., 2019) by proposing a multi-scale triplet GCN

framework in which functional connectivity for each subject has been generated by using multi-scale templates for coarse-to-fine ROIs parcellation, followed by a triplet GCN model to learn graph representations of brain functional connectivity networks.

Apart from the mentioned limitation of spectral-based GCN, applying all nodes of the graph during training is the other restriction in most spectral-based GCN models which may result in poor performance on unseen nodes. To deal with this restriction, Li et al. (X. Li et al., 2019) proposed a two-stage pipeline to identify ASD brain biomarkers from task-fMRI. Unlike spectral-based GCN models, the proposed GCN algorithm is a graph isomorphism network (GIN) (Xu et al., 2018) which divides the whole graph structure into some equivalence sub-graphs with different nodes and edges. The aim of the proposed model is to update the feature vector of each node by recursively aggregating representations of its neighborhood. Further improvement of these authors presented in (Li, Zhou, *et al.*, 2020; X. Li *et al.*, 2021) by proposing a GAT architecture and a pooling regularized GNN model, respectively. Due to the low signal-to-noise ratio and high dimensionality of fMRI data, embedding node representations for classifying ASD and HC groups arises a limitation for graph-based classification. Li et al. (Li, Dvornek, et al., 2020) dealt with this challenge by using the Infomax graph embedding with Infomax loss which improved node representation. This novelty led to learning a better graph embedding and improving the classification of ASD or HC in a group of children collected at Yale Child Study Center (X. Li et al., 2019).

(Rakhimberdina and Murata, 2020) proposed a simple graph convolution (SGC) (Wu et al., no date) by removing nonlinearities between layers, and aggregating weight matrices of each layer into a single matrix. Based on the reported results, the proposed SGC-based model showed a high classification performance and efficiency over GCN based model for ASD classification in

the ABIDE (Di Martino et al., 2013) dataset. However, these GCN models have some inherent limitations in extracting sufficient features. Kazi et al. (Kazi, Shekarforoush, et al., 2019) addressed this limitation by introducing the Inception GCN model as a spectral domain architecture for deep learning on non-Euclidean space. In the proposed model, multiple kernel sizes have been employed across graph convolution layers to leverage spectral convolutions. Thereby, the Inception GCN improved the performance of node classification by using a population graph. In addition, (Huang and Chung, 2020) proposed the Edge-Variational GCN (EV-GCN) to reduce the uncertainty estimation associated with disease prediction.

In addition to the various above extensions, (Anirudh and Thiagarajan, 2019) proposed a bootstrapped approach to the GCN model to reduce the sensitivity of GCN models to the choice of the population graph. The bootstrapped GCN generated randomized graphs from the initial population graph to train the set of weak GCN for ASD and HC classification, and integrate their prediction as to the final result which achieved better classification accuracy than the similar work done in reference (Parisot et al., 2017). Hierarchical GCN (Hi-GCN) (H. Jiang *et al.*, 2020) is another spectral approach targeting the classification task. (H. Jiang *et al.*, 2020) proposed Hi-GCN to learn the graph feature embedding to a low-dimensional vector. The Hi-GCN framework consists of two independent GCNs: f-GCN and p-GCN which preserve the topology information in the population network and subject's association brain function network, respectively. The model has been used to extract features of the brain, resulting in better classification of ASD vs AD from the ABIDE dataset in comparison to Eigenpooling GCN (Yao Ma et al., 2019) and population GCN (Parisot et al., 2017).

### Schizophrenia

Schizophrenia (SZ) is a mental disease with brain dysconnectivity (Schmitt et al., 2011) with behavioral symptoms such as disorganized speech and decreased participation in daily activities. fMRI studies in patients with SZ have revealed local abnormalities in brain activity resulting in disrupted functional connectivity networks (S. Li et al., 2019). (Mahmood et al., 2021) proposed the BrainGNN framework consisting of a CNN encoder, a self-attention model, and a gated recurrent unit (GRU) network. The performance of the proposed framework was tested on the data repository from Function Biomedical Informatics Research Network (FBIRN) (Keator et al., 2016) and showed the state-of-the-art performance for the classification of SZ patients and healthy controls (HC) task. Further, (Rakhimberdina and Murata, 2020) also implemented a SGC model for SZ detection with an 80.55% classification accuracy with the COBRE[1] dataset. The authors constructed population graphs in which the patients diagnosed with SZ and healthy subjects as nodes and the hamming distance between phenotypic attributes of the subjects as the weights of the edges. The use of the SGC model can dramatically reduce the computational cost, however, the edge construction method can be improved by using techniques to learn the edge weights.

### Alzheimer's Disease

The AD is a prevalent neurodegenerative disorder accompanied by decreased cognitive functions in memory and motor disorders (Albert et al., 2011). The AD can be diagnosed based on changes in the functional connectivity architecture of the brain and computational models have undergone dramatic developments to discover biomarkers related to AD (Trojanowski et al., 2010). Inspired by geometric deep learning to learn relevant connectional features, several studies attempted to

[1] http://fcon_1000.projects.nitrc.org/indi/retro/cobre.html (accessed on 29 October 2020).

reduce the brain network complexity by projecting high-dimensional graph nodes into low-dimensional Euclidean space (Banka and Rekik, 2019; Cosmo et al., 2020). Despite the remarkable performance of GCN, existing GCN-based methods usually use a fixed graph topology to extract temporal features. To address this issue, a dynamic spectral-based GCN was proposed by (Xing et al., 2019, 2021) in which a LSTM network was used to extract temporal information related to the early mild cognitive impairment. (L. Zhang *et al.*, 2019) also applied a graph convolutional recurrent neural network (GCRNN) that is a combination of GCN and recurrent neural network (RNN) models to integrate multi-modal data from diffusion tensor imaging (DTI) and rs-fMRI signals. In that work, GCN layers used multi-modality data structure to learn the spatial features, then, RNN was developed to capture temporal information in fMRI signals for AD/MCI classification.

In two interesting studies using multi-level GCN models, (Kazi, Krishna, et al., 2019) and (Yu et al., 2019) examined the contribution of the image information and non-image information (i.e., gender and age) to construct the sparse graphs. To improve model efficiency, the former study applied weights for every demographic element towards the decision layer through attention mechanisms, whereas the latter study improved the feature selection process by using different kernel sizes. Given the proposed models, the accuracy performance showed superiority compared to the state-of-the-art methods for MCI prediction in the ADNI (Petersen et al., 2010) dataset. Motivated by (Yu et al., 2019), Yu and his colleagues improved the performance of the model by presenting a multi-scale enhanced GCN model in which random walk embedding techniques have been used to get the node representation (S. Yu et al., 2020). Further, (J. Liu et al., 2020) applied GCN models by using multi-modal data, MRI and rs-fMRI, to perform the early MCI classification task from the ADNI dataset. In this study, multi-task feature selection

was conducted to obtain more relevant features. Then, a non-fully labeled subject graph was developed as the input of a GCN model to get a fully labeled subject graph.

### Attention-Deficit/Hyperactivity Disorder

The ADHD is one of the common childhood neurodevelopmental disorders that usually lasts into adulthood (Nair et al., 2006; Marcos-Vidal et al., 2018). ADHD is a condition that exhibits age-inappropriate levels of inattention, hyperactivity, and behavior problems (Norman et al., 2016). In references (Yao et al., 2019) and (Yao et al., 2021), Yao et al. implemented the multi-scale tripled GCN to classify ADHD patients by using fMRI data from ADHD-200 (Bellec et al., 2017) dataset. The authors first generated multi-scale functional connectivity for each subject. Then a triplet GCN model is designed to learn multiscale graph representations of brain functional connectivity, followed by a weighted fusion strategy for classification. Further, (Rakhimberdina and Murata, 2020) applied the SGC model for brain disorder classification. The proposed model was on the basis of the population graph in which phenotypic features (e.g., gender, handedness, and acquisition site) were used to construct the graph. The performance of the model outperformed other GCN-based models with high levels of efficiency. Another population-based approach was proposed in (Saboksayr, Foxe and Wismüller, 2020) to identify ADHD patients using the ADHD-200 dataset.

### Application of GNNs in Gender Classification

Human gender classification is one of the key assignments of neuroscience, and it finds practical applications to identify brain regions based on masculinity and femininity characteristics. To explore the task of brain ROI identification, there is evidence that gender-related differences are accompanied by related changes in brain functional connectivity (Satterthwaite et al., 2015). For

example, some studies have applied GNN to classify gender-related status based on the graph structure of the brain. (Kim and Ye, 2020) adapted a framework to identify the important brain regions related to the subject's phenotypic difference by using a GIN model (Xu et al., 2018). (Arslan et al., 2018) applied a spectral-based GCN model on brain connectivity networks for ROIs identification task in gender classification of more than 5000 participants from the UK Biobank (Sudlow et al., 2015) dataset. The gender classification experiment showed the robustness of the proposed model across all runs. Further, the graph similarity metric implemented by (Ktena et al., 2018), was a Siamese GCN using a set of 2500 participants from the UK Biobank dataset. The Siamese GCN took a pair of graphs with the same structure but different signals as inputs and used spectral GCN to get graph embedding for each input graph which resulted in producing the similarity estimate between the two graphs.

Deep learning methods used for rs-fMRI data analysis are promising techniques to decode the brain, however, those methods cannot simultaneously consider the functional dependency between different brain regions in a network and the time dynamics of brain activity (Cheng, Ning and Du, 2021). To address these limitations, Spatio-Temporal GCN (ST-GCN) model has been proposed by (Gadgil et al., 2020) and (Kim, Ye and Kim, 2021). (Gadgil et al., 2020) examined the BOLD time series to model the non-stationary nature of functional connectivity and has achieved success in the classification of gender tasks. The ST-GCN used data from HCP 1200 (Van Essen et al., 2013) and National Consortium on Alcohol and Neurodevelopment in Adolescence (NCANDA) (Brown et al., 2015) datasets and the accuracy outperformed RNN-Based networks associated with gender differences. The spatio-Temporal Attention Graph Isomorphism Network (STAGIN) model was proposed by (Kim, Ye and Kim, 2021) to obtain dynamic graph representation as well. Different from the proposed model in (Gadgil et al.,

2020), STAGIN applied two types of attention functions: Graph-Attention Readout and Squeeze-Excitation Readout that significantly improved the gender classification of healthy individuals on the HCP dataset. In addition, (Azevedo, Passamonti, Lio, et al., 2020) proposed a model on the basis of Geometric Deep Learning that was the preliminary version of the model (Azevedo, Campbell, et al., 2020). The proposed model used 1D convolution operations in the neural network and a GNN model to leverage both the spatial and temporal information in rs-fMRI data, followed by a set of linear transformations to make the final gender prediction.

(Filip et al., 2020) proposed an adaptation of the GAT architecture with inductive learning in which three aggregation strategies have been employed to produce an integrated feature vector over all nodes. Specifically, the idea of a master node as a proposed aggregation strategy creates a new graph construction by connecting it to all the other nodes and discarding other connections between nodes. In addition, (Zhang et al., 2020) used the autoencoder architecture for a dynamic adjustment of the aggregation weights. The authors proposed a novel GAT model for a dynamic adjustment of the weights. To do that, three aggregation mechanisms: graph attention weight, the original edge weight, and the binary weight are combined through a multi-stage graph convolutional kernel.

Application of GNNs in Brain Response Cognitive Stimuli

Understanding which brain regions are related to a certain cognitive stimulus is a key goal in neuroscience studies. Researchers are interested in examining changes in brain functional networks during different cognitive tasks and decoding visual stimuli in human brains (Braun et al., 2015; Liang et al., 2016; Zhang et al., 2021). GNNs have recently been successful in learning the representation of graph-structured data (Z. Wu et al., 2021) and decoding brain activities

using fMRI signals to identify brain mechanisms of cognitive functions. (Zhang et al., 2021) have used a deep GNN consisting of six graph convolutional layers, on the basis of the spectral-based GCN model for brain decoding. Their model applied a DL approach to learning the spatiotemporal dynamics of brain activity from fMRI time series. Furthermore, (X. Li *et al.*, 2021) have improved the GNN model by proposing the BrainGNN framework with pooling layers. The framework has been used to map regional and cross-regional functional activation patterns for decoding cognitive states in the HCP S1200 dataset.

Research Gap in task-evoked fMRI data analysis with GCN

Task fMRI provides an opportunity to analyze the working mechanisms of the human brain during specific task performance. Our review revealed that GCN has shown promising performance in the neural decoding of fMRI signals in various applications, particularly in the disease association classification domain. However, there is a research gap with respect to applying GCN to decode task-based fMRI data. Furthermore, there are limited studies investigating the impact of node embedding methods on classification performance. Depending on the particular data structure of a graph, the performance of embedding methods in extracting the structural properties of graph nodes varies; thus, classification algorithms may perform differently according to the node embedding used (Goyal and Ferrara, 2018). Although previous studies have attempted to increase the classification performance of task fMRI data by using various node embedding methods (Li, Dvornek, *et al.*, 2020), no effort has been directed toward inferring how various node embeddings perform differently in classification task fMRI data. Most of the reviewed GNN studies used fMRI time-series data and the functional connectivity matrix as inputs for their model, however, we indicated that defining node weight by extracting

topological features of nodes before feeding the GNN model can significantly improve the performance of the model.

In addition, several studies have reported the good performance of classification models on limited datasets (Fabry-Asztalos *et al.*, 2008; Li *et al.*, 2016; Chen *et al.*, 2017) and have proposed several methods to augment the training set (Mao *et al.*, 2006; Althnian *et al.*, 2021). However, this assumption has not yet been tested against task fMRI data. On the basis of prior studies indicating a close link between individual variability and the organization of brain function (Santarnecchi *et al.*, 2017; R. Jiang *et al.*, 2020; X. Zhang *et al.*, 2020; Bruzzone *et al.*, 2022), there is a significant gap to research whether individual differences can affect a classification model. To the best of our knowledge, this is the first task fMRI study to examine the impact of individual discrepancy (i.e., gender and fluid intelligence) on task classification performance by using a GCN model.

Based on our systematic review of the applications of GNN to process fMRI data in neuroscience, our investigation indicates that the application of GNNs to process fMRI data has been rapidly developed in the last three years, and the number of publications in this field has shown significant growth. Figure 2.6 displays the number of published GNN articles in fMRI data analysis from 2017 to 2021. Although the application of GNN in fMRI data analysis is relatively limited, this figure shows the researchers' special attention to neurological and psychiatric disease prediction studies. Furthermore, the number of publications on analysing brain response cognitive stimuli by using GNN is three and we can infer that there is still room to develop computational models to improve task-evoke classification performance.

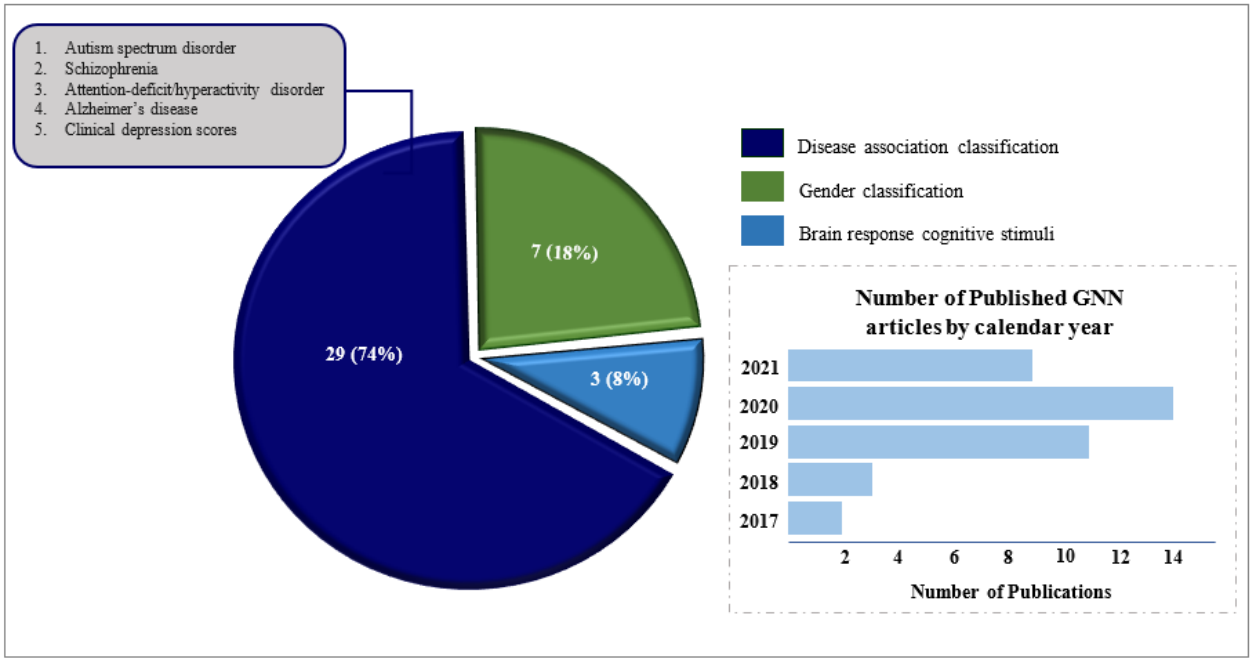


Figure 2.6. The bar chart shows the number of published graph neural network articles in fMRI analysis from 2017 to 2021. The pie chart shows the categorization of included studies.

# CHAPTER THREE: METHODOLOGY

Some of the material in this chapter are adapted from the published paper by (Saeidi *et al.*, 2022) which has been published in the Brain Sciences[1] journal.

## fMRI Dataset and Data Acquisition

We obtained task fMRI data for 302 participants, consisting of 164 women and 138 men (22–35 years, mean $= 28.7 \pm 3.6$) from the HCP 1200 Subject Release (S1200) (Van Essen *et al.*, 2013). HCP participants are drawn from a population of healthy individuals, and scans are performed during seven different tasks—emotion, gambling, working memory, language, relational, social, and motor (Barch *et al.*, 2013)—with a single dedicated 3 Tesla scanner at Washington University. Here, we give a summary of the task and a more detailed description can be found in (Barch et al., 2013).

**Emotion processing task:** The emotion task consists of two sub-tasks: face and shape images in which the face image has either angry or fearful expressions. Participants are presented with blocks of trial and asked to match the two images shown on the bottom of the screen to the target image. There are 7 blocks per run including 3 face blocks, 3 shape blocks and 1 fixation block at the end of each run.

**Gambling task:** The gambling task consists of two sub-tasks including win and loss. Participants are presented with cards and asked to guess a possible number ranging from 1 to 9 on a mystery card by selecting one of two buttons on a response box.

[1] https://www.mdpi.com/2076-3425/12/8/1094.

**Working memory task:** Participants are presented with four different stimulus types including pictures of places, tools, faces, and body parts in separate blocks, with half of the blocks using a 2-back working memory task and the other half using a 0-back working memory task. There are 12 blocks per run with 8 task blocks and 4 fixation blocks. For each task trial, the stimulus is presented for 2 seconds followed by a 500 millisecond inter-task interval.

**Language task:** The language task consists of two sub-tasks: story and math, and each sub-task has 4 blocks. The average lengths of the blocks are approximately 30 seconds. In the story trials, participants are asked to listen to a short auditory story (5-9 sentences), followed by a two-alternative choice question about the topic of the story. During the math trials, participants are asked to answer addition and subtraction operations, followed by a two-alternative choice question about the result of the operations.

**Relational processing task:** The relational task consists of two sub-tasks: relational processing and matching. In the relational processing sub-task, participants are presented with 2 pairs of objects, which are shown in 6 various shapes and filled with 6 various textures. There are four trials per each relational block and the stimuli are presented for 3500 milliseconds, with a 500 millisecond inter-task interval. In the control matching sub-task, two objects at the top of the screen and one object at the bottom of the screen are shown followed by a word in the middle of the screen. Participants are asked to decide whether the bottom object matches either of the top objects on the dimension. In this sub-task, there are 5 trials per block where stimuli are presented for 2800 millisecond, with a 400 millisecond inter-task interval.

**Social cognitive task:** Participants are presented with short video clips of objects including squares, circles, and triangles that interacted in some way, or moved randomly on the screen. After each video clip, participants decide that whether the objects had a mental interaction, Not Sure, or No interaction. Each of the two runs consists of 5 video blocks and 5 fixation blocks.

**Motor task:** Participants are presented with visual cues that ask them to response by tapping their fingers, squeezing their toes, or moving their tongue. Each block of a movement type lasts 12 seconds for 10 movements and is preceded by a 3 second cue. This task is carried out in 2 runs with 13 blocks for each run including 2 of tongue movements, 4 of hand movements, 4 of foot movement, and 3 extra fixation blocks per run.

Furthermore, a complete explanation of image acquisition has been provided in reference (Van Essen et al., 2013). Briefly, the image data was acquired with TR = 0.72s, TE = 33.1ms, flip angle = 52 degree, FOV = 208 ×180mm, and voxel size = 2.0mm isotropic with opposite phase encoding directions (left-to-right and right-to-left).

To perform our experiments aimed at evaluating the influence of individual differences, we considered two categories of task fMRI data: gender and fluid intelligence (gF). The first category consisted of two (female and male) sub-datasets in which task fMRI data for 164 and 138 participants were assigned to each sub-dataset according to gender. In the second category, we sorted gF scores of 302 participants in descending order and divided the dataset of 302 participants into two sub-datasets, LM-gF and HM-gF, of participants with gF scores lower than the median value (gF score $< 18$) and with gF score higher than the median value (gF score $\geq 18$), respectively. Consequently, a total of 144 and 158 participants' task fMRI data were

assigned to the LM-gF and HM-gF sub-datasets, respectively. Table 3.1 presents the demographics and subject distribution of the four defined sub-datasets.

Table 3.1. Demographics and participant distribution results.

| Groups | Number of participants | Age (mean±SD) | gF-score (mean±$SD$) |
|---|---|---|---|
| Female | 164 | $29.2 \pm 3.6$ | − |
| Male | 138 | $28.1 \pm 3.6$ | − |
| LM-gF | $F = 91, M = 53$ | $29.1 \pm 3.6$ | $12.5 \pm 3.4$ |
| HM-gF | $F = 83, M = 75$ | $28.4 \pm 3.6$ | $20.6 \pm 1.7$ |

Abbreviations: LM-gF, low median-gF score; HM-gF, high median-gF score; F, female; M, male.

## Data Pre-processing

The preprocessing of the task fMRI volume time series was performed by the HCP consortium as previously described (Glasser et al., 2013). The preprocessing pipeline included artifact removal and gradient distortion correction, motion correction, and registration to the standard Montreal Neurological Institute space using DARTEL and voxel size of $2 \times 2 \times 2$ mm$^3$. Spatial smoothing and activation maps generation were performed with a GLM implemented in FSL's FILM (FMRIB's Improved Linear Model with autocorrelation) (Beckmann and Smith, 2004). More details about the HCP preprocessing pipeline can be found in Barch et al. (Barch et al., 2013).

## Brain Functional Graph

An overview of our analysis pipeline is presented in Figure 3.1. First, the raw task fMRI data were collected and preprocessed by means of the HCP minimal preprocessing pipeline (Glasser et al., 2013) and denoised by using ICA-FIX (Salimi-Khorshidi et al., 2014) to remove spatial

artifacts and motion correction. Then, we used a large-scale multimodal brain atlas to parcellate the brain regions into 360 anatomical areas using the Human Connectome Project Multi-Modal Parcellation that is based on a combination of cortical architecture, function, connectivity, and topography (Glasser et al., 2016). By parcellation, we define ROIs that represent graph nodes for brain network construction. Theoretically, the construction of a functional graph involves two steps. First, the time series of all voxels in the region were averaged. Then, we computed the functional connectivity between each pair of averaged time series of brain regions by means of Pearson's correlation coefficient. We used Fisher's z transformation to normalized r value to improve the normality and obtained a $360 \times 360$ symmetric matrix A (adjacency matrix) for each subject. Figure 3.2, Figure 3.3, and Figure 3.4 illustrate functional connectivity averaged based on task fMRI across the whole dataset, gender sub-dataset, and fluid intelligence sub-datasets, respectively. The regions (nodes) are ordered according to which cognitive system they belong to.

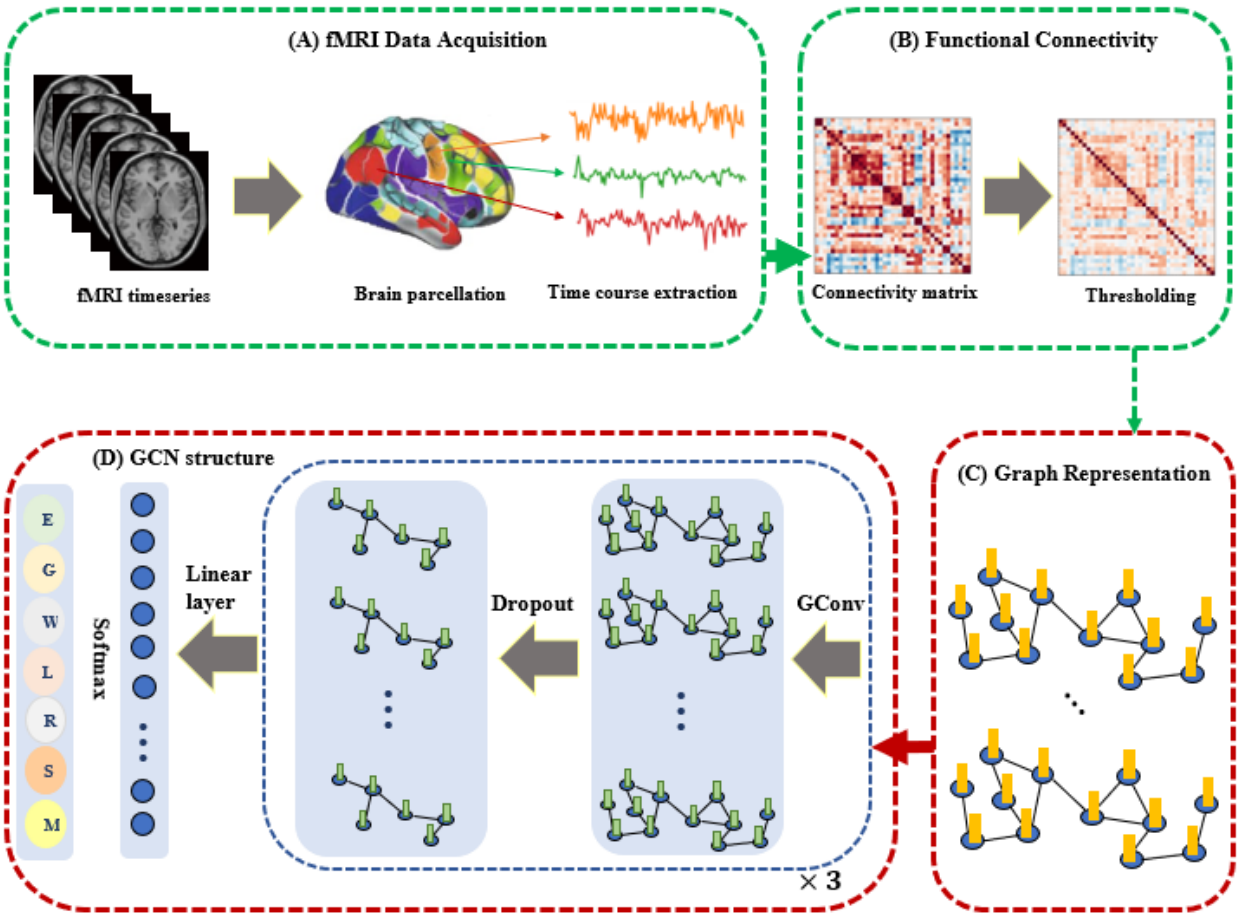


Figure 3.1. Overview of Graph Convolutional Network (GCN) model for task fMRI classification. After acquisition of the raw task fMRI data and identification of the brain's divisions into various parcels, several time courses of each parcel were extracted (A) to create the functional connectivity matrix. To reduce the complexity of the graph, a threshold was applied to the connectivity matrix (B) and transferred to a graph. The initial representation of each node was extracted by using the FRESH algorithm and node embedding methods (C).Finally, the feature vectors were used to perform the classification task with the proposed GCN framework including three Conv layers followed by a dropout layer after each Conv layer (D).

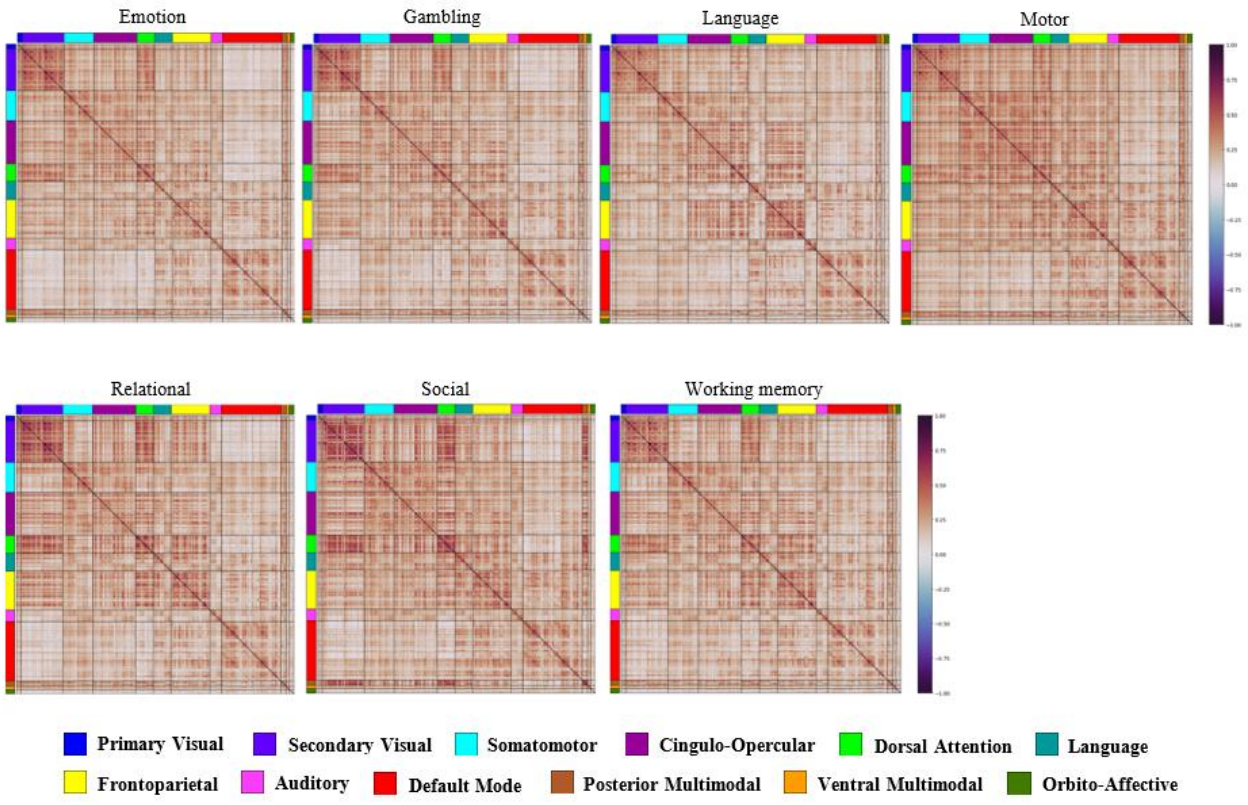


Figure 3.2. Functional connectivity averaged across N = 302 subjects based on task fMRI. The regions were sorted according to which cognitive system they belong to. Network names are listed on the left.

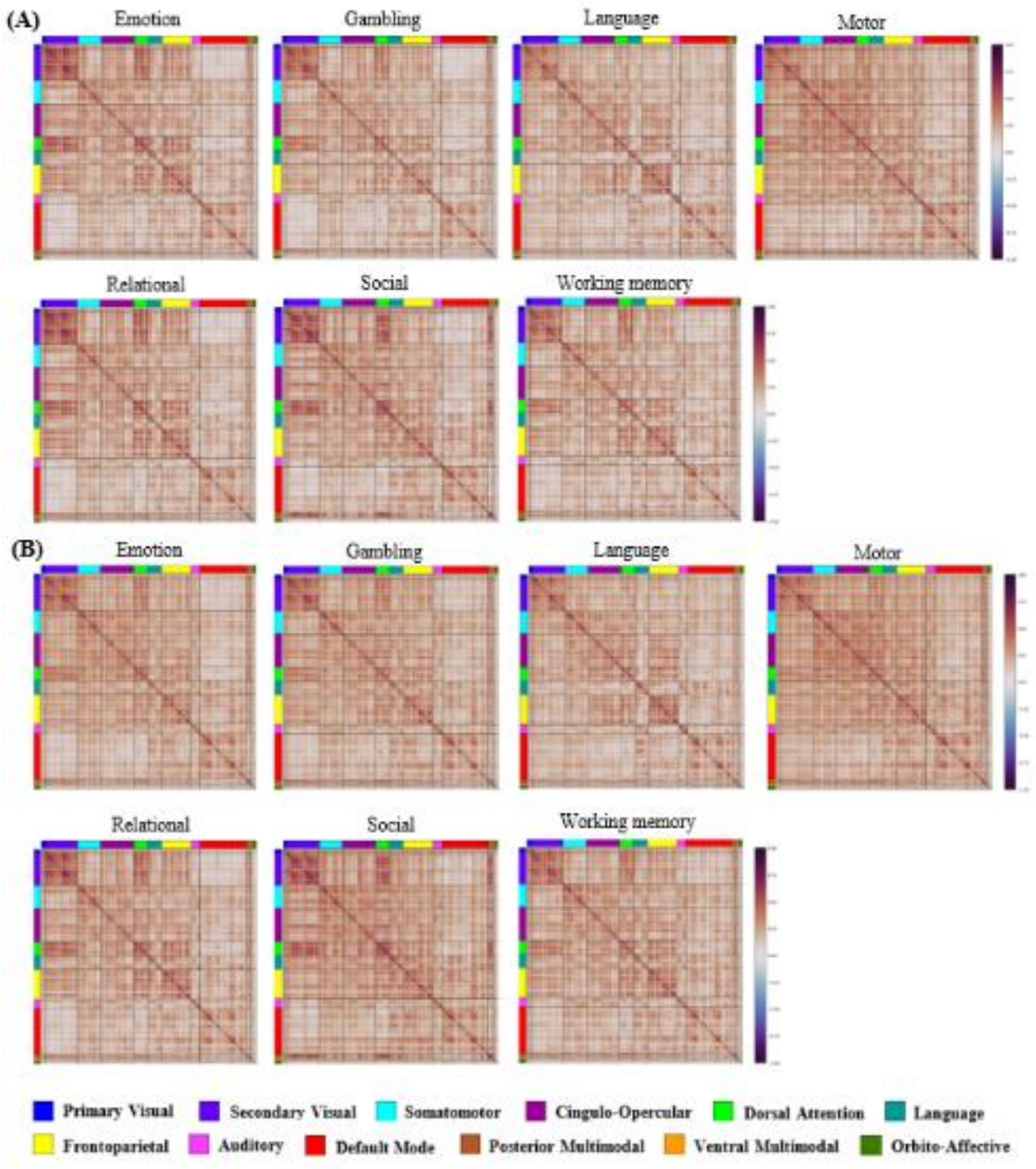


Figure 3.3. Correlation-based task fMRI connectivity for both female (A) and male (B) sub-datasets. The regions were sorted according to which cognitive system they belong to. Network names are listed on the left.

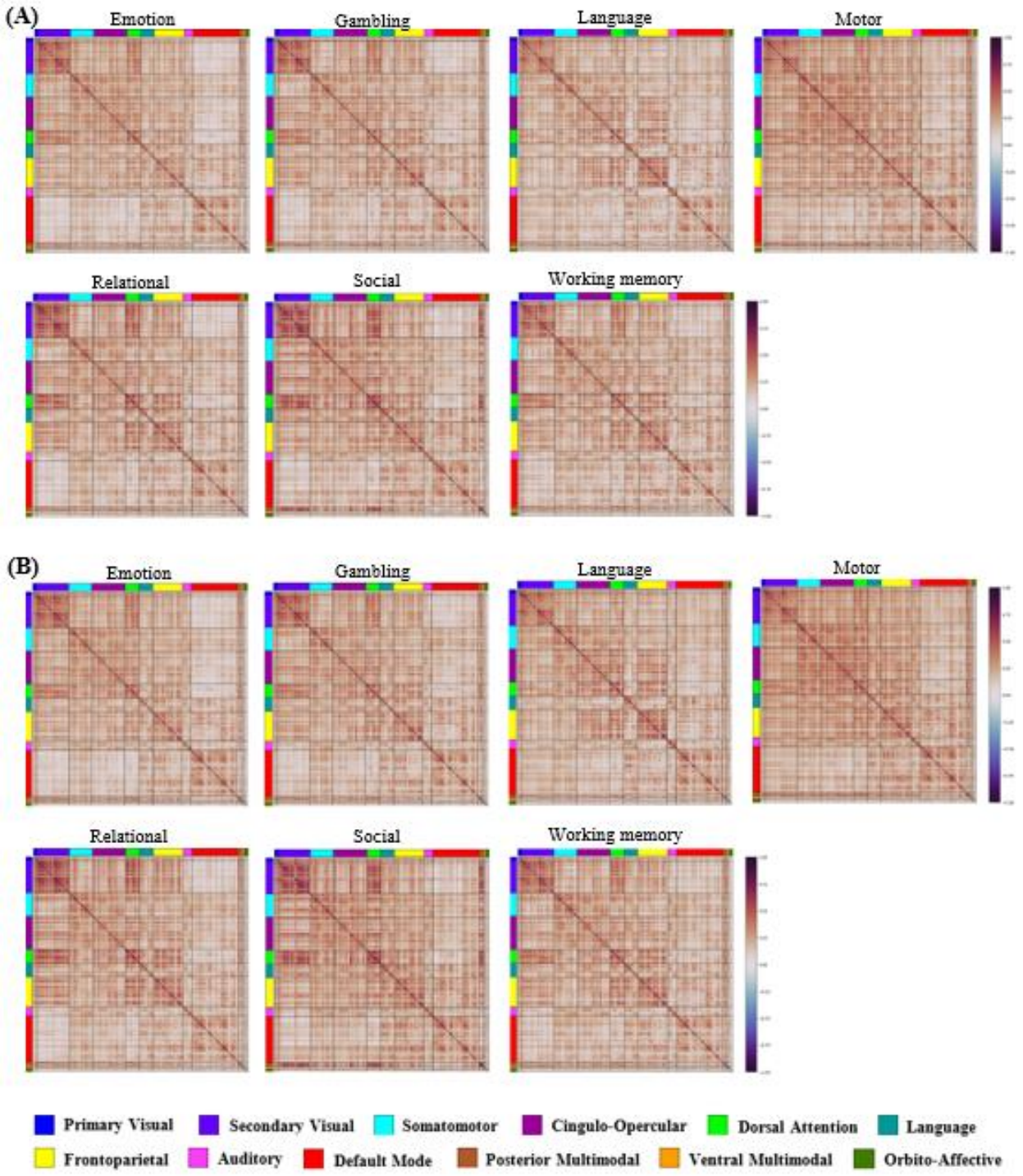


Figure 3.4. Correlation-based task fMRI connectivity for both LM-gF (A) and HM-gF (B) sub-datasets. The regions were sorted according to which cognitive system they belong to. Network names are listed on the left.

## Feature Engineering and Node Embedding Algorithms

Features from averaged time series of brain regions were extracted by using Time Series FeatuRe Extraction on basis of Scalable Hypothesis tests (tsfresh), an efficient and scalable feature extraction algorithm for time series based on a Python package (Christ *et al.*, 2018). The tsfresh algorithm integrates the components from the hypothesis tests with the feature significance testing on the basis of the FRESH algorithm (Christ, Kempa-Liehr and Feindt, 2016). Each generated feature vector is independently assessed to identify its significance for the given target by quantifying p-values and is further evaluated through the Benjamini-Yekutieli procedure (Benjamini and Yekutieli, 2001) to decide which features to keep. The features extracted by tsfresh consist of both basic and advanced characteristics of the time series, and a complete list of features along with their mathematical descriptions can be found in the reference (Christ, Kempa-Liehr and Feindt, 2016). We selected a minimum set of relevant statistical features to prepare feature representations for each node as follows: "absolute_sum_of_changes," "benford_correlation," "c3" (i.e., a measure of nonlinearity in the time series), "cid_ce" (i.e., a measure of complexity in the time series), "longest_strike_above_mean," "variance," "standard deviation," "skewness," and "quantile" (i.e., 0.25 quantile).

In addition to the statistical features obtained through the tsfresh algorithm, Node embeddings were applied to automatically extract node attributes in graphs. Node embedding algorithms project nodes into low-dimensional vectors such that nodes with similar topological structures are in proximity in the embedding space (Cai, Zheng and Chang, 2018) through an encoder function. Specifically, the aim of the encoder function is to take the data from the original space or graph and then provide us with the data in the embedding space. The illustration is presented in Figure 3.5.

We used the Python framework Karate Club (Rozemberczki, Kiss and Sarkar, 2020), which consists of at least 30 graph mining algorithms, for node and graph embedding. We compared the performance of four state-of-the-art node embedding algorithms: Walklets (Perozzi *et al.*, 2017) and Node2Vec (Grover and Leskovec, no date), which use sampled random walks to make the node embeddings; NetMF (Qiu *et al.*, 2018), a factorization-based model; and the recently proposed RandNE (Z. Zhang *et al.*, 2018), which is based on a Gaussian random projection approach with the default dimension ordering.

**Walklets.** In this method, instead of the random walk process used in DeepWalk (Perozzi, Al-Rfou and Skiena, 2014), Walklets approximates sample node neighborhoods by skipping over nodes in each short random walk. Then, the set of results of multiple skip lengths are used to train the model (Goyal and Ferrara, 2018).

**Node2Vec.** This method is a modification of DeepWalk by introducing parameters p and q to smoothly interpolate between breadth-first sampling and depth-first sampling. Parameter p controls the likelihood of immediately revisiting a node in the walk whereas parameter q allows the search to differentiate between "inward" and "outward" nodes. In Node2Vec, a vector representation of a node is computed based on the second order random walks in the graph, and the core assumption is that Node2Vec's sampling strategy is based on the mixture of breadth-first sampling and depth-first sampling which are suited for structural equivalence (i.e., similar roles of nodes) and homophily (i.e., network community) respectively (Dalmia, Ganesh and Gupta, 2018).

**NetMF.** This method is a matrix factorization-based algorithm that is based on the connection between DeepWalk's implicit matrix and graph Laplacians (Z. Zhang *et al.*, 2018). NetMF uses a

small subset of nodes and extracts embedding vectors by approximating the proximity between nodes and the subset with the help of graph Laplacians (B. Yu et al., 2020).

**RandNE.** This method of iterative random projection network embedding preserves high order proximity between nodes using Gaussian random projection method while reduces the time complexity (Z. Zhang *et al.*, 2018).

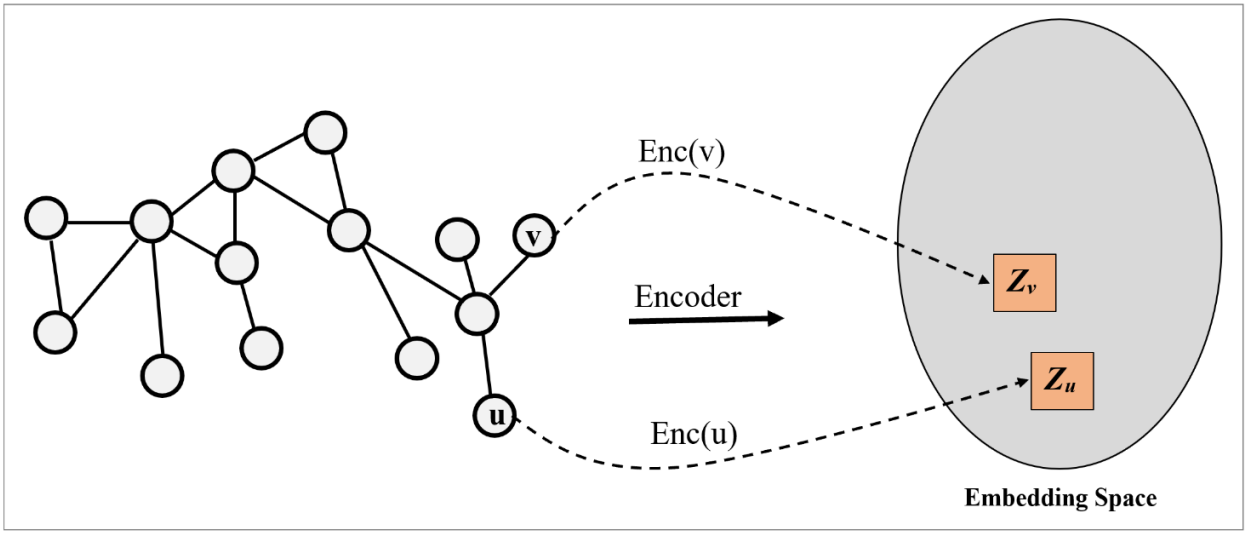


Figure 3.5. Schematic of embedding process. The goal in embedding is to encode nodes into low-dimensional space/embedding space.

## Proposed Model

### Modular Architecture

Our proposed model was developed by using PyTorch (Paszke *et al.*, 2019) and PyTorch Geometric (Fey and Lenssen, 2019). The model takes a time series of fMRI volumes as input, in which each time series is a 2D matrix $X$ of size $T \times N$ where $T$ is the number of time steps, and $N$ is the number of brain regions. The tsfresh algorithm was used for statistical feature extraction for each node, and then high-level node features associated with each node were extracted with

node embedding methods. The overall GCN model architecture for task fMRI classification is summarized in Figure 3.1.D.

The GCN model consists of three Conv layers with 92 neurons per layer. ReLU and batch normalization layers are applied between each Conv layer to accelerate the convergence and enhance stability, and dropout layers are added after each Conv layer. Then, a global mean pooling layer is applied to calculate the final graph representation vector. We performed experiments on the same computing machine equipped with a single NVIDIA Tesla T4 24 GB RAM GPU.

## Training and Testing

This study used five-fold Stratified cross-validation within a training/validation/test setup. Four-fifths of the available data were allocated to a training set within each fold. The remaining one-fifth of the data were partitioned with a 60:40 ratio into a validation set and a final test set. The hyperparameter search consisted of a grid of learning rate, dropout, and weight decay values. The model with the lowest loss in the validation set was considered the best model for the final test. The following ideal parameters were used: learning rate: 0.001, dropout: 0.65, weight decay: 0.0. Furthermore, because batch size is among the most important hyperparameters to tune, we considered a set of values of batch sizes. The batch sizes used in all experiments were $B = [16, 32, 48, 64]$ over 100 epochs, all using the Adam optimizer and reducing the learning rate on a plateau with a patience of 10. Furthermore, cross-entropy loss was used for the optimization function.

## Evaluation Metrics

The metrics used for comparison embedding methods and evaluation of classification performance included accuracy, balanced accuracy, F1 scores (macro, micro, and weighted), Mathews correlation coefficient (MCC), precision, and recall. F1 macro and MCC have been widely considered as metrics to evaluate imbalanced datasets in which all classes are weighted equally (Géron, 2019; Chicco and Jurman, 2020). Therefore, we applied accuracy, F1 macro, and MCC for further node embedding method comparisons and evaluation of GCN model performance. For statistical analysis, we used a significance threshold of 0.05. We also used the Shapiro-Wilk normality test (Shapiro and Wilk, 1965) followed by the t-test to evaluate the statistical significance of the model's classification performance in different scenarios.

$$\text{Accuracy} = \frac{\text{TP} + \text{TN}}{\text{TP} + \text{TN} + \text{FP} + \text{FN}} \tag{3.1}$$

where TP, TN, FP, and FN represent True Positive, True Negative, False Positive, and False Negative measures respectively.

$$\text{Balanced Accuracy} = \frac{\text{sensitivity} + \text{specificity}}{2} \tag{3.2}$$

Where $\text{sensitivity} = \frac{\text{TP}}{\text{TP+FN}}$ and $\text{specificity} = \frac{\text{TN}}{\text{TN+FP}}$

$$\text{Macro F1 score} = \frac{1}{\text{N}}\sum_{\text{i=0}}^{\text{N}} \text{F1score}_{\text{i}} \tag{3.3}$$

Where i is the class/label index and N is the number of classes/labels.

$$\text{Micro F1 score} = 2 \times \frac{\text{Precision} \times \text{Recall}}{\text{Precision} + \text{Recall}} \tag{3.4}$$

$$\text{Precision} = \frac{\text{TP}}{\text{TP} + \text{FP}} \tag{3.5}$$

$$\text{Recall} = \frac{\text{TP}}{\text{TP} + \text{FN}} \tag{3.6}$$

$$\text{MCC} = \frac{\text{TN} \times \text{TP} - \text{FN} \times \text{FP}}{\sqrt{(\text{TP} + \text{FP})(\text{TP} + \text{FN})(\text{TN} + \text{FP})(\text{TN} + \text{FN})}} \tag{3.7}$$

# CHAPTER FOUR: RESULTS

In this section, the experimental results are presented for the GCN model implementation and classification performance in different scenarios. Furthermore, detailed information regarding the evaluation of node embeddings in the context of task fMRI decoding concerning gender and gF score differences is provided. Finally, we implemented a t-test to determine whether the difference in classification performance was statistically significant.

## Classification of task fMRI data

The first set of results included the evaluation of our proposed GCN framework to classify task fMRI data with respect to node embeddings. The experiment was performed by using task fMRI data from the 302 participants, and the framework was set up by application of the four defined node embeddings regarding different batch sizes during training. The results shown in Table 4.1 illustrated that RandNE, NetMF embedding methods outperformed DeepWalk methods (Node2Vec, Walklets). This result might have been because DeepWalk-based methods require many sampled node neighborhoods to create node embedding vectors (Dong *et al.*, 2021). The F1 macro scores for RandNE and NetMF revealed similar performance across the GCN framework, and the application of different batch sizes had a minor effect on the classification performance.

Figure 4.1 illustrates the effect of batch size on classification performance. As the number of batch sizes increased from 16 to 64, the F1 macro score and MCC increased. We also observed that using a batch size of 64 achieved superior results if any node embeddings were selected. However, our GCN model showed the best classification performance with NetMF when a batch size of 64 was chosen. We set up our GCN model and obtained the confusion matrix for task

fMRI classification after the training step, as shown in Figure 4.2. The normalized confusion matrix indicated that the top confusions were between 1) the social and motor tasks and 2) the gambling and social tasks.

## Performance Comparison

We compared the proposed GCN model with Logistic Regression (LR) that used L2 regularization, as our baseline model, to prove if the classification performance represented a noticeable improvement over the traditional machine learning model. LR works well as a baseline model since it is relatively easy to implement. The use of regularization prevents overfitting of the task fMRI data so that the model features are shrunk towards zero and perform feature selection automatically. We evaluated the same brain decoding tasks and ran LR on our task fMRI dataset, splitting it into the train, validation, and test sets. To tune the regularization parameter, we used a range of values and perform 5-fold cross-validation to achieve the optimal regularization parameter of 0.1. The result of L2- regularized LR showed a lower prediction accuracy in the seven-class classification task (97.7% vs. 86.4%, respectively, for GCN and LR with L2 regularization).

Table 4.1. Two-factor performance comparison on predicting experimental task, taking into account the influence of node embedding methods and batch sizes for the task fMRI classification. The training processes were set with 100 epochs, 10 step patience for early stopping, and learning rate = 0.001 for Adam. The proposed GCN model showed impressive results with both RandNE and NetMF node embedding methods. Classification performance values for 302 participants' task fMRI data were in the range of 94% to 98%. Bold values represent the best classification performance obtained for each batch size.

| Batch size | Node embeddings | Metrics | | | | | | | |
|---|---|---|---|---|---|---|---|---|---|
| | | Accuracy | Balanced accuracy | F1 macro | F1 micro | F1 weighted | MCC | Precision | Recall |
| 16 | Walklets | 0.886 | 0.893 | 0.89 | 0.886 | 0.885 | 0.867 | 0.891 | 0.893 |
| | Node2Vec | 0.854 | 0.866 | 0.863 | 0.854 | 0.854 | 0.831 | 0.869 | 0.866 |
| | RandNE | **0.939** | **0.942** | **0.941** | **0.939** | **0.939** | **0.928** | **0.941** | **0.942** |
| | NetMF | 0.933 | 0.937 | 0.936 | 0.933 | 0.933 | 0.921 | 0.936 | 0.937 |
| 32 | Walklets | 0.911 | 0.917 | 0.915 | 0.91 | 0.911 | 0.895 | 0.916 | 0.917 |
| | Node2Vec | 0.873 | 0.888 | 0.886 | 0.873 | 0.874 | 0.854 | 0.891 | 0.888 |
| | RandNE | 0.969 | 0.971 | 0.97 | 0.969 | 0.969 | 0.954 | 0.97 | 0.971 |
| | NetMF | **0.974** | **0.976** | **0.976** | **0.974** | **0.974** | **0.97** | **0.975** | **0.976** |
| 48 | Walklets | 0.915 | 0.922 | 0.92 | 0.915 | 0.914 | 0.901 | 0.919 | 0.922 |
| | Node2Vec | 0.898 | 0.903 | 0.9 | 0.898 | 0.895 | 0.882 | 0.904 | 0.904 |
| | RandNE | 0.971 | 0.974 | 0.973 | 0.971 | 0.971 | 0.966 | 0.973 | 0.974 |
| | NetMF | **0.976** | **0.978** | **0.977** | **0.976** | **0.976** | **0.971** | **0.976** | **0.978** |
| 64 | Walklets | 0.932 | 0.937 | 0.936 | 0.933 | 0.933 | 0.922 | 0.935 | 0.937 |
| | Node2Vec | 0.902 | 0.907 | 0.908 | 0.902 | 0.902 | 0.886 | 0.911 | 0.937 |
| | RandNE | 0.975 | 0.977 | 0.976 | 0.973 | 0.975 | 0.971 | 0.976 | 0.977 |
| | NetMF | **0.977** | **0.979** | **0.978** | **0.977** | **0.977** | **0.974** | **0.978** | **0.979** |

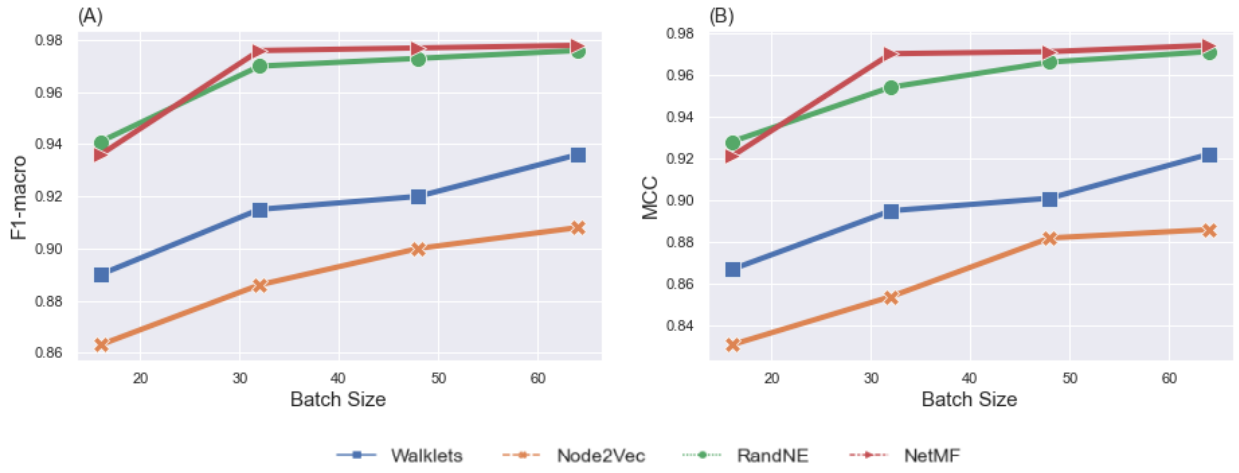


Figure 4.1. F1 macro (A) and MCC (B) comparison of GCN model, taking into account the influence of node embedding methods and batch sizes for the task fMRI classification task, by using the 302 participants' fMRI data.

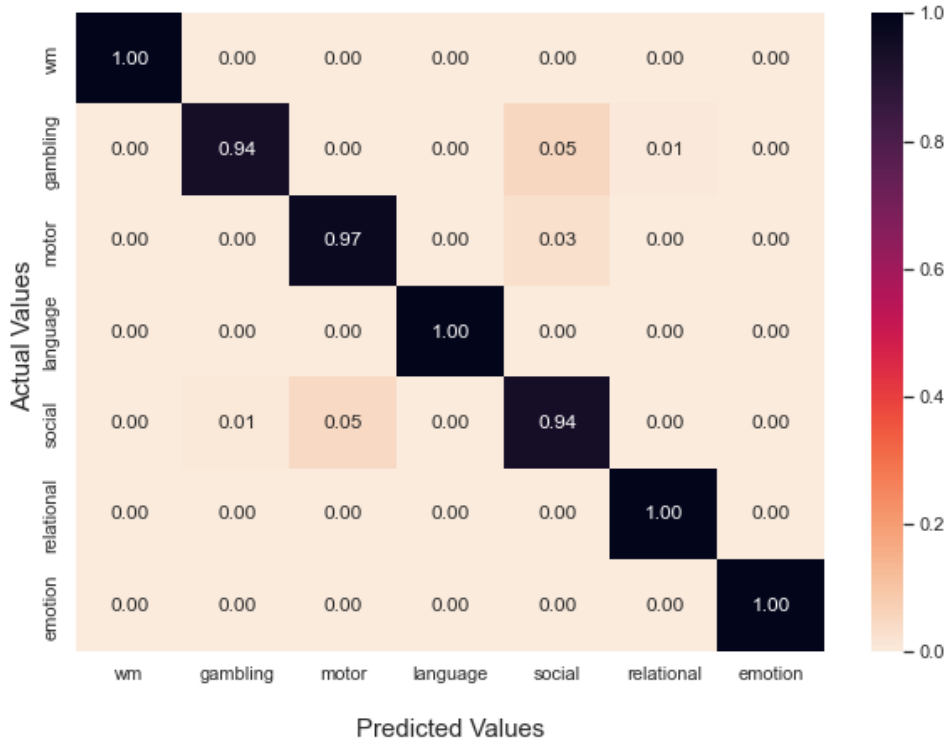


Figure 4.2. Confusion matrix of the GCN classification results on the 302 participants' task fMRI data that is normalized to the seven tasks in the five-fold cross-validation. The top two confusions were caused by the social task versus motor task and the gambling task versus social task. The F1 macro and MCC of classification were 0.977 and 0.974, respectively.

## Effects of individual discrepancy (gender and fluid intelligence) on classification

We performed experiments to evaluate the effects of gender and gF score on classification performance by using task fMRI data. The experiments were performed separately on the datasets described in the fMRI Dataset and Data Acquisition section. We applied the proposed GCN framework with the same hyperparameters above for all classification experiments.

### Gender discrepancy

#### Classification

We first assessed the predictive performance of our model on predicting gender. The classification performance of the GCN model with the four node embedding methods when varying batch sizes were used during training is presented in Table 4.2 and Table 4.3 for the female and male sub-datasets, respectively.

Several observations were made in Table 4.2 and Table 4.3. First, we observed that the average F1 macro of the classifier on both sub-datasets ranged from 79.5% to 97.9%. Second, the GCN model achieved the best classification performance with NetMF for both sub-datasets. Third, the GCN model was sensitive to the choice of batch size, such that the best performance was obtained with a batch size of 64 for male and female sub-datasets.

Similar trends were observed in the performance of the GCN model for F1 macro and MCC in Figure 4.3. For MCC, model performance across both sub-datasets ranges from 82% to 97% with batch sizes of 48 and 64, respectively.

Table 4.2. Two-factor performance comparison, taking into account the influence of node embedding methods and batch sizes in the GCN model, by using the female fMRI data. Bold values represent the best classification performance obtained for each batch size.

| Batch size | Node embeddings | Metrics | | | | | | | |
|---|---|---|---|---|---|---|---|---|---|
| | | Accuracy | Balanced accuracy | F1 macro | F1 micro | F1 weighted | MCC | Precision | Recall |
| 16 | Walklets | 0.881 | 0.886 | 0.882 | 0.881 | 0.881 | 0.862 | 0.882 | 0.886 |
| | Node2Vec | 0.792 | 0.806 | 0.795 | 0.793 | 0.794 | 0.764 | 0.794 | 0.805 |
| | RandNE | 0.916 | 0.921 | 0.916 | 0.916 | 0.916 | 0.902 | 0.915 | 0.921 |
| | NetMF | **0.927** | **0.932** | **0.928** | **0.927** | **0.927** | **0.915** | **0.926** | **0.932** |
| 32 | Walklets | 0.919 | 0.922 | 0.919 | 0.919 | 0.918 | 0.905 | 0.915 | 0.922 |
| | Node2Vec | 0.835 | 0.839 | 0.837 | 0.836 | 0.835 | 0.807 | 0.849 | 0.838 |
| | RandNE | 0.938 | 0.941 | 0.939 | 0.938 | 0.938 | 0.927 | 0.937 | 0.941 |
| | NetMF | **0.959** | **0.961** | **0.959** | **0.959** | **0.959** | **0.952** | **0.959** | **0.96** |
| 48 | Walklets | 0.931 | 0.936 | 0.932 | 0.931 | 0.931 | 0.92 | 0.931 | 0.936 |
| | Node2Vec | 0.871 | 0.871 | 0.869 | 0.871 | 0.867 | 0.851 | 0.874 | 0.874 |
| | RandNE | 0.952 | 0.955 | 0.952 | 0.951 | 0.948 | 0.944 | 0.951 | 0.955 |
| | NetMF | **0.967** | **0.968** | **0.967** | **0.966** | **0.966** | **0.961** | **0.965** | **0.968** |
| 64 | Walklets | 0.928 | 0.932 | 0.928 | 0.928 | 0.928 | 0.916 | 0.927 | 0.932 |
| | Node2Vec | 0.859 | 0.869 | 0.861 | 0.861 | 0.858 | 0.837 | 0.867 | 0.87 |
| | RandNE | 0.971 | 0.971 | 0.972 | 0.972 | 0.969 | 0.966 | 0.969 | 0.972 |
| | NetMF | **0.979** | **0.98** | **0.979** | **0.98** | **0.978** | **0.974** | **0.976** | **0.979** |

Table 4.3. Two-factor performance comparison, taking into account the influence of node embedding methods and batch sizes in the GCN model, by using the male fMRI data. Bold values represent the best classification performance obtained for each batch size.

| Batch size | Node embeddings | Metrics | | | | | | | |
|---|---|---|---|---|---|---|---|---|---|
| | | Accuracy | Balanced accuracy | F1 macro | F1 micro | F1 weighted | MCC | Precision | Recall |
| 16 | Walklets | 0.849 | 0.861 | 0.85 | 0.849 | 0.848 | 0.823 | 0.847 | 0.861 |
| | Node2Vec | 0.841 | 0.857 | 0.845 | 0.842 | 0.84 | 0.817 | 0.846 | 0.858 |
| | RandNE | 0.907 | 0.911 | 0.909 | 0.908 | 0.907 | 0.891 | 0.907 | 0.911 |
| | NetMF | **0.908** | **0.913** | **0.911** | **0.908** | **0.908** | **0.892** | **0.911** | **0.913** |
| 32 | Walklets | 0.879 | 0.891 | 0.882 | 0.879 | 0.879 | 0.859 | 0.88 | 0.891 |
| | Node2Vec | 0.878 | 0.887 | 0.879 | 0.878 | 0.877 | 0.856 | 0.878 | 0.884 |
| | RandNE | **0.949** | **0.951** | **0.951** | **0.949** | **0.949** | **0.94** | **0.952** | **0..951** |
| | NetMF | 0.939 | 0.943 | 0.941 | 0.939 | 0.939 | 0.928 | 0.941 | 0.943 |
| 48 | Walklets | 0.887 | 0.895 | 0.889 | 0.884 | 0.887 | 0.862 | 0.887 | 0.895 |
| | Node2Vec | 0.852 | 0.865 | 0.857 | 0.852 | 0.852 | 0.827 | 0.857 | 0.862 |
| | RandNE | 0.955 | 0.959 | 0.957 | 0.955 | 0.956 | 0.947 | 0.957 | 0.959 |
| | NetMF | **0.962** | **0.965** | **0.964** | **0.962** | **0.962** | **0.953** | **0.964** | **0.965** |
| 64 | Walklets | 0.871 | 0.885 | 0.874 | 0.871 | 0.87 | 0.844 | 0.87 | 0.885 |
| | Node2Vec | 0.845 | 0.855 | 0.849 | 0.845 | 0.845 | 0.817 | 0.853 | 0.852 |
| | RandNE | 0.958 | 0.961 | 0.961 | 0.958 | 0.959 | 0.951 | 0.96 | 0.961 |
| | NetMF | **0.962** | **0.966** | **0.965** | **0.962** | **0.961** | **0.953** | **0.964** | **0.963** |

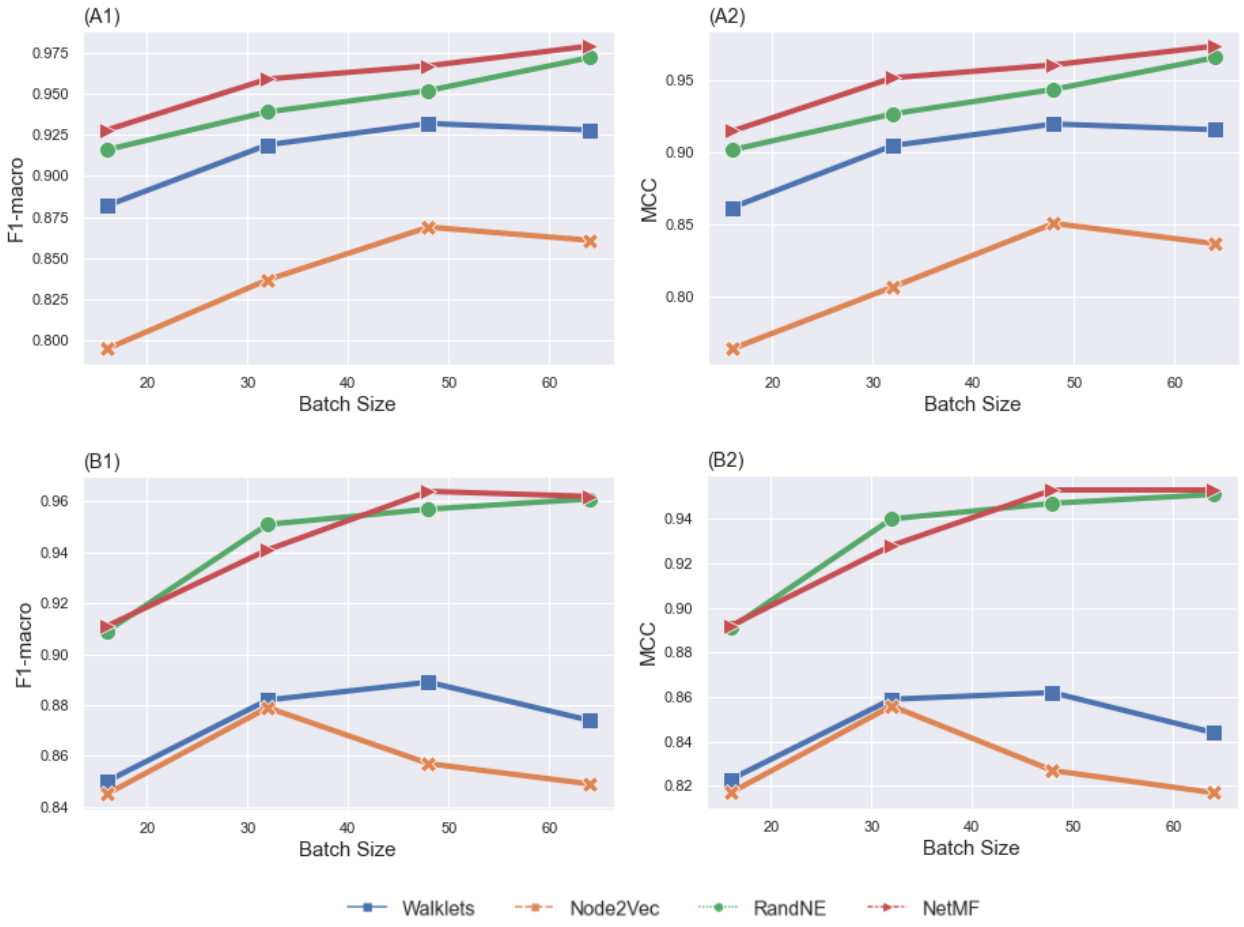


Figure 4.3. F1 macro and MCC comparisons of GCN model, taking into account the effects of node embedding methods and batch sizes, by using female task fMRI data (A1, A2) and male task fMRI data (B1, B2).

Statistical analysis concerning MCC

According to the results of our model applied independently to female and male sub-datasets, the proposed GCN model had the best classification performance when NetMF was the node embedding method, and the batch size of 64 was selected during training. We set up the GCN model with NetMF and trained it with a batch size of 64, by using a learning rate of 0.001 for 100 epochs to classify task fMRI data for each sub-dataset separately. This process was

performed iteratively a total of 35 times, and related MCC values were used to assess the statistical significance of the differences in classification performance. Figure 4.5.A represents the results of this process. The GCN model performed relatively similarly, whereas each run showed varying performance between two sub-datasets.

To perform statistical significance testing, we used the Shapiro-Wilk normality test to assess normality. After assessing the statistical significance of the difference between the classification performance of two sub-datasets (i.e., female and male), we performed a t-test, which indicated a significant difference ($p = 0.000001022$), at $p < 0.05$. The null hypothesis for this test was that the mean of classification performance for two sub-datasets was identical. Together, these results revealed that differences between the male and female task fMRI data were significant, such that classification was more accurate for female than male task fMRI data. Therefore, gender differences should be considered a feature in performing a task fMRI classification.

## Fluid intelligence level discrepancy

### Classification

We evaluated the gF-score through the same procedures used for the assessment of the influence of gender differences on classification task fMRI data. We set up the model and independently performed classification experiments on two sub-datasets: LM-gF and HM-gF. Table 4.4 and Table 4.5 show the model's performance regarding defined node embedding methods after training with a batch size range from 16 to 64 for LM-gF and HM-gF. Correspondingly, Figure 4.4 represents the visualization of the model's performance for various node embeddings for F1 macro and MCC. The x-axis in the figures shows the batch sizes. The GCN classification showed high performance on LM-gF and HM-gF sub-datasets with RandNE and NetMF node

embedding methods, which exhibited similar trends. In addition, the results indicated a change in the performance of the model when the size of the batch size increased from 16 to 64. The most striking observation was that for both sub-datasets, classification performance with RandNE achieved the best MCC.

Statistical analysis concerning MCC

To assess the influence of individuals' gF-scores on the classification performance, we conducted the same procedure as the previous scenario for gender differences. However, we found that the GCN model had the best classification performance when RandNE was used as the node embedding method. Similarly, the model was set up and trained with a batch size of 48 and a learning rate of 0.001 for 100 epochs to classify task fMRI data by using LM-gF and HM-gF. We obtained two groups of values indicating the accuracy performance (i.e., MCC) of the classification model in different sub-datasets (Figure 4.5.B). The Shapiro-Wilk normality test was performed to assess normality, and a t-test was used to assess the statistical significance of the differences in classification performance. The difference was found to be non-significant ($p = 0.604$), at $p < 0.05$. Therefore, the accuracy performance of classification task fMRI data for participants with lower and higher fluid intelligence was comparable. Thus, individuals' gF scores do not affect task fMRI classification performance.

Table 4.4. Two-factor performance comparisons, taking into account the influence of node embedding methods and batch sizes in the GCN model, by using LM-gF task fMRI data. Bold values represent the best classification performance obtained for each batch size.

| Batch size | Node embeddings | Metrics | | | | | | | |
|---|---|---|---|---|---|---|---|---|---|
| | | Accuracy | Balanced accuracy | F1 macro | F1 micro | F1 weighted | MCC | Precision | Recall |
| 16 | Walklets | 0.869 | 0.872 | 0.873 | 0.869 | 0.868 | 0.847 | 0.875 | 0.873 |
| | Node2Vec | 0.895 | 0.896 | 0.896 | 0.895 | 0.893 | 0.877 | 0.901 | 0.897 |
| | RandNE | **0.936** | **0.937** | **0.937** | **0.936** | **0.932** | **0.925** | **0.938** | **0.937** |
| | NetMF | 0.906 | 0.909 | 0.908 | 0.906 | 0.906 | 0.89 | 0.907 | 0.909 |
| 32 | Walklets | 0.899 | 0.902 | 0.902 | 0.899 | 0.899 | 0.882 | 0.903 | 0.902 |
| | Node2Vec | 0.891 | 0.894 | 0.893 | 0.891 | 0.89 | 0.869 | 0.895 | 0.894 |
| | RandNE | **0.977** | **0.977** | **0.977** | **0.977** | **0.976** | **0.973** | **0.977** | **0.976** |
| | NetMF | 0.93 | 0.932 | 0.93 | 0.929 | 0.929 | 0.918 | 0.931 | 0.932 |
| 48 | Walklets | 0.908 | 0.911 | 0.91 | 0.908 | 0.904 | 0.891 | 0.91 | 0.91 |
| | Node2Vec | 0.9 | 0.902 | 0.902 | 0.9 | 0.9 | 0.883 | 0.904 | 0.902 |
| | RandNE | **0.991** | **0.991** | **0.991** | **0.99** | **0.991** | **0.989** | **0.991** | **0.991** |
| | NetMF | 0.934 | 0.935 | 0.934 | 0.934 | 0.933 | 0.922 | 0.935 | 0.935 |
| 64 | Walklets | 0.899 | 0.901 | 0.901 | 0.899 | 0.898 | 0.881 | 0.903 | 0.901 |
| | Node2Vec | 0.901 | 0.904 | 0.903 | 0.902 | 0.901 | 0.885 | 0.905 | 0.905 |
| | RandNE | **0.991** | **0.991** | **0.991** | **0.99** | **0.991** | **0.99** | **0.991** | **0.991** |
| | NetMF | 0.936 | 0.938 | 0.938 | 0.936 | 0.935 | 0.925 | 0.938 | 0.938 |

Table 4.5. Two-factor performance comparisons, taking into account the influence of node embedding methods and batch sizes in the GCN model, by using LM-gF task fMRI data. Bold values represent the best classification performance obtained for each batch size.

| Batch size | Node embeddings | Metrics | | | | | | | |
|---|---|---|---|---|---|---|---|---|---|
| | | Accuracy | Balanced accuracy | F1 macro | F1 micro | F1 weighted | MCC | Precision | Recall |
| 16 | Walklets | 0.876 | 0.877 | 0.876 | 0.876 | 0.875 | 0.855 | 0.878 | 0.878 |
| | Node2Vec | 0.876 | 0.878 | 0.878 | 0.876 | 0.877 | 0.855 | 0.882 | 0.879 |
| | RandNE | **0.945** | **0.944** | **0.944** | **0.945** | **0.945** | **0.936** | **0.946** | **0.944** |
| | NetMF | 0.921 | 0.92 | 0.921 | 0.921 | 0.92 | 0.909 | 0.922 | 0.92 |
| 32 | Walklets | 0.901 | 0.90 | 0.901 | 0.901 | 0.90 | 0.883 | 0.902 | 0.90 |
| | Node2Vec | 0.92 | 0.921 | 0.92 | 0.921 | 0.921 | 0.907 | 0.92 | 0.921 |
| | RandNE | **0.98** | **0.979** | **0.979** | **0.98** | **0.98** | **0.975** | **0.979** | **0.979** |
| | NetMF | 0.942 | 0.941 | 0.942 | 0.942 | 0.942 | 0.932 | 0.943 | 0.941 |
| 48 | Walklets | 0.92 | 0.919 | 0.919 | 0.92 | 0.919 | 0.906 | 0.92 | 0.919 |
| | Node2Vec | 0.915 | 0.915 | 0.915 | 0.916 | 0.915 | 0.901 | 0.916 | 0.916 |
| | RandNE | **0.988** | **0.987** | **0.988** | **0.988** | **0.988** | **0.983** | **0.987** | **0.987** |
| | NetMF | 0.948 | 0.947 | 0.947 | 0.947 | 0.948 | 0.939 | 0.947 | 0.947 |
| 64 | Walklets | 0.92 | 0.92 | 0.918 | 0.919 | 0.92 | 0.907 | 0.922 | 0.921 |
| | Node2Vec | 0.906 | 0.906 | 0.905 | 0.906 | 0.906 | 0.891 | 0.908 | 0.907 |
| | RandNE | **0.988** | **0.988** | **0.988** | **0.988** | **0.987** | **0.986** | **0.988** | **0.988** |
| | NetMF | 0.944 | 0.943 | 0.943 | 0.944 | 0.944 | 0.935 | 0.946 | 0.94 |

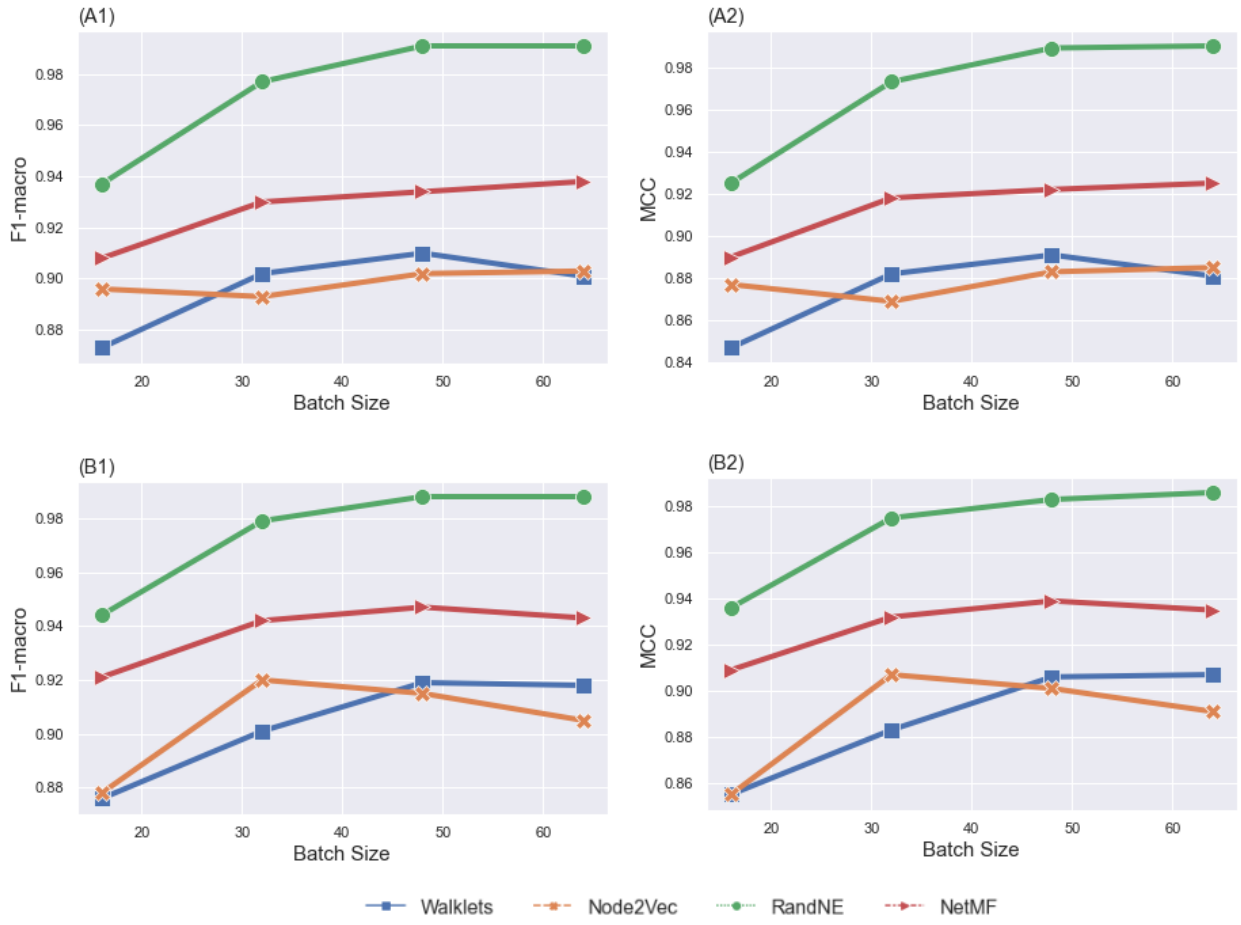


Figure 4.4. F1 macro and MCC comparison of the GCN model, taking into account the effects of node embedding methods and batch sizes, by using LM-gF task fMRI data (A1, A2) and HM-gF task fMRI data (B1, B2).

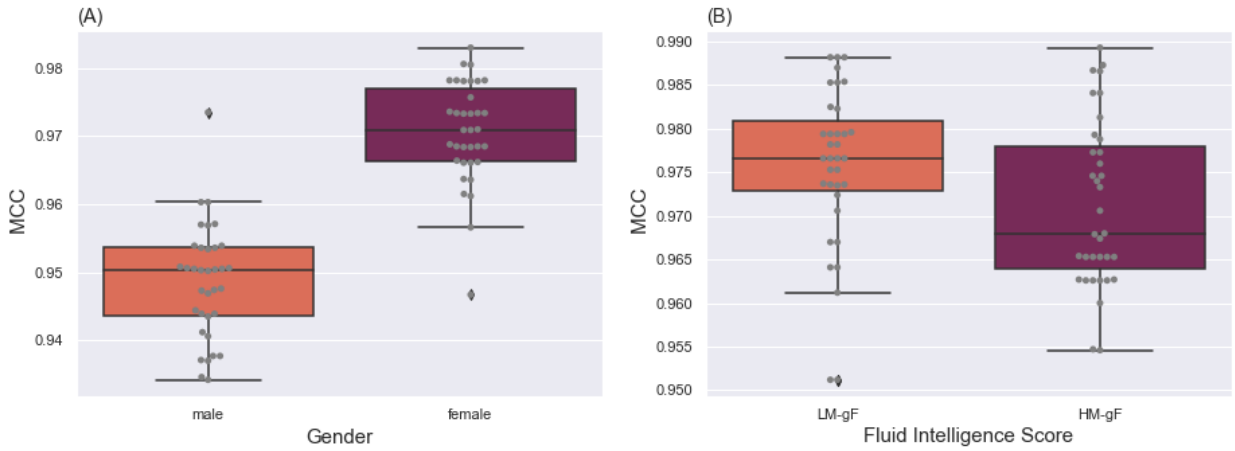


Figure 4.5. Box plots of classification performance of the GCN model in 35 independent runs, by using gender sub-datasets (A) and fluid intelligence sub-datasets (B). Significant differences in classification performance of task fMRI data were observed between female and male data, but not between high and low fluid intelligence data.

# CHAPTER FIVE: DISCUSSION

## Overview

In this study, we developed a classification framework based on a GCN model, which has been recently been proposed as a successful solution to the node classification task in graph-structured data. GCN can aggregate the high-order information of neighborhoods from graph nodes representing regions of interest and edges representing the functional connectivity between brain regions. This important feature allows researchers to use GCN to efficiently model the human brain network in various applications (Xing *et al.*, 2019; Yu *et al.*, 2019; Zhang and Huang, 2019; S. Yu *et al.*, 2020). Our study achieved an accuracy of 97.7% in a seven-class classification task, thus demonstrating a competitive classification performance for brain state decoding, with respect to those recently reported across task fMRI data by using the HCP dataset (Gui, Chen and Nie, 2020; Wang *et al.*, 2020; Huang, Xiao and Wu, 2021; X. Li *et al.*, 2021). Inspired by reference (X. Li *et al.*, 2021), our proposed model included three Conv layers, in which we first implemented several node embedding methods to extract the topological features of nodes and defined node weight. Then the first Conv layer was fed by using different node embedding weights instead of using the same weights for all nodes. To this end, we tested four node embeddings (i.e., NetMF, RandNE, Node2Vec, and Walklets) and observed that our GCN model using NetMF and RandNE tended to yield the best results for classification task fMRI data.

Furthermore, our findings confirmed the importance of selecting a proper node embedding method to extract topological features of graph nodes before feeding the GCN model, in

agreement with previous research detecting influenza-like symptoms with a GNN model (Dong *et al.*, 2021).

## Effects of Individual Differences

We examined the effects of individual differences on task fMRI classification in terms of gender and gF score discrepancy. With respect to gender differences, the performance of the proposed GCN model was tested on two sub-datasets (female/male) by considering four node embedding methods. The same procedure was applied to gF-associated sub-datasets (LM-gF/HM-gF). The p-value for classification performance between female and male sub-datasets was significantly less than 0.05, indicating a significant difference in task fMRI classification performance between these sub-datasets. However, no significant difference was observed in classification performance at a 95% confidence interval, because the p-value was greater than 0.05. These results can be considered evidence of gender-related differences in brain functional connectivity. Gender differences are associated with performance in spatial perception, memory, and verbal skills (Miller and Halpern, 2014; Siedlecki, Falzarano and Salthouse, 2019). Extensive research has addressed resting-state brain functional connectivity differences between men and women (Bluhm *et al.*, 2008; C. Zhang *et al.*, 2018; J. Zhang *et al.*, 2018), and reported that women have strong functional connectivity in the default mode of the brain's network (Sen and Parhi, 2019a). Furthermore, Sen and Parhi (Sen and Parhi, 2019a) have investigated the ability of task fMRI functional connectivity discrepancies to predict gender. The results of that study, in agreement with our findings, have shown that functional connectivity associated with relational, motor, social, gambling, and emotion differs between women and men, so that gender identity can be efficiently assessed on the basis of these differences.

## Impact of Batch Size

Training a DL model involves selecting a large set of hyperparameters, among which batch size is important (Ioffe, machine and 2015, no date). Batch size defines the number of training samples used in one iteration to update the internal network parameters. To achieve the best accuracy performance of the GCN model associated with the batch size values, we chose a sequence of batch sizes of 16, 32, 48, and 64, and applied GCN architectures to each dataset. This approach allowed us to obtain the best classification performance for each experiment. The trend of the batch size change influenced the classification performance for all considered datasets. The worst classification performance values were obtained with a batch size of 16, and the best results were achieved with batch sizes of 48 and 64.

# CHAPTER SIX: CONCLUSION

We proposed a GCN framework to decode task fMRI data. Four node embedding methods—NetMF, RandNE, Node2Vec, and Walklets—were used to extract the topological features of graph nodes. We compared the performance of the model with different node embeddings through experiments and assessed classification accuracy. We further examined whether individual differences, specifically gender and fluid intelligence discrepancies, affect task fMRI data classification performance. Several conclusions were drawn. First, the overall task fMRI classification of the GCN model resulted in an F1 macro and MCC of 0.977 and 0.974, respectively. Second, the most robust node embedding methods for task fMRI data were NetMF and RandNE, whereas the least robust node embedding method was Node2Vec. Third, the influence of gender differences on task fMRI classification performance was significant, whereas no significant difference was observed between gF score categories.

## Research Contribution

The major contribution of this study are as follow:

1. We propose an end-to-end GCN framework to classify task-evoked fMRI data. The objective is to examine the performance of various node embeddings to generate topological embeddings of the graph's nodes. To our knowledge, this is the first investigation of different node embeddings on task fMRI classification performance using the HCP dataset.

2. We demonstrate the performance of the proposed GCN framework according to individual differences (i.e., gender and fluid intelligence). To this end, we constructed four small sub-datasets of gender (female/male) and gF score (LM-gF/HM-gF) with replacement. We endeavored to examine whether gender and gF score might affect task fMRI classification performance.

## Limitation and Future Directions

Our current study has several limitations that should be considered in future research. Although this study examined several node embedding methods to represent the graph nodes as low dimensional vectors, we disregarded the influence of the dimensionality of the node embeddings. Although finding the optimal dimension for embedding methods is challenging, some studies have applied several embedding dimensions on various datasets and achieved varying performance (Goyal and Ferrara, 2018; Martin and Riebeling, 2020). Therefore, the node embedding method must be customized to our dataset in future work. Furthermore, although batch size is an important hyperparameter to be considered in training a DL model (Ioffe, machine and 2015, no date), and we refitted our GCN model with different batch sizes and analyzed the effects of the change in batch size on classification performance, more hyperparameters should be studied, such as the number of convolutional layers, pooling ratio, and different readout operations. Finally, we analyzed only the task fMRI dataset for 302 participants and concluded that gender differences can affect classification performance. However, the ability to generalize our findings should be studied over a large number of participants and evaluated our decoding model for experimental conditions under each task fMRI.

# APPENDIX A: HCP DATA USE AGREEMENT

Human Connectome Project

# HCP Data Use Agreement

**I request access to data collected by the Human Connectome Project (HCP) for the purpose of scientific investigation, teaching or the planning of clinical research studies and agree to the following terms:**

1. I will receive access to de-identified data and will not attempt to establish the identity of, or attempt to contact any of the HCP subjects.
2. I will not further disclose these data beyond the uses outlined in this agreement and my data use application.
3. I will require anyone on my team who utilizes these data, or anyone with whom I share these data to comply with this data use agreement.
4. I will accurately provide the requested information for persons who will use these data and the analyses that are planned using these data.
5. I will respond promptly and accurately to requests to update this information.
6. I will comply with any rules and regulations imposed by my institution and its institutional review board in requesting these data.
7. I will ensure that Investigators who utilize HCP data use appropriate administrative, physical and technical safeguards to prevent use or disclosure of the data other than as provided for by this Agreement.
8. I will report any use or disclosure of the data not provided for by this Agreement of which I become aware within 15 days of becoming aware of such use or disclosure.

If I publish abstracts using data from HCP, I agree to the following:

9. I will cite HCP as the source of data and the HCP funding sources in the abstract as space allows in the acknowledgements.
10. Group authorship of HCP will not be cited in the authorship line of the abstract.If I publish manuscripts using data from HCP, I agree to the following:
11. I will acknowledge the HCP project as a source of data and include language similar to the following:

    * Data collection and sharing for this project was provided by the **Human Connectome Project** (HCP; Principal Investigators: Bruce Rosen, M.D., Ph.D., Arthur W. Toga, Ph.D., Van J. Weeden, MD). HCP funding was provided by the National Institute of Dental and Craniofacial Research (NIDCR), the National Institute of Mental Health (NIMH), and the National Institute of Neurological Disorders and Stroke (NINDS). HCP data are disseminated by the Laboratory of Neuro Imaging at the University of Southern California.

12. I will include language similar to the following in the methods section of my manuscripts in order to accurately acknowledge data gathering by the HCP investigators. Depending upon the length and focus of the article, it may be appropriate to include more or less than the example below, however, inclusion of some variation of the language shown below is mandatory. "Data used in the preparation of this work were obtained from the **Human Connectome Project (HCP)** database (https://ida.loni.usc.edu/login.jsp). The HCP project (Principal Investigators: Bruce Rosen, M.D., Ph.D., Martinos Center at Massachusetts General Hospital; Arthur W. Toga, Ph.D., University of Southern California, Van J. Weeden, MD, Martinos Center at Massachusetts General Hospital) is supported by the National Institute of Dental and Craniofacial Research (NIDCR), the National Institute of Mental Health (NIMH) and the National Institute of Neurological Disorders and Stroke (NINDS). HCP is the result of efforts of co-investigators from the University of Southern California, Martinos Center for Biomedical Imaging at Massachusetts General Hospital (MGH), Washington University, and the University of Minnesota."

I understand that failure to abide by these guidelines will result in termination of my privileges to access HCP data.

# APPENDIX B: IRB DETERMINATION

UNIVERSITY OF CENTRAL FLORIDA

**Institutional Review Board**
FWA00000351
IRB00001138, IRB00012110
Office of Research
12201 Research Parkway
Orlando, FL 32826-3246

NOT HUMAN RESEARCH DETERMINATION

June 17, 2022

Dear Maham Saeidi:

On 6/17/2022, the IRB reviewed the following protocol:

| | |
|---|---|
| Type of Review: | Modification / Update |
| Title of Study: | Decoding task-based fMRI data with graph neural networks, considering individual differences |
| Investigator: | Maham Saeidi |
| IRB ID: | MOD00003001 |
| Funding: | None |
| Grant ID: | None |
| Documents Reviewed: | • HRP-250-FORM- Request for NHSR, Category: IRB Protocol; |

The IRB determined that the proposed activity is not research involving human subjects as defined by DHHS and FDA regulations.

IRB review and approval by this organization is not required. This determination applies only to the activities described in the IRB submission and does not apply should any changes be made. If changes are made and there are questions about whether these activities are research involving human in which the organization is engaged, please submit a new request to the IRB for a determination. You can create a modification by clicking **Create Modification / CR** within the study.

If you have any questions, please contact the UCF IRB at 407-823-2901 or irb@ucf.edu. Please include your project title and IRB number in all correspondence with this office.

Sincerely,

Renea Carver
UCF IRB

# LIST OF REFERENCES

Abiodun, O. I. *et al.* (2018) 'State-of-the-art in artificial neural network applications: A survey', *Heliyon*. Elsevier, 4(11), p. e00938. doi: 10.1016/J.HELIYON.2018.E00938.

Ahmedt-Aristizabal, D. *et al.* (2021) 'Graph-Based Deep Learning for Medical Diagnosis and Analysis: Past, Present and Future', *Sensors 2021, Vol. 21, Page 4758*. Multidisciplinary Digital Publishing Institute, 21(14), p. 4758. doi: 10.3390/S21144758.

Al-Kadi, M. I., Reaz, M. B. I. and Mohd Ali, M. A. (2013) 'Evolution of Electroencephalogram Signal Analysis Techniques during Anesthesia', *Sensors 2013, Vol. 13, Pages 6605-6635*. Multidisciplinary Digital Publishing Institute, 13(5), pp. 6605–6635. doi: 10.3390/S130506605.

Al-Saegh, A., Dawwd, S. A. and Abdul-Jabbar, J. M. (2021) 'Deep learning for motor imagery EEG-based classification: A review', *Biomedical Signal Processing and Control*. Elsevier, 63, p. 102172. doi: 10.1016/J.BSPC.2020.102172.

Al-Shboul, B. *et al.* (2016) 'Voting-based Classification for E-mail Spam Detection.', *researchgate.net*. doi: 10.5614/itbj.ict.res.appl.2016.10.1.3.

Al-Zubaidi, A. *et al.* (2019) 'Machine learning based classification of resting-state fMRI features exemplified by metabolic state (hunger/satiety)', *Frontiers in Human Neuroscience*. Frontiers Media S.A., 13, p. 164. doi: 10.3389/FNHUM.2019.00164/BIBTEX.

Albert, M. S. *et al.* (2011) 'The diagnosis of mild cognitive impairment due to Alzheimer's disease: Recommendations from the National Institute on Aging-Alzheimer's Association workgroups on diagnostic guidelines for Alzheimer's disease', *Alzheimer's & Dementia*. John

Wiley & Sons, Ltd, 7(3), pp. 270–279. doi: 10.1016/J.JALZ.2011.03.008.

Althnian, A. *et al.* (2021) 'Impact of Dataset Size on Classification Performance: An Empirical Evaluation in the Medical Domain', *Applied Sciences 2021, Vol. 11, Page 796*. Multidisciplinary Digital Publishing Institute, 11(2), p. 796. doi: 10.3390/APP11020796.

An, X. *et al.* (2020) 'Dynamic Functional Connectivity and Graph Convolution Network for Alzheimer's Disease Classification', *ACM International Conference Proceeding Series*. Association for Computing Machinery, pp. 1–4. doi: 10.1145/3444884.3444885.

Anirudh, R. and Thiagarajan, J. J. (2019) 'Bootstrapping Graph Convolutional Neural Networks for Autism Spectrum Disorder Classification', *ICASSP, IEEE International Conference on Acoustics, Speech and Signal Processing - Proceedings*. Institute of Electrical and Electronics Engineers Inc., 2019-May, pp. 3197–3201. doi: 10.1109/ICASSP.2019.8683547.

Arslan, S. *et al.* (2018) 'Graph saliency maps through spectral convolutional networks: Application to sex classification with brain connectivity', *Lecture Notes in Computer Science (including subseries Lecture Notes in Artificial Intelligence and Lecture Notes in Bioinformatics)*. Springer Verlag, 11044 LNCS, pp. 3–13. doi: 10.1007/978-3-030-00689-1_1/FIGURES/3.

Atwood, J. and Towsley, D. (2015) 'Diffusion-Convolutional Neural Networks', *Advances in Neural Information Processing Systems*. Neural information processing systems foundation, pp. 2001–2009. doi: 10.48550/arxiv.1511.02136.

Azevedo, T., Campbell, A., *et al.* (2020) 'A Deep Graph Neural Network Architecture for Modelling Spatio-temporal Dynamics in resting-state functional MRI Data', *bioRxiv*. Cold

Spring Harbor Laboratory, p. 2020.11.08.370288. doi: 10.1101/2020.11.08.370288.

Azevedo, T., Passamonti, L., Lio, P., *et al.* (2020) 'A deep spatiotemporal graph learning architecture for brain connectivity analysis', *Proceedings of the Annual International Conference of the IEEE Engineering in Medicine and Biology Society, EMBS*. Institute of Electrical and Electronics Engineers Inc., 2020-July, pp. 1120–1123. doi: 10.1109/EMBC44109.2020.9175360.

Azevedo, T., Passamonti, L., Liò, P., *et al.* (2020) 'Towards a predictive spatio-temporal representation of brain data'. doi: 10.48550/arxiv.2003.03290.

Balakrishnama, S., Ganapathiraju, A. and Picone, J. (1999) 'Linear discriminant analysis for signal processing problems', *Conference Proceedings - IEEE SOUTHEASTCON*. Institute of Electrical and Electronics Engineers Inc., 1999-March, pp. 78–81. doi: 10.1109/SECON.1999.766096.

Bandos, T. V., Bruzzone, L. and Camps-Valls, G. (2009) 'Classification of hyperspectral images with regularized linear discriminant analysis', *IEEE Transactions on Geoscience and Remote Sensing*, 47(3), pp. 862–873. doi: 10.1109/TGRS.2008.2005729.

Banka, A. and Rekik, I. (2019) 'Adversarial connectome embedding for mild cognitive impairment identification using cortical morphological networks', *Lecture Notes in Computer Science (including subseries Lecture Notes in Artificial Intelligence and Lecture Notes in Bioinformatics)*. Springer, 11848 LNCS, pp. 74–82. doi: 10.1007/978-3-030-32391-2_8/FIGURES/2.

Barch, D. M. *et al.* (2013) 'Function in the human connectome: Task-fMRI and individual differences in behavior', *NeuroImage*. Academic Press, 80, pp. 169–189. doi:

10.1016/J.NEUROIMAGE.2013.05.033.

Bassett, D. S. and Bullmore, E. T. (2009) ‘Human Brain Networks in Health and Disease’, *Current opinion in neurology*. NIH Public Access, 22(4), p. 340. doi: 10.1097/WCO.0B013E32832D93DD.

Beckett, L. A. *et al.* (2015) ‘The Alzheimer’s Disease Neuroimaging Initiative phase 2: Increasing the length, breadth, and depth of our understanding’, *Alzheimer’s & Dementia*. No longer published by Elsevier, 11(7), pp. 823–831. doi: 10.1016/J.JALZ.2015.05.004.

Beckmann, C. F. *et al.* (2005) ‘Investigations into resting-state connectivity using independent component analysis’, *Philosophical Transactions of the Royal Society B: Biological Sciences*. The Royal SocietyLondon, 360(1457), pp. 1001–1013. doi: 10.1098/RSTB.2005.1634.

Beckmann, C. F. and Smith, S. M. (2004) ‘Probabilistic Independent Component Analysis for Functional Magnetic Resonance Imaging’, *IEEE Transactions on Medical Imaging*, 23(2), pp. 137–152. doi: 10.1109/TMI.2003.822821.

Behri, M., Subasi, A. and Qaisar, S. M. (2018) ‘Comparison of machine learning methods for two class motor imagery tasks using EEG in brain-computer interface’, *2018 Advances in Science and Engineering Technology International Conferences, ASET 2018*. Institute of Electrical and Electronics Engineers Inc., pp. 1–5. doi: 10.1109/ICASET.2018.8376886.

Bellec, P. *et al.* (2017) ‘The Neuro Bureau ADHD-200 Preprocessed repository’, *NeuroImage*. Academic Press, 144, pp. 275–286. doi: 10.1016/J.NEUROIMAGE.2016.06.034.

Bengio, Y. *et al.* (no date) ‘Unsupervised feature learning and deep learning: A review and new

perspectives', *docs.huihoo.com*. Available at: https://docs.huihoo.com/deep-learning/Representation-Learning-A-Review-and-New-Perspectives-v1.pdf (Accessed: 30 April 2022).

Benjamini, Y. and Yekutieli, D. (2001) 'The control of the false discovery rate in multiple testing under dependency', *https://doi.org/10.1214/aos/1013699998*. Institute of Mathematical Statistics, 29(4), pp. 1165–1188. doi: 10.1214/AOS/1013699998.

Bernhardt, B. C., Bonilha, L. and Gross, D. W. (2015) 'Network analysis for a network disorder: The emerging role of graph theory in the study of epilepsy', *Epilepsy & Behavior*. Academic Press, 50, pp. 162–170. doi: 10.1016/J.YEBEH.2015.06.005.

Beyer, K. *et al.* (1999) 'When Is "Nearest Neighbor" Meaningful?', *Lecture Notes in Computer Science (including subseries Lecture Notes in Artificial Intelligence and Lecture Notes in Bioinformatics)*. Springer, Berlin, Heidelberg, 1540, pp. 217–235. doi: 10.1007/3-540-49257-7_15.

Bhattacharya, S. *et al.* (2021) 'Deep learning and medical image processing for coronavirus (COVID-19) pandemic: A survey', *Sustainable Cities and Society*. Elsevier, 65, p. 102589. doi: 10.1016/J.SCS.2020.102589.

Bi, X. *et al.* (2020) 'GNEA: A Graph Neural Network with ELM Aggregator for Brain Network Classification', *Complexity*. Hindawi Limited, 2020. doi: 10.1155/2020/8813738.

Bi, Y. *et al.* (2020) 'Graph-Based Spatiooral Feature Learning for Neuromorphic Vision Sensing', *IEEE Transactions on Image Processing*. Institute of Electrical and Electronics Engineers Inc., 29, pp. 9084–9098. doi: 10.1109/TIP.2020.3023597.

Bishara, A. J. and Hittner, J. B. (2012) ‘Testing the significance of a correlation with nonnormal data: Comparison of Pearson, Spearman, transformation, and resampling approaches’, *Psychological Methods*, 17(3), pp. 399–417. doi: 10.1037/A0028087.

Bluhm, R. L. *et al.* (2008) ‘Default mode network connectivity: Effects of age, sex, and analytic approach’, *NeuroReport*, 19(8), pp. 887–891. doi: 10.1097/WNR.0B013E328300EBBF.

Bojchevski, A. and Günnemann, S. (2017) ‘Deep Gaussian Embedding of Graphs: Unsupervised Inductive Learning via Ranking’, *6th International Conference on Learning Representations, ICLR 2018 - Conference Track Proceedings*. International Conference on Learning Representations, ICLR. doi: 10.48550/arxiv.1707.03815.

Borgomaneri, S. *et al.* (2020) ‘State-Dependent TMS over Prefrontal Cortex Disrupts Fear-Memory Reconsolidation and Prevents the Return of Fear’, *Current Biology*. Cell Press, 30(18), pp. 3672-3679.e4. doi: 10.1016/J.CUB.2020.06.091.

Braun, U. *et al.* (2015) ‘Dynamic reconfiguration of frontal brain networks during executive cognition in humans’, *Proceedings of the National Academy of Sciences of the United States of America*. National Academy of Sciences, 112(37), pp. 11678–11683. doi: 10.1073/PNAS.1422487112.

Brown, S. A. *et al.* (2015) ‘The National Consortium on Alcohol and NeuroDevelopment in Adolescence (NCANDA): A Multisite Study of Adolescent Development and Substance Use’, *http://dx.doi.org/10.15288/jsad.2015.76.895*. Rutgers University, 76(6), pp. 895–908. doi: 10.15288/JSAD.2015.76.895.

Bruna, J. *et al.* (2013) ‘Spectral Networks and Locally Connected Networks on Graphs’, *2nd*

*International Conference on Learning Representations, ICLR 2014 - Conference Track Proceedings*. International Conference on Learning Representations, ICLR. doi: 10.48550/arxiv.1312.6203.

Bruzzone, S. E. P. *et al.* (2022) 'Dissociated brain functional connectivity of fast versus slow frequencies underlying individual differences in fluid intelligence: a DTI and MEG study', *Scientific Reports 2022 12:1*. Nature Publishing Group, 12(1), pp. 1–15. doi: 10.1038/s41598-022-08521-5.

Bullmore, E. and Sporns, O. (2009) 'Complex brain networks: graph theoretical analysis of structural and functional systems', *Nature Reviews Neuroscience 2009 10:3*. Nature Publishing Group, 10(3), pp. 186–198. doi: 10.1038/nrn2575.

Cai, H., Zheng, V. W. and Chang, K. C. C. (2018) 'A Comprehensive Survey of Graph Embedding: Problems, Techniques, and Applications', *IEEE Transactions on Knowledge and Data Engineering*. IEEE Computer Society, 30(9), pp. 1616–1637. doi: 10.1109/TKDE.2018.2807452.

Calhoun, V. D. *et al.* (2001) 'A method for making group inferences from functional MRI data using independent component analysis', *Human Brain Mapping*, 14(3), pp. 140–151. doi: 10.1002/HBM.1048.

Calhoun, V. D. and Adali, T. (2012) 'Multisubject independent component analysis of fMRI: A decade of intrinsic networks, default mode, and neurodiagnostic discovery', *IEEE Reviews in Biomedical Engineering*, 5, pp. 60–73. doi: 10.1109/RBME.2012.2211076.

Calhoun, V. D., Liu, J. and Adali, T. (2009) 'A review of group ICA for fMRI data and ICA for

joint inference of imaging, genetic, and ERP data', *NeuroImage*. Academic Press, 45(1), pp. S163–S172. doi: 10.1016/J.NEUROIMAGE.2008.10.057.

Casas, S. *et al.* (2020) 'SpAGNN: Spatially-Aware Graph Neural Networks for Relational Behavior Forecasting from Sensor Data', *Proceedings - IEEE International Conference on Robotics and Automation*. Institute of Electrical and Electronics Engineers Inc., pp. 9491–9497. doi: 10.1109/ICRA40945.2020.9196697.

Chen, Z. S. *et al.* (2017) 'A PSO based virtual sample generation method for small sample sets: Applications to regression datasets', *Engineering Applications of Artificial Intelligence*. Pergamon, 59, pp. 236–243. doi: 10.1016/J.ENGAPPAI.2016.12.024.

Cheng, X., Ning, H. and Du, B. (2021) 'A Survey: Challenges and Future Research Directions of fMRI Based Brain Activity Decoding Model', *2021 International Wireless Communications and Mobile Computing, IWCMC 2021*. Institute of Electrical and Electronics Engineers Inc., pp. 957–960. doi: 10.1109/IWCMC51323.2021.9498710.

Chicco, D. and Jurman, G. (2020) 'The advantages of the Matthews correlation coefficient (MCC) over F1 score and accuracy in binary classification evaluation', *BMC Genomics*. BioMed Central Ltd., 21(1), pp. 1–13. doi: 10.1186/S12864-019-6413-7/TABLES/5.

Cho, K. *et al.* (2014) 'Learning Phrase Representations using RNN Encoder-Decoder for Statistical Machine Translation', *EMNLP 2014 - 2014 Conference on Empirical Methods in Natural Language Processing, Proceedings of the Conference*. Association for Computational Linguistics (ACL), pp. 1724–1734. doi: 10.48550/arxiv.1406.1078.

Christ, M. *et al.* (2018) 'Time Series FeatuRe Extraction on basis of Scalable Hypothesis tests

(tsfresh – A Python package)', *Neurocomputing*. Elsevier, 307, pp. 72–77. doi: 10.1016/J.NEUCOM.2018.03.067.

Christ, M., Kempa-Liehr, A. W. and Feindt, M. (2016) 'Distributed and parallel time series feature extraction for industrial big data applications'. doi: 10.48550/arxiv.1610.07717.

Cocchi, L. *et al.* (2012) 'Altered Functional Brain Connectivity in a Non-Clinical Sample of Young Adults with Attention-Deficit/Hyperactivity Disorder', *Journal of Neuroscience*. Society for Neuroscience, 32(49), pp. 17753–17761. doi: 10.1523/JNEUROSCI.3272-12.2012.

Conklin, J. D. (2002) 'Applied logistic regression', *Technometrics*. Informa UK Limited, 44(1), pp. 81–82. doi: 10.1198/tech.2002.s650.

Cosmo, L. *et al.* (2020) 'Latent-Graph Learning for Disease Prediction', *Lecture Notes in Computer Science (including subseries Lecture Notes in Artificial Intelligence and Lecture Notes in Bioinformatics)*. Springer Science and Business Media Deutschland GmbH, 12262 LNCS, pp. 643–653. doi: 10.1007/978-3-030-59713-9_62/FIGURES/3.

Craddock, R. C. *et al.* (2013) 'Imaging human connectomes at the macroscale', *Nature Methods 2013 10:6*. Nature Publishing Group, 10(6), pp. 524–539. doi: 10.1038/nmeth.2482.

Craik, A., He, Y. and Contreras-Vidal, J. L. (2019) 'Deep learning for electroencephalogram (EEG) classification tasks: a review', *Journal of Neural Engineering*. IOP Publishing, 16(3), p. 031001. doi: 10.1088/1741-2552/AB0AB5.

Crosson, B. *et al.* (2010) 'Functional Imaging and Related Techniques: An Introduction for Rehabilitation Researchers', *Journal of rehabilitation research and development*. NIH Public

Access, 47(2), p. vii. doi: 10.1682/JRRD.2010.02.0017.

Dai, H. *et al.* (2017) 'Learning combinatorial optimization algorithms over graphs', *Advances in Neural Information Processing Systems*. Neural information processing systems foundation, 2017-December, pp. 6349–6359.

Dalmia, A., Ganesh, J. and Gupta, M. (2018) 'Towards Interpretation of Node Embeddings', *The Web Conference 2018 - Companion of the World Wide Web Conference, WWW 2018*. Association for Computing Machinery, Inc, pp. 945–952. doi: 10.1145/3184558.3191523.

Defferrard, M., Bresson, X. and Vandergheynst, P. (2016) 'Convolutional Neural Networks on Graphs with Fast Localized Spectral Filtering', *Advances in Neural Information Processing Systems*. Neural information processing systems foundation, pp. 3844–3852. doi: 10.48550/arxiv.1606.09375.

Dong, G. *et al.* (2021) 'Influenza-like symptom recognition using mobile sensing and graph neural networks', *ACM CHIL 2021 - Proceedings of the 2021 ACM Conference on Health, Inference, and Learning*. Association for Computing Machinery, Inc, 21, pp. 291–300. doi: 10.1145/3450439.3451880.

Dong, Q. *et al.* (2020) 'Modeling hierarchical brain networks via volumetric sparse deep belief network', *IEEE Transactions on Biomedical Engineering*. IEEE Computer Society, 67(6), pp. 1739–1748. doi: 10.1109/TBME.2019.2945231.

Du, S. C., Huang, D. L. and Wang, H. (2015) 'An Adaptive Support Vector Machine-Based Workpiece Surface Classification System Using High-Definition Metrology', *IEEE Transactions on Instrumentation and Measurement*. Institute of Electrical and Electronics Engineers Inc.,

64(10), pp. 2590–2604. doi: 10.1109/TIM.2015.2418684.

Duvenaud, D. *et al.* (2015) 'Convolutional Networks on Graphs for Learning Molecular Fingerprints', *Advances in Neural Information Processing Systems*. Neural information processing systems foundation, 2015-January, pp. 2224–2232. doi: 10.48550/arxiv.1509.09292.

Ecker, C., Spooren, W. and Murphy, D. G. M. (2012) 'Translational approaches to the biology of Autism: false dawn or a new era?', *Molecular Psychiatry 2013 18:4*. Nature Publishing Group, 18(4), pp. 435–442. doi: 10.1038/mp.2012.102.

Van Essen, D. C. *et al.* (2013) 'The WU-Minn Human Connectome Project: An overview', *NeuroImage*. Academic Press, 80, pp. 62–79. doi: 10.1016/J.NEUROIMAGE.2013.05.041.

Fabry-Asztalos, L. *et al.* (2008) 'A genetic algorithm optimized fuzzy neural network analysis of the affinity of inhibitors for HIV-1 protease', *Bioorganic and Medicinal Chemistry*, 16(6), pp. 2903–2911. doi: 10.1016/J.BMC.2007.12.055.

Farahani, F. V., Karwowski, W. and Lighthall, N. R. (2019) 'Application of graph theory for identifying connectivity patterns in human brain networks: A systematic review', *Frontiers in Neuroscience*. Frontiers Media S.A., 13(JUN), p. 585. doi: 10.3389/FNINS.2019.00585/BIBTEX.

Faust, O. *et al.* (2018) 'Deep learning for healthcare applications based on physiological signals: A review', *Computer Methods and Programs in Biomedicine*. Elsevier, 161, pp. 1–13. doi: 10.1016/J.CMPB.2018.04.005.

Felouat, H. and Oukid-Khouas, S. (2020) 'Graph Convolutional Networks and Functional

Connectivity for Identification of Autism Spectrum Disorder', *2020 2nd International Conference on Embedded and Distributed Systems, EDiS 2020*. Institute of Electrical and Electronics Engineers Inc., pp. 27–32. doi: 10.1109/EDIS49545.2020.9296476.

Ferrarini, L. *et al.* (2009) 'Hierarchical functional modularity in the resting-state human brain', *Human Brain Mapping*. John Wiley & Sons, Ltd, 30(7), pp. 2220–2231. doi: 10.1002/HBM.20663.

Fey, M. and Lenssen, J. E. (2019) 'Fast Graph Representation Learning with PyTorch Geometric'. doi: 10.48550/arxiv.1903.02428.

Filip, A. C. *et al.* (2020) 'A novel Graph Attention Network Architecture for modeling multimodal brain connectivity', *Proceedings of the Annual International Conference of the IEEE Engineering in Medicine and Biology Society, EMBS*. Institute of Electrical and Electronics Engineers Inc., 2020-July, pp. 1071–1074. doi: 10.1109/EMBC44109.2020.9176613.

Fiok, K. *et al.* (2021) 'A Study of the Effects of the COVID-19 Pandemic on the Experience of Back Pain Reported on Twitter® in the United States: A Natural Language Processing Approach', *International Journal of Environmental Research and Public Health 2021, Vol. 18, Page 4543*. Multidisciplinary Digital Publishing Institute, 18(9), p. 4543. doi: 10.3390/IJERPH18094543.

Fout, A. *et al.* (no date) 'Protein interface prediction using graph convolutional networks', *proceedings.neurips.cc*. Available at: https://proceedings.neurips.cc/paper/2017/hash/f507783927f2ec2737ba40afbd17efb5-Abstract.html (Accessed: 31 May 2022).

Friston, K. J. *et al.* (1994) ‘Statistical parametric maps in functional imaging: A general linear approach’, *Human Brain Mapping*. John Wiley & Sons, Ltd, 2(4), pp. 189–210. doi: 10.1002/HBM.460020402.

Gadgil, S. *et al.* (2020) ‘Spatio-Temporal Graph Convolution for Resting-State fMRI Analysis’, *Lecture Notes in Computer Science (including subseries Lecture Notes in Artificial Intelligence and Lecture Notes in Bioinformatics)*. Springer Science and Business Media Deutschland GmbH, 12267 LNCS, pp. 528–538. doi: 10.1007/978-3-030-59728-3_52/FIGURES/4.

García-Prieto, J., Bajo, R. and Pereda, E. (2017) ‘Efficient computation of functional brain networks: Toward real-time functional connectivity’, *Frontiers in Neuroinformatics*. Frontiers Research Foundation, 11, p. 8. doi: 10.3389/FNINF.2017.00008/BIBTEX.

Garcia, G. N., Ebrahimi, T. and Vesin, J. M. (2003) ‘Support vector EEG classification in the Fourier and time-frequency correlation domains’, *International IEEE/EMBS Conference on Neural Engineering, NER*. IEEE Computer Society, 2003-January, pp. 591–594. doi: 10.1109/CNE.2003.1196897.

Géron, A. (2019) *Hands-on machine learning with Scikit-Learn, Keras, and TensorFlow: Concepts, tools, and techniques to build intelligent systems*. Available at: https://books.google.com/books?hl=en&lr=&id=HnetDwAAQBAJ&oi=fnd&pg=PT9&dq=Hands-on+Machine+Learning+with+Scikit-Learn,+Keras,+and+TensorFlow:+Concepts,+Tools,+and+Techniques+to+Build+Intelligent+Systems&ots=kPVsFLCOzb&sig=ouZxx6E9PiaZEsmvdWbkj39Cj9k (Accessed: 17 May 2022).

Glasser, M. F. *et al.* (2013) ‘The minimal preprocessing pipelines for the Human Connectome

Project', *NeuroImage*. Academic Press, 80, pp. 105–124. doi: 10.1016/J.NEUROIMAGE.2013.04.127.

Glasser, M. F. *et al.* (2016) 'A multi-modal parcellation of human cerebral cortex', *Nature 2016 536:7615*. Nature Publishing Group, 536(7615), pp. 171–178. doi: 10.1038/nature18933.

Goense, J., Bohraus, Y. and Logothetis, N. K. (2016) 'fMRI at high spatial resolution implications for BOLD-models', *Frontiers in Computational Neuroscience*. Frontiers Research Foundation, 10(Jun), p. 66. doi: 10.3389/FNCOM.2016.00066/BIBTEX.

Gong, D. *et al.* (2016) 'Functional Integration between Salience and Central Executive Networks: A Role for Action Video Game Experience', *Neural Plasticity*. Hindawi Limited, 2016. doi: 10.1155/2016/9803165.

Gori, M., Monfardini, G. and Scarselli, F. (2005) 'A new model for earning in raph domains', *Proceedings of the International Joint Conference on Neural Networks*, 2, pp. 729–734. doi: 10.1109/IJCNN.2005.1555942.

Goyal, P. and Ferrara, E. (2018) 'Graph embedding techniques, applications, and performance: A survey', *Knowledge-Based Systems*. Elsevier, 151, pp. 78–94. doi: 10.1016/J.KNOSYS.2018.03.022.

Gross, J. L., Yellen, J. and Anderson, M. (2018) 'Graph Theory and Its Applications', *Graph Theory and Its Applications*. Chapman and Hall/CRC. doi: 10.1201/9780429425134.

Grover, A. and Leskovec, J. (no date) 'node2vec: Scalable Feature Learning for Networks', *Proceedings of the 22nd ACM SIGKDD International Conference on Knowledge Discovery and*

*Data Mining*. New York, NY, USA: ACM. doi: 10.1145/2939672.

Gui, R., Chen, T. and Nie, H. (2020) 'Classification of Task-State fMRI Data Based on Circle-EMD and Machine Learning', *Computational Intelligence and Neuroscience*. Hindawi Limited, 2020. doi: 10.1155/2020/7691294.

Guo, S. *et al.* (2019) 'Attention Based Spatial-Temporal Graph Convolutional Networks for Traffic Flow Forecasting', *Proceedings of the AAAI Conference on Artificial Intelligence*. AAAI Press, 33(01), pp. 922–929. doi: 10.1609/AAAI.V33I01.3301922.

Hamilton, W. L., Ying, R. and Leskovec, J. (2017a) 'Inductive Representation Learning on Large Graphs', *Advances in Neural Information Processing Systems*. Neural information processing systems foundation, 2017-December, pp. 1025–1035. doi: 10.48550/arxiv.1706.02216.

Hamilton, W. L., Ying, R. and Leskovec, J. (2017b) 'Representation Learning on Graphs: Methods and Applications'. doi: 10.48550/arxiv.1709.05584.

Haykin, S., networks, N. N.-N. and 2004, undefined (no date) 'A comprehensive foundation', *ieeexplore.ieee.org*. Available at: https://ieeexplore.ieee.org/iel4/91/8807/x0153119.pdf (Accessed: 30 April 2022).

He, Y. and Evans, A. (2010) 'Graph theoretical modeling of brain connectivity', *Current Opinion in Neurology*, 23(4), pp. 341–350. doi: 10.1097/WCO.0B013E32833AA567.

Herculano-Houzel, S. (2009) 'The human brain in numbers: A linearly scaled-up primate brain', *Frontiers in Human Neuroscience*. Frontiers Media S. A., 3(NOV), p. 31. doi:

10.3389/NEURO.09.031.2009/BIBTEX.

Hjelm, R. D. *et al.* (2014) ‘Restricted Boltzmann machines for neuroimaging: An application in identifying intrinsic networks’, *NeuroImage*. Academic Press, 96, pp. 245–260. doi: 10.1016/J.NEUROIMAGE.2014.03.048.

Hochreiter, S. and Schmidhuber, J. (1997) ‘Long Short-Term Memory’, *Neural Computation*. MIT Press Journals, 9(8), pp. 1735–1780. doi: 10.1162/NECO.1997.9.8.1735.

Hosseini, M. *et al.* (no date) ‘A review on machine learning for EEG signal processing in bioengineering’, *ieeexplore.ieee.org*. Available at: https://ieeexplore.ieee.org/abstract/document/8972542/ (Accessed: 30 April 2022).

Hu, J. *et al.* (2019) ‘A Multichannel 2D Convolutional Neural Network Model for Task-Evoked fMRI Data Classification’, *Computational Intelligence and Neuroscience*. Hindawi Limited, 2019. doi: 10.1155/2019/5065214.

Hu, X. *et al.* (2015) ‘Sparsity-constrained fMRI decoding of visual saliency in naturalistic video streams’, *IEEE Transactions on Autonomous Mental Development*. Institute of Electrical and Electronics Engineers Inc., 7(2), pp. 65–75. doi: 10.1109/TAMD.2015.2409835.

Huang, C. L. and Wang, C. J. (2006) ‘A GA-based feature selection and parameters optimizationfor support vector machines’, *Expert Systems with Applications*. Pergamon, 31(2), pp. 231–240. doi: 10.1016/J.ESWA.2005.09.024.

Huang, H., Hu, X., Zhao, Y., *et al.* (2018) ‘Modeling Task fMRI Data Via Deep Convolutional Autoencoder’, *IEEE Transactions on Medical Imaging*. Institute of Electrical and Electronics

Engineers Inc., 37(7), pp. 1551–1561. doi: 10.1109/TMI.2017.2715285.

Huang, H., Hu, X., Dong, Q., *et al.* (2018) 'Modeling task fMRI data via mixture of deep expert networks', *Proceedings - International Symposium on Biomedical Imaging*. IEEE Computer Society, 2018-April, pp. 82–86. doi: 10.1109/ISBI.2018.8363528.

Huang, J. *et al.* (2020) 'Attention-Diffusion-Bilinear Neural Network for Brain Network Analysis', *IEEE Transactions on Medical Imaging*. Institute of Electrical and Electronics Engineers Inc., 39(7), pp. 2541–2552. doi: 10.1109/TMI.2020.2973650.

Huang, X., Xiao, J. and Wu, C. (2021) 'Design of Deep Learning Model for Task-Evoked fMRI Data Classification', *Computational Intelligence and Neuroscience*. Hindawi Limited, 2021. doi: 10.1155/2021/6660866.

Huang, Y. and Chung, A. C. S. (2020) 'Edge-Variational Graph Convolutional Networks for Uncertainty-Aware Disease Prediction', *Lecture Notes in Computer Science (including subseries Lecture Notes in Artificial Intelligence and Lecture Notes in Bioinformatics)*. Springer Science and Business Media Deutschland GmbH, 12267 LNCS, pp. 562–572. doi: 10.1007/978-3-030-59728-3_55/TABLES/4.

Ioffe, S., machine, C. S.-I. conference on and 2015, undefined (no date) 'Batch normalization: Accelerating deep network training by reducing internal covariate shift', *proceedings.mlr.press*. Available at: http://proceedings.mlr.press/v37/ioffe15.html (Accessed: 21 May 2022).

Jain, A. *et al.* (2015) 'Structural-RNN: Deep Learning on Spatio-Temporal Graphs', *Proceedings of the IEEE Computer Society Conference on Computer Vision and Pattern Recognition*. IEEE Computer Society, 2016-December, pp. 5308–5317. doi: 10.48550/arxiv.1511.05298.

Jang, H. *et al.* (no date) ‘Task-specific feature extraction and classification of fMRI volumes using a deep neural network initialized with a deep belief network: Evaluation using’, *Elsevier*. Available at: https://www.sciencedirect.com/science/article/pii/S1053811916300362?casa_token=DtwRv4GXbX4AAAAA:cyksg2NDphrG1fOOj4Ccgm1af3gRgy2wx_XzAI1FCMVhLHi5XWVDWm95ILf6B0zxGCqaOgeLag (Accessed: 3 June 2022).

Ji, C., Maurits, N. M. and Roerdink, J. B. T. M. (2019) ‘Comparison of brain connectivity networks using local structure analysis’, *Studies in Computational Intelligence*. Springer Verlag, 813, pp. 639–651. doi: 10.1007/978-3-030-05414-4_51/FIGURES/5.

Jiang, H. *et al.* (2020) ‘Hi-GCN: A hierarchical graph convolution network for graph embedding learning of brain network and brain disorders prediction’, *Computers in Biology and Medicine*. Pergamon, 127, p. 104096. doi: 10.1016/J.COMPBIOMED.2020.104096.

Jiang, R. *et al.* (2020) ‘Gender Differences in Connectome-based Predictions of Individualized Intelligence Quotient and Sub-domain Scores’, *Cerebral Cortex*. Oxford Academic, 30(3), pp. 888–900. doi: 10.1093/CERCOR/BHZ134.

Kaiser, M. D. *et al.* (2010) ‘Neural signatures of autism’, *Proceedings of the National Academy of Sciences of the United States of America*, 107(49), pp. 21223–21228. doi: 10.1073/PNAS.1010412107.

Karas, G. B. *et al.* (2004) ‘Global and local gray matter loss in mild cognitive impairment and Alzheimer’s disease’, *NeuroImage*. Academic Press, 23(2), pp. 708–716. doi: 10.1016/J.NEUROIMAGE.2004.07.006.

Kazeminejad, A. and Sotero, R. C. (2019) ‘Topological properties of resting-state FMRI functional networks improve machine learning-based autism classification’, *Frontiers in Neuroscience*. Frontiers Media S.A., 13(JAN), p. 1018. doi: 10.3389/FNINS.2018.01018/BIBTEX.

Kazi, A., Shekarforoush, S., *et al.* (2019) ‘InceptionGCN: Receptive Field Aware Graph Convolutional Network for Disease Prediction’, *Lecture Notes in Computer Science (including subseries Lecture Notes in Artificial Intelligence and Lecture Notes in Bioinformatics)*. Springer Verlag, 11492 LNCS, pp. 73–85. doi: 10.1007/978-3-030-20351-1_6/TABLES/3.

Kazi, A., Krishna, S. A., *et al.* (2019) ‘Self-attention equipped graph convolutions for disease prediction’, *Proceedings - International Symposium on Biomedical Imaging*. IEEE Computer Society, 2019-April, pp. 1896–1899. doi: 10.1109/ISBI.2019.8759274.

Keator, D. B. *et al.* (2016) ‘The Function Biomedical Informatics Research Network Data Repository’, *NeuroImage*. Academic Press, 124, pp. 1074–1079. doi: 10.1016/J.NEUROIMAGE.2015.09.003.

Kim, B.-H., Ye, J. C. and Kim, J.-J. (2021) ‘Learning Dynamic Graph Representation of Brain Connectome with Spatio-Temporal Attention’. Available at: http://arxiv.org/abs/2105.13495 (Accessed: 30 April 2022).

Kim, B. H. and Ye, J. C. (2020) ‘Understanding Graph Isomorphism Network for rs-fMRI Functional Connectivity Analysis’, *Frontiers in Neuroscience*. Frontiers Media S.A., 14, p. 630. doi: 10.3389/FNINS.2020.00630/BIBTEX.

Kipf, T. N. and Welling, M. (2016) ‘Semi-Supervised Classification with Graph Convolutional

Networks', *5th International Conference on Learning Representations, ICLR 2017 - Conference Track Proceedings*. International Conference on Learning Representations, ICLR. doi: 10.48550/arxiv.1609.02907.

Krause, B. *et al.* (2016) 'Multiplicative LSTM for sequence modelling', *5th International Conference on Learning Representations, ICLR 2017 - Workshop Track Proceedings*. International Conference on Learning Representations, ICLR. doi: 10.48550/arxiv.1609.07959.

Ktena, S. I. *et al.* (2017) 'Distance metric learning using graph convolutional networks: Application to functional brain networks', *Lecture Notes in Computer Science (including subseries Lecture Notes in Artificial Intelligence and Lecture Notes in Bioinformatics)*. Springer Verlag, 10433 LNCS, pp. 469–477. doi: 10.1007/978-3-319-66182-7_54/FIGURES/3.

Ktena, S. I. *et al.* (2018) 'Metric learning with spectral graph convolutions on brain connectivity networks', *NeuroImage*. Academic Press, 169, pp. 431–442. doi: 10.1016/J.NEUROIMAGE.2017.12.052.

Lecun, Y., Bengio, Y. and Hinton, G. (2015) 'Deep learning', *Nature 2015 521:7553*. Nature Publishing Group, 521(7553), pp. 436–444. doi: 10.1038/nature14539.

Li, D. C. *et al.* (2016) 'The attribute-trend-similarity method to improve learning performance for small datasets', *http://dx.doi.org/10.1080/00207543.2016.1213447*. Taylor & Francis, 55(7), pp. 1898–1913. doi: 10.1080/00207543.2016.1213447.

Li, H. *et al.* (2017) 'Brain explorer for connectomic analysis', *Brain Informatics*. Springer Berlin Heidelberg, 4(4), pp. 253–269. doi: 10.1007/S40708-017-0071-9/TABLES/1.

Li, Q. *et al.* (2021) 'Simultaneous spatial-temporal decomposition for connectome-scale brain networks by deep sparse recurrent auto-encoder', *Brain Imaging and Behavior*. Springer, 15(5), pp. 2646–2660. doi: 10.1007/S11682-021-00469-W/FIGURES/14.

Li, S. *et al.* (2019) 'Dysconnectivity of multiple brain networks in schizophrenia: A meta-analysis of resting-state functional connectivity', *Frontiers in Psychiatry*. Frontiers Media S.A., 10(JULY), p. 482. doi: 10.3389/FPSYT.2019.00482/BIBTEX.

Li, X. *et al.* (2019) 'Graph Neural Network for Interpreting Task-fMRI Biomarkers', *Lecture Notes in Computer Science (including subseries Lecture Notes in Artificial Intelligence and Lecture Notes in Bioinformatics)*. Springer Science and Business Media Deutschland GmbH, 11768 LNCS, pp. 485–493. doi: 10.1007/978-3-030-32254-0_54/FIGURES/5.

Li, X., Dvornek, N. C., *et al.* (2020) 'Graph embedding using Infomax for ASD classification and brain functional difference detection', *https://doi.org/10.1117/12.2549451*. SPIE, 11317, p. 1131702. doi: 10.1117/12.2549451.

Li, X., Zhou, Y., *et al.* (2020) 'Pooling Regularized Graph Neural Network for fMRI Biomarker Analysis', *Lecture Notes in Computer Science (including subseries Lecture Notes in Artificial Intelligence and Lecture Notes in Bioinformatics)*. Springer Science and Business Media Deutschland GmbH, 12267 LNCS, pp. 625–635. doi: 10.1007/978-3-030-59728-3_61/FIGURES/4.

Li, X. *et al.* (2021) 'BrainGNN: Interpretable Brain Graph Neural Network for fMRI Analysis', *Medical Image Analysis*. Elsevier, 74, p. 102233. doi: 10.1016/J.MEDIA.2021.102233.

Li, Y. *et al.* (2015) 'Gated Graph Sequence Neural Networks', *4th International Conference on*

*Learning Representations, ICLR 2016 - Conference Track Proceedings*. International Conference on Learning Representations, ICLR. doi: 10.48550/arxiv.1511.05493.

Liang, X. *et al.* (2016) 'Topologically Reorganized Connectivity Architecture of Default-Mode, Executive-Control, and Salience Networks across Working Memory Task Loads', *Cerebral Cortex*. Oxford Academic, 26(4), pp. 1501–1511. doi: 10.1093/CERCOR/BHU316.

Liégeois, R. *et al.* (no date) 'Resting brain dynamics at different timescales capture distinct aspects of human behavior', *nature.com*. Available at: https://www.nature.com/articles/s41467-019-10317-7 (Accessed: 31 May 2022).

Liu, J. *et al.* (2018) 'MMM: classification of schizophrenia using multi-modality multi-atlas feature representation and multi-kernel learning', *Multimedia Tools and Applications*. Springer New York LLC, 77(22), pp. 29651–29667. doi: 10.1007/S11042-017-5470-7/TABLES/4.

Liu, J. *et al.* (2020) 'Identification of early mild cognitive impairment using multi-modal data and graph convolutional networks', *BMC Bioinformatics*. BioMed Central Ltd, 21(6), pp. 1–12. doi: 10.1186/S12859-020-3437-6/TABLES/4.

Liu, L. *et al.* (2020) 'Deep convolutional neural network for accurate segmentation and quantification of white matter hyperintensities', *Neurocomputing*. Elsevier, 384, pp. 231–242. doi: 10.1016/J.NEUCOM.2019.12.050.

Lotte, F. *et al.* (2007) 'A review of classification algorithms for EEG-based brain–computer interfaces', *Journal of Neural Engineering*. IOP Publishing, 4(2), p. R1. doi: 10.1088/1741-2560/4/2/R01.

Lv, J. *et al.* (2017) ‘Task fMRI data analysis based on supervised stochastic coordinate coding’, *Medical Image Analysis*. Elsevier, 38, pp. 1–16. doi: 10.1016/J.MEDIA.2016.12.003.

Ma, Yao *et al.* (2019) ‘Graph Convolutional Networks with EigenPooling’, *Proceedings of the 25th ACM SIGKDD International Conference on Knowledge Discovery & Data Mining*. New York, NY, USA: ACM. doi: 10.1145/3292500.

Ma, Yi *et al.* (2019) ‘Spectral-based Graph Convolutional Network for Directed Graphs’. doi: 10.48550/arxiv.1907.08990.

Mahmood, U. *et al.* (2021) ‘A Deep Learning Model for Data-Driven Discovery of Functional Connectivity’, *Algorithms 2021, Vol. 14, Page 75*. Multidisciplinary Digital Publishing Institute, 14(3), p. 75. doi: 10.3390/A14030075.

Mao, R. *et al.* (2006) ‘A new method to assist small data set neural network learning’, *Proceedings - ISDA 2006: Sixth International Conference on Intelligent Systems Design and Applications,* 1, pp. 17–22. doi: 10.1109/ISDA.2006.67.

Marcos-Vidal, L. *et al.* (2018) ‘Local functional connectivity suggests functional immaturity in children with attention-deficit/hyperactivity disorder’, *Human Brain Mapping*. John Wiley & Sons, Ltd, 39(6), pp. 2442–2454. doi: 10.1002/HBM.24013.

Marinescu, R. V. *et al.* (2018) ‘TADPOLE Challenge: Prediction of Longitudinal Evolution in Alzheimer’s Disease’. doi: 10.48550/arxiv.1805.03909.

Markett, S. *et al.* (2018) ‘Working memory capacity and the functional connectome - insights from resting-state fMRI and voxelwise centrality mapping’, *Brain Imaging and Behavior*.

Springer New York LLC, 12(1), pp. 238–246. doi: 10.1007/S11682-017-9688-9/FIGURES/3.

Martin, C. and Riebeling, M. (2020) ‘A Process for the Evaluation of Node Embedding Methods in the Context of Node Classification’. doi: 10.48550/arxiv.2005.14683.

Di Martino, A. *et al.* (2013) ‘The autism brain imaging data exchange: towards a large-scale evaluation of the intrinsic brain architecture in autism’, *Molecular Psychiatry 2014 19:6*. Nature Publishing Group, 19(6), pp. 659–667. doi: 10.1038/mp.2013.78.

Mastrovito, D., Hanson, C. and Hanson, S. J. (2018) ‘Differences in atypical resting-state effective connectivity distinguish autism from schizophrenia’, *NeuroImage: Clinical*. Elsevier, 18, pp. 367–376. doi: 10.1016/J.NICL.2018.01.014.

McCulloch, W. S. and Pitts, W. (1943) ‘A logical calculus of the ideas immanent in nervous activity’, *The bulletin of mathematical biophysics 1943 5:4*. Springer, 5(4), pp. 115–133. doi: 10.1007/BF02478259.

Meunier, D. *et al.* (2009) ‘Hierarchical modularity in human brain functional networks’, *Frontiers in Neuroinformatics*. Frontiers Media S.A., 3(OCT), p. 37. doi: 10.3389/NEURO.11.037.2009/BIBTEX.

Miao, Y., Gowayyed, M. and Metze, F. (2016) ‘EESEN: End-to-end speech recognition using deep RNN models and WFST-based decoding’, *2015 IEEE Workshop on Automatic Speech Recognition and Understanding, ASRU 2015 - Proceedings*. Institute of Electrical and Electronics Engineers Inc., pp. 167–174. doi: 10.1109/ASRU.2015.7404790.

Miller, D. I. and Halpern, D. F. (2014) ‘The new science of cognitive sex differences’, *Trends in*

*Cognitive Sciences*. Elsevier Current Trends, 18(1), pp. 37–45. doi: 10.1016/J.TICS.2013.10.011.

Moher, D. *et al.* (2009) 'Preferred reporting items for systematic reviews and meta-analyses: The PRISMA statement', *Annals of Internal Medicine*. American College of Physicians, 151(4), pp. 264–269. doi: 10.7326/0003-4819-151-4-200908180-00135.

Molfese, D. L., Molfese, V. J. and Kelly, S. (2016) 'The Use of Brain Electrophysiology Techniques to Study Language: A Basic Guide for the Beginning Consumer of Electrophysiology Information':, *http://dx.doi.org/10.2307/1511242*. SAGE PublicationsSage CA: Los Angeles, CA, 24(3), pp. 177–188. doi: 10.2307/1511242.

Nair, J. *et al.* (2006) 'Clinical review: evidence-based diagnosis and treatment of ADHD in children.', *Missouri Medicine*, 103(6), pp. 617–621. Available at: https://europepmc.org/article/med/17256270 (Accessed: 4 May 2022).

Norman, L. J. *et al.* (2016) 'Structural and Functional Brain Abnormalities in Attention-Deficit/Hyperactivity Disorder and Obsessive-Compulsive Disorder: A Comparative Meta-analysis', *JAMA Psychiatry*. American Medical Association, 73(8), pp. 815–825. doi: 10.1001/JAMAPSYCHIATRY.2016.0700.

Osowski, S., Siwek, K. and Markiewicz, T. (no date) 'MLP and SVM Networks-a Comparative Study'.

Pakkenberg, B. *et al.* (2003) 'Aging and the human neocortex', *Experimental Gerontology*. Pergamon, 38(1–2), pp. 95–99. doi: 10.1016/S0531-5565(02)00151-1.

Palaniappan, R., Sundaraj, K. and Sundaraj, S. (2014) 'A comparative study of the svm and k-nn

machine learning algorithms for the diagnosis of respiratory pathologies using pulmonary acoustic signals', *BMC Bioinformatics*. BioMed Central Ltd., 15(1), pp. 1–8. doi: 10.1186/1471-2105-15-223/TABLES/6.

Parisi, G. I. *et al.* (2019) 'Continual lifelong learning with neural networks: A review', *Neural Networks*. Pergamon, 113, pp. 54–71. doi: 10.1016/J.NEUNET.2019.01.012.

Parisot, S. *et al.* (2017) 'Spectral graph convolutions for population-based disease prediction', *Lecture Notes in Computer Science (including subseries Lecture Notes in Artificial Intelligence and Lecture Notes in Bioinformatics)*. Springer Verlag, 10435 LNCS, pp. 177–185. doi: 10.1007/978-3-319-66179-7_21/FIGURES/2.

Parisot, S. *et al.* (2018) 'Disease prediction using graph convolutional networks: Application to Autism Spectrum Disorder and Alzheimer's disease', *Medical Image Analysis*. Elsevier, 48, pp. 117–130. doi: 10.1016/J.MEDIA.2018.06.001.

Park, H. J. and Friston, K. (2013) 'Structural and functional brain networks: From connections to cognition', *Science*. American Association for the Advancement of Science, 342(6158). doi: 10.1126/SCIENCE.1238411/ASSET/C8A581FE-33ED-405E-B2C2-AFA912B9F016/ASSETS/GRAPHIC/342_1238411_F4.JPEG.

Paszke, A. *et al.* (2019) 'PyTorch: An Imperative Style, High-Performance Deep Learning Library'. doi: 10.5555/3454287.3455008.

Perozzi, B. *et al.* (2017) 'Don't walk, skip! online learning of multi-scale network embeddings', *Proceedings of the 2017 IEEE/ACM International Conference on Advances in Social Networks Analysis and Mining, ASONAM 2017*. Association for Computing Machinery, Inc, pp. 258–265.

doi: 10.1145/3110025.3110086.

Perozzi, B., Al-Rfou, R. and Skiena, S. (2014) 'DeepWalk: Online learning of social representations', *Proceedings of the ACM SIGKDD International Conference on Knowledge Discovery and Data Mining*. Association for Computing Machinery, pp. 701–710. doi: 10.1145/2623330.2623732.

Petersen, R. C. *et al.* (2010) 'Alzheimer's Disease Neuroimaging Initiative (ADNI)', *Neurology*. Wolters Kluwer Health, Inc. on behalf of the American Academy of Neurology, 74(3), pp. 201–209. doi: 10.1212/WNL.0B013E3181CB3E25.

Petersen, S. E. and Sporns, O. (2015) 'Brain Networks and Cognitive Architectures', *Neuron*. Cell Press, 88(1), pp. 207–219. doi: 10.1016/J.NEURON.2015.09.027.

Qiu, J. *et al.* (2018) 'Network embedding as matrix factorization: Unifying DeepWalk, LINE, PTE, and node2vec', *WSDM 2018 - Proceedings of the 11th ACM International Conference on Web Search and Data Mining*. Association for Computing Machinery, Inc, 2018-Febuary, pp. 459–467. doi: 10.1145/3159652.3159706.

Rakhimberdina, Z. and Murata, T. (2020) 'Linear Graph Convolutional Model for Diagnosing Brain Disorders', *Studies in Computational Intelligence*. Springer, 882 SCI, pp. 815–826. doi: 10.1007/978-3-030-36683-4_65/FIGURES/4.

Ramzan, M. and Dawn, S. (2019) 'Learning-based classification of valence emotion from electroencephalography', *https://doi.org/10.1080/00207454.2019.1634070*. Taylor & Francis, 129(11), pp. 1085–1093. doi: 10.1080/00207454.2019.1634070.

Razavian, A. S. *et al.* (no date) ‘CNN features off-the-shelf: an astounding baseline for recognition’, *cv-foundation.org*. Available at: https://www.cv-foundation.org/openaccess/content_cvpr_workshops_2014/W15/html/Razavian_CNN_Features_Off-the-Shelf_2014_CVPR_paper.html (Accessed: 31 May 2022).

Reijneveld, J. C. *et al.* (2007) ‘The application of graph theoretical analysis to complex networks in the brain’, *Clinical Neurophysiology*. Elsevier, 118(11), pp. 2317–2331. doi: 10.1016/J.CLINPH.2007.08.010.

Rocca, D. La *et al.* (2014) ‘Human brain distinctiveness based on EEG spectral coherence connectivity’, *IEEE Transactions on Biomedical Engineering*. IEEE Computer Society, 61(9), pp. 2406–2412. doi: 10.1109/TBME.2014.2317881.

Roux, A. M. *et al.* (2012) ‘Developmental and Autism Screening Through 2-1-1: Reaching Underserved Families’, *American Journal of Preventive Medicine*. Elsevier, 43(6), pp. S457–S463. doi: 10.1016/J.AMEPRE.2012.08.011.

Roy, S., Kiral-Kornek, I. and Harrer, S. (2019) ‘Chrononet: A deep recurrent neural network for abnormal EEG identification’, *Lecture Notes in Computer Science (including subseries Lecture Notes in Artificial Intelligence and Lecture Notes in Bioinformatics)*. Springer Verlag, 11526 LNAI, pp. 47–56. doi: 10.1007/978-3-030-21642-9_8/TABLES/1.

Rozemberczki, B., Kiss, O. and Sarkar, R. (2020) ‘Karate Club: An API Oriented Open-Source Python Framework for Unsupervised Learning on Graphs’, *International Conference on Information and Knowledge Management, Proceedings*. Association for Computing Machinery, pp. 3125–3132. doi: 10.1145/3340531.3412757.

Rubinov, M. and Sporns, O. (2010) ‘Complex network measures of brain connectivity: Uses and interpretations’, *NeuroImage*. Academic Press, 52(3), pp. 1059–1069. doi: 10.1016/J.NEUROIMAGE.2009.10.003.

Saboksayr, S. S., Foxe, J. J. and Wismüller, A. (2020) ‘Attention-deficit/hyperactivity disorder prediction using graph convolutional networks’, *https://doi.org/10.1117/12.2551364*. SPIE, 11314, pp. 430–437. doi: 10.1117/12.2551364.

Saeidi, M. *et al.* (2021) ‘Neural Decoding of EEG Signals with Machine Learning: A Systematic Review’, *Brain Sciences 2021, Vol. 11, Page 1525*. Multidisciplinary Digital Publishing Institute, 11(11), p. 1525. doi: 10.3390/BRAINSCI11111525.

Saeidi, M. *et al.* (2022) ‘Decoding Task-Based fMRI Data with Graph Neural Networks, Considering Individual Differences’, *Brain Sciences 2022, Vol. 12, Page 1094*. Multidisciplinary Digital Publishing Institute, 12(8), p. 1094. doi: 10.3390/BRAINSCI12081094.

Sakhavi, S., Guan, C. and Yan, S. (2018) ‘Learning Temporal Information for Brain-Computer Interface Using Convolutional Neural Networks’, *IEEE Transactions on Neural Networks and Learning Systems*. Institute of Electrical and Electronics Engineers Inc., 29(11), pp. 5619–5629. doi: 10.1109/TNNLS.2018.2789927.

Salimi-Khorshidi, G. *et al.* (2014) ‘Automatic denoising of functional MRI data: Combining independent component analysis and hierarchical fusion of classifiers’, *NeuroImage*. Academic Press, 90, pp. 449–468. doi: 10.1016/J.NEUROIMAGE.2013.11.046.

Santarnecchi, E. *et al.* (2017) ‘Network connectivity correlates of variability in fluid intelligence performance’, *Intelligence*. JAI, 65, pp. 35–47. doi: 10.1016/J.INTELL.2017.10.002.

Sarica, A., Cerasa, A. and Quattrone, A. (2017) 'Random forest algorithm for the classification of neuroimaging data in Alzheimer's disease: A systematic review', *Frontiers in Aging Neuroscience*. Frontiers Media S.A., 9(OCT), p. 329. doi: 10.3389/FNAGI.2017.00329/BIBTEX.

Satterthwaite, T. D. *et al.* (2015) 'Linked Sex Differences in Cognition and Functional Connectivity in Youth', *Cerebral Cortex*. Oxford Academic, 25(9), pp. 2383–2394. doi: 10.1093/CERCOR/BHU036.

Scarselli, F. *et al.* (2009) 'The graph neural network model', *IEEE Transactions on Neural Networks*. Institute of Electrical and Electronics Engineers Inc., 20(1), pp. 61–80. doi: 10.1109/TNN.2008.2005605.

Schmitt, A. *et al.* (2011) 'Schizophrenia as a disorder of disconnectivity', *European Archives of Psychiatry and Clinical Neuroscience*. Springer, 261(SUPPL. 2), pp. 150–154. doi: 10.1007/S00406-011-0242-2/FIGURES/1.

Schweitzer PASCAL, P. *et al.* (2011) 'Weisfeiler-lehman graph kernels.', *jmlr.org*, 12, pp. 2539–2561. Available at: https://www.jmlr.org/papers/volume12/shervashidze11a/shervashidze11a.pdf (Accessed: 1 May 2022).

Sen, B. and Parhi, K. K. (2017) 'Extraction of common task signals and spatial maps from group fMRI using a PARAFAC-based tensor decomposition technique', *ICASSP, IEEE International Conference on Acoustics, Speech and Signal Processing - Proceedings*. Institute of Electrical and Electronics Engineers Inc., pp. 1113–1117. doi: 10.1109/ICASSP.2017.7952329.

Sen, B. and Parhi, K. K. (2019a) 'Predicting Male vs. Female from Task-fMRI Brain Connectivity', *Proceedings of the Annual International Conference of the IEEE Engineering in Medicine and Biology Society, EMBS*. Institute of Electrical and Electronics Engineers Inc., pp. 4089–4092. doi: 10.1109/EMBC.2019.8857236.

Sen, B. and Parhi, K. K. (2019b) 'Predicting Tasks from Task-fMRI Using Blind Source Separation', *Conference Record - Asilomar Conference on Signals, Systems and Computers*. IEEE Computer Society, 2019-November, pp. 2201–2205. doi: 10.1109/IEEECONF44664.2019.9049015.

Sen, P. C., Hajra, M. and Ghosh, M. (2020) 'Supervised Classification Algorithms in Machine Learning: A Survey and Review', *Advances in Intelligent Systems and Computing*. Springer Verlag, 937, pp. 99–111. doi: 10.1007/978-981-13-7403-6_11/TABLES/1.

Seo, Y. *et al.* (2018) 'Structured sequence modeling with graph convolutional recurrent networks', *Lecture Notes in Computer Science (including subseries Lecture Notes in Artificial Intelligence and Lecture Notes in Bioinformatics)*. Springer Verlag, 11301 LNCS, pp. 362–373. doi: 10.1007/978-3-030-04167-0_33/TABLES/2.

Shapiro, S. S. and Wilk, M. B. (1965) 'An Analysis of Variance Test for Normality (Complete Samples)', *Biometrika*. JSTOR, 52(3/4), p. 591. doi: 10.2307/2333709.

Siedlecki, K. L., Falzarano, F. and Salthouse, T. A. (2019) 'Examining Gender Differences in Neurocognitive Functioning Across Adulthood', *Journal of the International Neuropsychological Society*. Cambridge University Press, 25(10), pp. 1051–1060. doi: 10.1017/S1355617719000821.

Simonovsky, M. and Komodakis, N. (2017) ‘Dynamic edge-conditioned filters in convolutional neural networks on graphs’, *Proceedings - 30th IEEE Conference on Computer Vision and Pattern Recognition, CVPR 2017*. Institute of Electrical and Electronics Engineers Inc., 2017-January, pp. 29–38. doi: 10.1109/CVPR.2017.11.

Spasov, S. *et al.* (2019) ‘A parameter-efficient deep learning approach to predict conversion from mild cognitive impairment to Alzheimer’s disease’, *NeuroImage*. Academic Press, 189, pp. 276–287. doi: 10.1016/J.NEUROIMAGE.2019.01.031.

Sporns, O. (2022) ‘Graph theory methods: applications in brain networks’, *https://doi.org/10.31887/DCNS.2018.20.2/osporns*. Taylor & Francis, 20(2), pp. 111–120. doi: 10.31887/DCNS.2018.20.2/OSPORNS.

Stam, C. J. (2014) ‘Modern network science of neurological disorders’, *Nature Reviews Neuroscience 2014 15:10*. Nature Publishing Group, 15(10), pp. 683–695. doi: 10.1038/nrn3801.

Stankevičiūtė, K. *et al.* (2020) ‘Population Graph GNNs for Brain Age Prediction’, *bioRxiv*. Cold Spring Harbor Laboratory, p. 2020.06.26.172171. doi: 10.1101/2020.06.26.172171.

Sudlow, C. *et al.* (2015) ‘UK Biobank: An Open Access Resource for Identifying the Causes of a Wide Range of Complex Diseases of Middle and Old Age’, *PLOS Medicine*. Public Library of Science, 12(3), p. e1001779. doi: 10.1371/JOURNAL.PMED.1001779.

Tai, K. S., Socher, R. and Manning, C. D. (2015) ‘Improved Semantic Representations From Tree-Structured Long Short-Term Memory Networks’, *ACL-IJCNLP 2015 - 53rd Annual Meeting of the Association for Computational Linguistics and the 7th International Joint Conference on Natural Language Processing of the Asian Federation of Natural Language*

*Processing, Proceedings of the Conference*. Association for Computational Linguistics (ACL), 1, pp. 1556–1566. doi: 10.48550/arxiv.1503.00075.

Tan, J. H. *et al.* (2018) 'Application of stacked convolutional and long short-term memory network for accurate identification of CAD ECG signals', *Computers in Biology and Medicine*. Pergamon, 94, pp. 19–26. doi: 10.1016/J.COMPBIOMED.2017.12.023.

Tavor, I. *et al.* (2016) 'Task-free MRI predicts individual differences in brain activity during task performance', *Science*. American Association for the Advancement of Science, 352(6282), pp. 216–220. doi: 10.1126/SCIENCE.AAD8127/SUPPL_FILE/AAD8127S7.GIF.

Tharwat, A. *et al.* (2017) 'Linear discriminant analysis: A detailed tutorial', *AI Communications*. IOS Press, 30(2), pp. 169–190. doi: 10.3233/AIC-170729.

Trojanowski, J. Q. *et al.* (2010) 'Update on the biomarker core of the Alzheimer's Disease Neuroimaging Initiative subjects', *Alzheimer's & Dementia*. No longer published by Elsevier, 6(3), pp. 230–238. doi: 10.1016/J.JALZ.2010.03.008.

Valliani, A. A. A., Ranti, D. and Oermann, E. K. (2019) 'Deep Learning and Neurology: A Systematic Review', *Neurology and Therapy*. Adis, 8(2), pp. 351–365. doi: 10.1007/S40120-019-00153-8/FIGURES/2.

Veličković, P. *et al.* (2017) 'Graph Attention Networks', *6th International Conference on Learning Representations, ICLR 2018 - Conference Track Proceedings*. International Conference on Learning Representations, ICLR. doi: 10.48550/arxiv.1710.10903.

van de Ven, G. M., Siegelmann, H. T. and Tolias, A. S. (2020) 'Brain-inspired replay for

continual learning with artificial neural networks', *Nature Communications 2020 11:1*. Nature Publishing Group, 11(1), pp. 1–14. doi: 10.1038/s41467-020-17866-2.

Venkataraman, A. *et al.* (2016) 'Bayesian Community Detection in the Space of Group-Level Functional Differences', *IEEE Transactions on Medical Imaging*. Institute of Electrical and Electronics Engineers Inc., 35(8), pp. 1866–1882. doi: 10.1109/TMI.2016.2536559.

Ventresca, M. (2019) 'Using algorithmic complexity to differentiate Cognitive states in fMRI', *Studies in Computational Intelligence*. Springer Verlag, 813, pp. 663–674. doi: 10.1007/978-3-030-05414-4_53/FIGURES/6.

Wang, G., Qiu, Y. F. and Li, H. X. (2010) 'Temperature forecast based on SVM optimized by PSO algorithm', *Proceedings - 2010 International Conference on Intelligent Computing and Cognitive Informatics, ICICCI 2010*, pp. 259–262. doi: 10.1109/ICICCI.2010.24.

Wang, H. *et al.* (2019) 'Recognizing Brain States Using Deep Sparse Recurrent Neural Network', *IEEE Transactions on Medical Imaging*. Institute of Electrical and Electronics Engineers Inc., 38(4), pp. 1058–1068. doi: 10.1109/TMI.2018.2877576.

Wang, J., Zuo, X. and He, Y. (2010) 'Graph-based network analysis of resting-state functional MRI', *Frontiers in Systems Neuroscience*. Frontiers, 4, p. 16. doi: 10.3389/FNSYS.2010.00016/BIBTEX.

Wang, P. *et al.* (2018) 'LSTM-based EEG classification in motor imagery tasks', *IEEE Transactions on Neural Systems and Rehabilitation Engineering*. Institute of Electrical and Electronics Engineers Inc., 26(11), pp. 2086–2095. doi: 10.1109/TNSRE.2018.2876129.

Wang, S. *et al.* (no date) ‘Structural Deep Brain Network Mining’, *Proceedings of the 23rd ACM SIGKDD International Conference on Knowledge Discovery and Data Mining*. New York, NY, USA: ACM, 17. doi: 10.1145/3097983.

Wang, X. *et al.* (2020) ‘Decoding and mapping task states of the human brain via deep learning’, *Human Brain Mapping*. John Wiley & Sons, Ltd, 41(6), pp. 1505–1519. doi: 10.1002/HBM.24891.

Wang, Y., Cang, S. and Yu, H. (2019) ‘A survey on wearable sensor modality centred human activity recognition in health care’, *Expert Systems with Applications*. Pergamon, 137, pp. 167–190. doi: 10.1016/J.ESWA.2019.04.057.

Wang, Z. *et al.* (2018) ‘Deep Reasoning with Knowledge Graph for Social Relationship Understanding’, *IJCAI International Joint Conference on Artificial Intelligence*. International Joint Conferences on Artificial Intelligence, 2018-July, pp. 1021–1028. doi: 10.48550/arxiv.1807.00504.

Weisfeiler, B. *et al.* (no date) ‘The reduction of a graph to canonical form and the algebra which appears therein’, *iti.zcu.cz*. Available at: https://www.iti.zcu.cz/wl2018/pdf/wl_paper_translation.pdf (Accessed: 1 May 2022).

Wen, D. *et al.* (2018) ‘Deep learning methods to process fmri data and their application in the diagnosis of cognitive impairment: A brief overview and our opinion’, *Frontiers in Neuroinformatics*. Frontiers Media S.A., 12, p. 23. doi: 10.3389/FNINF.2018.00023/BIBTEX.

Wiggins, W. F. *et al.* (2021) ‘Natural Language Processing of Radiology Text Reports: Interactive Text Classification’, *https://doi.org/10.1148/ryai.2021210035*. Radiological Society

of North America , 3(4). doi: 10.1148/RYAI.2021210035.

Wu, D. *et al.* (2021) ‘Connectome-based individual prediction of cognitive behaviors via graph propagation network reveals directed brain network topology’, *iopscience.iop.org*, 18, pp. 460–463. doi: 10.1088/1741-2552/ac0f4d.

Wu, F. *et al.* (no date) ‘Simplifying graph convolutional networks’, *proceedings.mlr.press*. Available at: https://proceedings.mlr.press/v97/wu19e.html (Accessed: 4 May 2022).

Wu, Z. *et al.* (2021) ‘A Comprehensive Survey on Graph Neural Networks’, *IEEE Transactions on Neural Networks and Learning Systems*. Institute of Electrical and Electronics Engineers Inc., 32(1), pp. 4–24. doi: 10.1109/TNNLS.2020.2978386.

Xing, X. *et al.* (2019) ‘Dynamic spectral graph convolution networks with assistant task training for early MCI diagnosis’, *Lecture Notes in Computer Science (including subseries Lecture Notes in Artificial Intelligence and Lecture Notes in Bioinformatics)*. Springer Science and Business Media Deutschland GmbH, 11767 LNCS, pp. 639–646. doi: 10.1007/978-3-030-32251-9_70/FIGURES/3.

Xing, X. *et al.* (2021) ‘DS-GCNs: Connectome Classification using Dynamic Spectral Graph Convolution Networks with Assistant Task Training’, *Cerebral Cortex*. Oxford Academic, 31(2), pp. 1259–1269. doi: 10.1093/CERCOR/BHAA292.

Xu, K. *et al.* (2018) ‘How Powerful are Graph Neural Networks?’, *7th International Conference on Learning Representations, ICLR 2019*. International Conference on Learning Representations, ICLR. doi: 10.48550/arxiv.1810.00826.

Xu, M. (2021) ‘Understanding Graph Embedding Methods and Their Applications’, *https://doi.org/10.1137/20M1386062*. Society for Industrial and Applied Mathematics, 63(4), pp. 825–853. doi: 10.1137/20M1386062.

Yan, C. G. *et al.* (2019) ‘Reduced default mode network functional connectivity in patients with recurrent major depressive disorder’, *Proceedings of the National Academy of Sciences of the United States of America*. National Academy of Sciences, 116(18), pp. 9078–9083. doi: 10.1073/PNAS.1900390116.

Yao, D. *et al.* (2019) ‘Triplet Graph Convolutional Network for Multi-scale Analysis of Functional Connectivity Using Functional MRI’, *Lecture Notes in Computer Science (including subseries Lecture Notes in Artificial Intelligence and Lecture Notes in Bioinformatics)*. Springer, 11849 LNCS, pp. 70–78. doi: 10.1007/978-3-030-35817-4_9/FIGURES/4.

Yao, D. *et al.* (2020) ‘Temporal-Adaptive Graph Convolutional Network for Automated Identification of Major Depressive Disorder Using Resting-State fMRI’, *Lecture Notes in Computer Science (including subseries Lecture Notes in Artificial Intelligence and Lecture Notes in Bioinformatics)*. Springer Science and Business Media Deutschland GmbH, 12436 LNCS, pp. 1–10. doi: 10.1007/978-3-030-59861-7_1/FIGURES/3.

Yao, D. *et al.* (2021) ‘A Mutual Multi-Scale Triplet Graph Convolutional Network for Classification of Brain Disorders Using Functional or Structural Connectivity’, *IEEE Transactions on Medical Imaging*. Institute of Electrical and Electronics Engineers Inc., 40(4), pp. 1279–1289. doi: 10.1109/TMI.2021.3051604.

Yu, B. *et al.* (2020) ‘Node proximity preserved dynamic network embedding via matrix

perturbation', *Knowledge-Based Systems*. Elsevier, 196, p. 105822. doi: 10.1016/J.KNOSYS.2020.105822.

Yu, S. *et al.* (2019) 'Multi-scale Graph Convolutional Network for Mild Cognitive Impairment Detection', *Lecture Notes in Computer Science (including subseries Lecture Notes in Artificial Intelligence and Lecture Notes in Bioinformatics)*. Springer, 11849 LNCS, pp. 79–87. doi: 10.1007/978-3-030-35817-4_10/FIGURES/4.

Yu, S. *et al.* (2020) 'Multi-scale Enhanced Graph Convolutional Network for Early Mild Cognitive Impairment Detection', *Lecture Notes in Computer Science (including subseries Lecture Notes in Artificial Intelligence and Lecture Notes in Bioinformatics)*. Springer Science and Business Media Deutschland GmbH, 12267 LNCS, pp. 228–237. doi: 10.1007/978-3-030-59728-3_23/TABLES/2.

Zeng, K. *et al.* (2017) 'Disrupted Brain Network in Children with Autism Spectrum Disorder', *Scientific Reports 2017 7:1*. Nature Publishing Group, 7(1), pp. 1–12. doi: 10.1038/s41598-017-16440-z.

Zhang, C. *et al.* (2018) 'Functional connectivity predicts gender: Evidence for gender differences in resting brain connectivity', *Human Brain Mapping*. John Wiley & Sons, Ltd, 39(4), pp. 1765–1776. doi: 10.1002/HBM.23950.

Zhang, J. *et al.* (2018) 'Gender differences in global functional connectivity during facial emotion processing: A visual MMN study', *Frontiers in Behavioral Neuroscience*. Frontiers Media S.A., 12, p. 220. doi: 10.3389/FNBEH.2018.00220/BIBTEX.

Zhang, L. *et al.* (2019) 'A Cascaded Multi-modality Analysis in Mild Cognitive Impairment',

*Lecture Notes in Computer Science (including subseries Lecture Notes in Artificial Intelligence and Lecture Notes in Bioinformatics)*. Springer, 11861 LNCS, pp. 557–565. doi: 10.1007/978-3-030-32692-0_64/FIGURES/5.

Zhang, M. and Chen, Y. (2018) 'Link Prediction Based on Graph Neural Networks', *Advances in Neural Information Processing Systems*. Neural information processing systems foundation, 2018-December, pp. 5165–5175. doi: 10.48550/arxiv.1802.09691.

Zhang, W. *et al.* (2019) 'Experimental Comparisons of Sparse Dictionary Learning and Independent Component Analysis for Brain Network Inference from fMRI Data', *IEEE Transactions on Biomedical Engineering*. IEEE Computer Society, 66(1), pp. 289–299. doi: 10.1109/TBME.2018.2831186.

Zhang, W. *et al.* (2020) 'Deep Representation Learning for Multimodal Brain Networks', *Lecture Notes in Computer Science (including subseries Lecture Notes in Artificial Intelligence and Lecture Notes in Bioinformatics)*. Springer Science and Business Media Deutschland GmbH, 12267 LNCS, pp. 613–624. doi: 10.1007/978-3-030-59728-3_60/FIGURES/3.

Zhang, X. *et al.* (2020) 'Gender Differences Are Encoded Differently in the Structure and Function of the Human Brain Revealed by Multimodal MRI', *Frontiers in Human Neuroscience*. Frontiers Media S.A., 14, p. 244. doi: 10.3389/FNHUM.2020.00244/BIBTEX.

Zhang, Y. *et al.* (2020) 'Adaptive Spatio-Temporal Graph Convolutional Neural Network for Remaining Useful Life Estimation', *Proceedings of the International Joint Conference on Neural Networks*. Institute of Electrical and Electronics Engineers Inc. doi: 10.1109/IJCNN48605.2020.9206739.

Zhang, Y. *et al.* (2021) ‘Functional annotation of human cognitive states using deep graph convolution’, *NeuroImage*. Academic Press, 231, p. 117847. doi: 10.1016/J.NEUROIMAGE.2021.117847.

Zhang, Y. and Huang, H. (2019) ‘New Graph-Blind Convolutional Network for Brain Connectome Data Analysis’, *Lecture Notes in Computer Science (including subseries Lecture Notes in Artificial Intelligence and Lecture Notes in Bioinformatics)*. Springer Verlag, 11492 LNCS, pp. 669–681. doi: 10.1007/978-3-030-20351-1_52/FIGURES/4.

Zhang, Z. *et al.* (2018) ‘Billion-Scale Network Embedding with Iterative Random Projection’, *Proceedings - IEEE International Conference on Data Mining, ICDM*. Institute of Electrical and Electronics Engineers Inc., 2018-November, pp. 787–796. doi: 10.1109/ICDM.2018.00094.

Zhang, Z., Cui, P. and Zhu, W. (2022) ‘Deep Learning on Graphs: A Survey’, *IEEE Transactions on Knowledge and Data Engineering*. IEEE Computer Society, 34(1), pp. 249–270. doi: 10.1109/TKDE.2020.2981333.

Zhao, Y. *et al.* (2020) ‘4D Modeling of fMRI Data via Spatio-Temporal Convolutional Neural Networks (ST-CNN)’, *IEEE transactions on cognitive and developmental systems*. NIH Public Access, 12(3), p. 451. doi: 10.1109/TCDS.2019.2916916.

Zhou, J. *et al.* (2017) ‘Applications of Resting-State Functional Connectivity to Neurodegenerative Disease’, *Neuroimaging Clinics*. Elsevier, 27(4), pp. 663–683. doi: 10.1016/J.NIC.2017.06.007.

Zhou, J. *et al.* (2020) ‘Graph neural networks: A review of methods and applications’, *AI Open*. Elsevier, 1, pp. 57–81. doi: 10.1016/J.AIOPEN.2021.01.001.

Zhou, Y. *et al.* (2022) ‘Graph Neural Networks: Taxonomy, Advances, and Trends’, *ACM Transactions on Intelligent Systems and Technology (TIST)*. ACMPUB27New York, NY, 13(1). doi: 10.1145/3495161.

Zhu, S. *et al.* (no date) ‘Graph geometry interaction learning’, *proceedings.neurips.cc*. Available at: https://proceedings.neurips.cc/paper/2020/hash/551fdbb810aff145c114b93867dd8bfd-Abstract.html (Accessed: 8 May 2022).

Zitnik, M., Agrawal, M. and Leskovec, J. (2018) ‘Modeling polypharmacy side effects with graph convolutional networks’, *Bioinformatics*. Oxford Academic, 34(13), pp. i457–i466. doi: 10.1093/BIOINFORMATICS/BTY294.